High-Throughput Phenotyping for Soybean Iron Deficiency Chlorosis Using an Unmanned Aircraft System: Applications in Breeding, Agronomy, and Genetics

A Thesis
SUBMITTED TO THE FACULTY OF
UNIVERSITY OF MINNESOTA
BY

Austin Andrew Dobbels

IN PARTIAL FULFILLMENT OF THE REQUIREMENTS
FOR THE DEGREE OF
DOCTOR OF PHILOSOPHY

Dr. Aaron Lorenz

July, 2020

Acknowledgements

I would like to thank all of the people who have helped and supported me in the completion of this dissertation. I would first like to thank my advisor, Dr. Aaron Lorenz, for input, guidance, and for the opportunity to work on these projects. I would also like to thank Drs. Seth Naeve, Dan Kaiser, Kevin Smith, and Joe Knight for serving on my committee and for all of their input and suggestions for my projects. In addition, I thank my funding sources: The Minnesota Soybean Research and Promotion Council and the United Soybean Board Fellowship.

I would like to thank all members of both the Lorenz Lab and Naeve Lab for their contributions. The lab technicians and MAST students deserve a huge thanks for their help coordinating field plans and assisting in data collection. This project could not have been completed without all your hard work.

Lastly, I would like to thank family, friends, and fellow graduate students. Thank you for your continued support of my academic and professional career. Thanks for the hours socializing and helping to alleviate stress when I needed it most and for helping me to become the person I am today.

Abstract

Iron deficiency chlorosis (IDC) is an abiotic stress in soybean [Glycine max (L.) Merr.] that causes significant yield reductions. Symptoms of IDC include interveinal chlorosis and stunting of the plant. While there are management practices that can overcome these drastic yield losses, the preferred approach to manage IDC is growing tolerant soybean varieties. To develop varieties tolerant to IDC, breeders may easily phenotype up to thousands of candidate soybean lines every year for severity of symptoms related to IDC, a task traditionally done with a 1–5 visual rating scale. The visual rating scale is subjective and, because it is time consuming and laborious, can typically only be accomplished once or twice during a growing season. The goal of this study was to use an unmanned aircraft system (UAS) to improve field screening for tolerance to soybean IDC. We achieved high efficiency in collecting data with autonomous UAS flights, greater than 77% accuracy in classifying plots on a 1-5 severity scale, and an average reduction in LSD values across a series of experimental trials. This method is high-throughput, objective, and more precise than traditional ground based visual assessments. The UAS-based system was further used to assess the interactions of IDC and soybean cyst nematode (SCN). A range of treatments were added to change the levels of IDC and SCN stress in a randomized complete block factorial design. Results from the three-year study showed that the treatments independently created IDC and SCN severity symptoms and associated yield differences. Nematode reproduction was significantly impacted by varietal resistance and was not impacted by IDC treatment. An interaction between IDC and SCN treatments was not found for yield, nematode

reproduction, or severity symptoms suggesting these stresses act additively. Finally, UAS-based phenotyping was used to assess temporal patterns of iron deficiency chlorosis symptoms in a genome-wide association study. The UAS-based system identified overlapping QTL with the same significance as traditional visual observations indicating that UAS estimates of IDC are useful in soybean genetics research programs. In addition, novel QTL were identified for the rate of IDC recovery. Overall, the efficiency and precision of UAS-based image analysis of IDC can be useful in breeding, agronomic, and genome-wide association studies.

Table of Contents

List of Tables

List of Figures

Chapter 1 – Literature Review

Soybean Iron Deficiency Chlorosis and High-Throughput Plant Phenotyping

Soybean Iron Deficiency Chlorosis

Factors and symptoms associated with soybean iron deficiency chlorosis

Soybean iron deficiency chlorosis (IDC) is a major soil borne stress that causes significant yield reduction in the Midwest. Iron deficiency chlorosis is caused by a lack of available iron [Fe(II)] to the plant. While iron is abundant in almost all soils, deficiencies are caused by several factors and their interactions that change the solubility of iron in the soil (Hansen *et al.* 2003). Soils with pH in the range of 7.4 – 8.5 cause low solubility of iron minerals (Lucena and Hernandez-Apaolaza 2017). Another soil factor that causes IDC is the amount of calcium carbonates in the soil. The calcium carbonates in the soil neutralize the excreted acids from the soybean roots that are meant to solubilize the iron in the soil (Kaiser *et al.* 2011). Nitrates (NO_{3-}) in the soil also increase IDC (Silva and Uchida 2000; Bloom *et al.* 2011a; Kaiser *et al.* 2011, 2014). Plants take up NO_{3-} from the soil and exchange a bicarbonate ion in the process. Bicarbonate neutralizes the acidity around the roots and the iron remains unavailable to the plant (Inskeep and Bloom 1987). Wet soils are another factor that increase IDC. Wet soils lead to a buildup of CO2 in the soil. The trapped CO2 results in a buildup of carbonic acid which forms bicarbonates. As described previously, the bicarbonate leads to a neutralization of the acidity around the roots and causes the iron to become unavailable to the plant. Symptoms of IDC include interveinal chlorosis of the leaves, yellowing of soybean foliage, and overall stunting of the plant. These symptoms appear as early as a few weeks after emergence and new growth by the plant is the most affected.

Management solutions for soybean iron deficiency chlorosis

Soybean iron deficiency chlorosis (IDC) causes annual losses of up to ~$260 million in the United States alone (Hansen *et al.* 2004; Peiffer *et al.* 2012). In Minnesota, IDC can be found in the regions of South Central, Southwest, West Central, and Northwest Minnesota, and is found on high pH soils and soils with large amounts of calcium carbonates.

Due to the large impact of IDC, many solutions have been studied and shown to prevent yield loss due to IDC. These solutions include growing a tolerant soybean variety, using a companion crop, reducing other forms of stress to the plant, increasing plant density, and supplementing the crop with iron chelates (Goos and Johnson 2000; Naeve 2006; Kaiser *et al.* 2011, 2014; Chatterjee *et al.* 2017). While there are management practices presented, note that soybean IDC is still challenging to manage due to the high amount of spatial and temporal variability of the stress (Hansen *et al.* 2004).

While there are several strategies presented to help manage IDC, it has been reported that growing a soybean variety tolerant to IDC stress is most beneficial (Goos and Johnson 2000; Hansen *et al.* 2004; Goos *et al.* 2009). Soybean varieties show a range in response to IDC with some very tolerant to the stress, while others are highly susceptible. Private companies and public institutions provide information on how different varieties rank in terms of IDC tolerance. Growers should look at these rankings when choosing a variety if their field has a known history of IDC. Growers can also discuss variety options with nearby farmers as well as perform on-site variety testing of

their own. When choosing a variety to plant, growers should consider the potential benefits of that variety in terms of cost and economic return.

Soil NO_{3-} levels (as discussed previously) can increase the severity of IDC. It has been shown that planting a companion crop such as oats can take up and use the NO_{3-}, thus helping to alleviate IDC. While planting a companion crop has been proven to be effective, it does require additional management of sowing the oats and terminating them at the right time (too early and the oats will not take up enough of the NO_{3-} and too late and they will compete with the soybean crop) (Naeve 2006, Bloom et al. 2011, Kaiser et al. 2014). In addition to companion crops, increased planting density of soybeans or planting soybeans into a wider row spacing can help a producer manage IDC (Goos and Johnson 2001).

Reducing other forms of stress is also important. A soil with high pH is a major factor that causes unavailability of iron to the soybean plant leading to IDC. In addition, it has been shown that nematodes are often present in higher numbers in high-pH soil (Francl 1993, Rogovska et al. 2006, Pedersen et al. 2010, Melakeberhan et al. 2013). It is very likely that IDC and SCN stresses are co-occurring in farmer's fields without the farmer recognizing the problem. It is likely that these two stresses are working together to make symptoms more severe. Other stresses that might affect iron uptake include herbicide damage and other plant diseases (Kaiser et al. 2011).

In-furrow application of an ortho-ortho EDDHA Fe chelate has been shown to be effective for reducing the impact of IDC on soybean. Soygreen is one example of an iron chelate product that contains 1.8% Fe by volume. While applying a chelated iron does help with stress, cost may be prohibitive for using such a product. Kaiser et al. in 2014

found that an in-furrow application of iron chelates provides a solution to reducing IDC stress in areas where IDC stress was moderate to severe. They also noted that the application of this product had less risk associated with it than using an oat companion crop (Kaiser et al. 2014). Other sources of Fe have been studied but have not been found to be overly effective (Chatterjee et al. 2017). Overall, the research studies have shown that it is best to pair IDC-tolerant varieties with other management options to improve yield in IDC prone fields (Mourtzinis and Conley 2017).

Genetics underlying tolerance to soybean iron deficiency chlorosis

Many studies have been conducted to identify quantitative trait loci (QTL) controlling IDC tolerance. As of 2019, Soybase has reported 39 QTL for IDC which are reported as iron efficiency QTL "Fe effic" (Soybase.org). Studies to identify QTL have included bi-parental linkage mapping and association mapping.

The first study on the genetics of IDC in soybean was conducted in 1943 by Weiss (Weiss 1943) who concluded that IDC was affected by a single recessive gene. Cianzio and Fehr 1980 also reported that IDC was controlled by a major gene based on backcrossing of susceptible and resistant IDC varieties (IVR EX5003 x Anoka) (Cianzio and Fehr 1980). The same group of researchers conducted follow-up studies and in 1982, reported that the inheritance of IDC was actually different than their reports in 1980 (Cianzio and Fehr 1982). In the follow-up manuscript, Cianzio and Fehr reported that the inheritance of IDC resistance was likely quantitative and can vary based on the parents that are used in the development of the populations. Fehr 1982 reported that after testing many plant introductions that no genotype was available that did not exhibit some level

of chlorosis, and thus, plant breeding efforts are needed to improve resistance to the stress.

Additional studies have been conducted on the genetics of IDC in soybean since the initial reports. Diers *et al.* 1992 conducted a bi-parental mapping population study and found three markers significantly associated with iron efficiency. Mansur 1992 identified a plant introduction that had an average reduction in IDC symptoms – PI 437654 (Mansur 1992).

Lin *et al.* 1997, 2000 identified a notable QTL on linkage group N (now identified as chromosome 3) for iron deficiency chlorosis indicating a major gene was involved in the segregation of the IDC response in one of the bi-parental populations of Anoka x A7. Lin *et al.* (2000) evaluated IDC symptoms of two separate bi-parental populations using both visual scores and spectrometric chlorophyll estimations to identify QTL affecting IDC. Overall, QTL with minor effects were found on five different linkage groups for one bi-parental population and two QTL mapped in the Anoka x A7 population. The same QTL on chromosome 3 was found in both studies (Lin *et al.* 1997a, 2000).

Severin *et al.* 2010 compared the near isogenic lines (NILs) Clark (PI 57430) and IsoClark (PI 548533) which were previously reported for differences in iron efficiency (O'Rourke *et al.* 2007b; a, 2009). They confirmed introgression sites of IsoClark on chromosomes 3, 4, 5, 13, and 16. Additionally, RNA-Seq was used to identify a much greater number of markers to increase the resolution of introgression sites.

Mamidi *et al.* 2011 studied the genetic architecture of IDC in soybean by SNP-based genome-wide association mapping and found nine consistent loci accounting for 43.7% of the variation in IDC severity, also confirming many previously reported loci.

In addition, fifteen genes known to be involved in iron metabolism were located within 500kb of the significant markers.

Peiffer *et al.* 2012 re-sequenced differentially expressed genes within the QTL region on chromosome 3 of the soybean genome, based on previous reporting of this QTL. Two genes encoding transcription factors within the chromosome 3 region were significantly altered during the induction of iron stress in the roots. Interestingly, these genes are known in Arabidopsis to regulate the strategy I response. Furthermore, the resequencing data revealed a significant deletion that is hypothesized to be associated with the iron acquisition genes. The results provide insights on the genes conferring the iron-efficient QTL in the Anoka x A7 population previously described.

King *et al.* 2013 found a QTL on chromosome 20 that showed a possible genetic link between the iron efficiency trait and iron accumulation in the soybean seed. Based on this, it may be possible to select genotypes based on iron composition in the seed as an indirect selection for IDC resistance. The authors conducted their analysis using the previously reported Anoka x A7 population and performed both nutrient analysis of the seed at harvest from each plot as well as the leaf tissue of fully expanded trifoliates within plots 3-4 weeks after planting. The candidate genes identified in this study could be involved in mineral uptake and transport and have the potential to be selected for in breeding Fe efficient crops (King *et al.* 2013).

Moran Lauter *et al.* 2014 conducted a RNA-Seq study at one and six hours after inducing iron stress by replacing iron abundant media with iron deficient media in a hydroponic assay. Genes were identified at each of the two time-points, but interestingly, there was little overlap in differentially expressed genes at each time of analysis.

Dynamic gene expression and differences between roots and leaves in this study suggests that there are likely many transcription factors involved that are changing the expression levels of genes involved in iron efficiency (Moran Lauter *et al.* 2014). The differentially expressed genes identified in the study can be considered for future investigation and selection for improvements in tolerance to iron deficiency chlorosis.

Mamidi *et al.* 2014a identified seven major effect QTL on seven different chromosomes using genome-wide association analysis. A total of twelve candidate genes were identified within the mapped regions based on their previously known associations to iron metabolism. In the study, two separate populations were grown over the course of two years and subsequently evaluated for IDC stress on a 1-5 visual scale. In the genome-wide association analysis, the authors found QTL overlapping with previous studies including the prominent QTL on chromosome 3. Additional QTL were identified on chromosomes 5, 7, 16, 17, 18, and 19. The markers combined explained a total of 46.3 percent of the variation in IDC severity score (Mamidi *et al.* 2014b; a). In addition to identifying QTL, the authors report narrowing QTL regions to identify a total of 12 candidate genes.

Zhang *et al.* 2017a used red-green-blue images to evaluate the severity of iron chlorosis symptoms for genome-wide association analysis. The machine learning scores based on image analysis provided a more objective measure of IDC stress and thus allowed for the detection of smaller effect QTL that would have otherwise been missed if solely relying on human based visual assessments of IDC symptoms. In the study, both visual score and machine learning scores were both successful in identifying the QTL on chromosome 3, as was previously reported. In addition, the machine learning score based

on image analysis allowed for the capture of a continuous variable rather than discrete classes on a 1-5 scale. This image based score, therefore, was used and identified two additional novel QTL on chromosomes 18 and 20. On the QTL of chromosome 18, a candidate gene (Glyma.18g111000) was identified for further investigation (Zhang *et al.* 2017b).

Merry *et al.* 2019 reported a significant IDC QTL on the short arm of chromosome 5 through a combination of two separate association mapping populations and a bi-parental mapping population. In that study, Merry et al. also identified significant QTL on chromosome 3 and chromosome 6 of the soybean genome. In addition to mapping several QTL, additional analysis was done to further investigate the region on chromosome 5. In Fiskeby III by Mandarin (Ottawa) near isogenic line pairs developed from residual heterogeneity, the causative region of IDC tolerance was narrowed to the end of chromosome 5. The final fine-mapped region was identified to be between 0 and 137,207 base pairs on chromosome 5 (Merry *et al.* 2019).

Another study by Assefa *et al.* 2020 used both genome-wide association analysis and genome-wide epistatic analysis to further investigate the genetic architecture of soybean iron deficiency chlorosis (Assefa *et al.* 2020). Phenotypic data was collected both in the field and in a hydroponic assay that introduces iron stress conditions. The authors demonstrate the power of combining genome-wide association analysis, genome-wide epistatic analysis, and gene expression analysis to identify novel QTL. The study suggested that a mutation in Isoclark was responsible for regulation of Fe uptake and transport genes (Assefa *et al.* 2020). In addition, significantly associated SNPs were identified on 19 of the 20 soybean chromosomes (all except chromosome 4). These

identified QTL have potential to be used for future genomic studies or for selection for future soybean improvement. Finally, the authors suggest that the region on chromosome 3 (previously reported) is likely caused by multiple candidate genes within the interval. Interestingly, there may be potential to alter multiple molecular pathways to improve tolerance to IDC (Assefa *et al.* 2020).

Methods of phenotyping soybean iron deficiency chlorosis

Traditionally, IDC severity is measured through a visual 1-5 or 1-9 rating system. In such systems, tolerant varieties would be given a 1-2 on a five-point scale or a 1-2.5 on a nine-point scale. Tolerant varieties show no yellowing and the full canopy is green. Moderately tolerant varieties will be given a 2.1-3 or 2.6-5 on a five-point and nine-point scale, respectively. Moderately susceptible lines show some signs of yellowing and are given a 3.1-4 or 5.1-7.5 on a five-point and nine-point scale, respectively. Finally, susceptible lines will be given a 4.1-5 or 7.5-9 rating on a five point and nine-point scale, respectively. Susceptible lines show severe chlorosis or necrosis and stunting of the plant.

Alternative methods for phenotyping IDC severity also exist. For example, relative leaf chlorophyll concentrations can be measured by destructively sampling soybean leaves and extracting the chlorophyll in acetone solutions (Lin *et al.* 1997a). Other researchers have measured chlorophyll concentration using a SPAD meter (Minolta, Ramsey, NJ) (Helms *et al.* 2010; Bloom *et al.* 2011a; Vasconcelos and Grusak 2014). In these cases, researchers typically measure random leaves within the plot and average the chlorophyll measurements. While this approach is more time and labor intensive, it provides an objective measurement of relative chlorophyll concentration.

Recently, researchers have developed alternative image-based IDC rating systems (Naik *et al.* 2017; Zhang *et al.* 2017b). In this approach, pictures of plots are taken with digital cameras and computer imaging software is used to extract three features - green pixel content, yellow pixel content, and brown pixel content. Using machine learning algorithms, these features are related to the IDC severity scores taken in the field. Approaches such as this one has offered great success in hill plots achieving a mean per class accuracy of ~96%.

Four-row field trial IDC plots have also been imaged to measure IDC severity (Bai *et al.* 2018). In the study by Bai et al. 2018, a high-throughput phenotyping cart was used to capture RGB images over the center two rows of each plot. In their approach, an overall classification accuracy of 81% was obtained (Bai *et al.* 2018). In the above image analysis papers, the authors mention the demand for a higher throughput method of image collection and analysis, such as unmanned aircraft systems.

High-Throughput Plant Phenotyping

High-throughput phenotyping

With advances in genomics and quantitative genetics, phenotyping remains a cornerstone of plant breeding (Godwin *et al.* 2019; Reynolds *et al.* 2020). Genetic markers have been a valuable tool for plant breeders in which the genes controlling a trait are of major effect. For complex traits and those of agronomic importance such as grain yield, individual markers are less valuable. However, whole genome prediction has shown success in improving genetic gain for these traits (Meuwissen *et al.* 2001; Heffner *et al.* 2010; Jannink *et al.* 2010; Lorenz 2013; Crossa *et al.* 2014). In light of these

advancements, high-throughput and reliable phenotypic information is still in high demand.

High-throughput phenotyping (HTP) refers to the ability for researchers to collect detailed information during a plant life cycle in a non-invasive way (Dhondt *et al.* 2013; Araus and Cairns 2014). A key to the success of HTP is the ability to non-destructively measure plant traits (Araus *et al.* 2015; Fahlgren *et al.* 2015). High-throughput image-based phenotyping can be defined as the ability to minimally image hundreds of plants per day (Fahlgren *et al.* 2015). High-throughput phenotyping, or phenomics, has also been defined as "the use of sensor and imaging technologies that permits the rapid, low-cost measurement of many phenotypes across time and space with less labor" (Pauli *et al.* 2016). In addition, HTP can be conducted in both controlled and field environments and with a wide array of platforms and sensors (Araus and Cairns 2014; Singh *et al.* 2016).

High-throughput phenotyping has recently been reviewed in several publications (Furbank and Tester 2011; Fiorani and Schurr 2013; Araus and Cairns 2014; Pauli *et al.* 2016c; Coppens *et al.* 2017; Tardieu *et al.* 2017; Reynolds *et al.* 2019; Roitsch *et al.* 2019). In these reviews, the technological advancements in image processing software, improvements in plant phenotyping, and relating these phenotypes to the environment are discussed in great detail. Regardless of these advancements, however, there is still a growing interest in "breeder-friendly" phenotyping, in which collecting data is easy and accessible, and the costs for implementation are low enough to permit its use (Reynolds *et al.* 2020).

In the area of HTP, improvements and new innovation continue to emerge. New sensors are being designed that are smaller and can capture more detailed information in

terms of spatial and spectral resolution. In addition, new computational techniques and machine learning algorithms are being incorporated to enable data assimilation and feature identification for plant phenotyping (Singh *et al.* 2016).

Sensors and vehicles for field based high-throughput phenotyping

There are many options for sensors and vehicles to perform high-throughput plant phenotyping (HTP), and the capabilities of these systems continue to evolve (Roitsch *et al.* 2019). White *et al.* (2012) discussed platform options for field-based phenomics including high-clearance tractors, cranes, cable robots, helicopters, and aerostats. Proximal sensing carts have also shown value in collecting high resolution phenotypic information (White and Conley 2013; Bai *et al.* 2018). Field-based phenotyping platforms vary in their ability to carry different sized payloads, their portability, and base cost. In addition, each platform will allow for different spatial and temporal resolution. Ultimately, the platform needs to provide a means to rapidly and accurately position instruments over field plots or individual plants (White *et al.* 2012).

In recent years there has been a growing interest in aerial HTP platforms, especially for the use in germplasm assessment within breeding programs. There are a few reasons for this upward attention including the affordability and accessibility of unmanned aircraft systems (UASs). One major advantage is that these platforms can cover thousands of plots in just minutes allowing for high temporal and spatial resolution of phenotypic data (Haghighattalab *et al.* 2016). The UASs can also be customized to carry a wide array of sensors, making them very appropriate for use as a phenotyping platform.

The platforms discussed previously are simply a means of carrying sensors to collect phenotypic information. These spectral sensors work either passively or actively. Passive sensors rely on an external source of energy, typically sunlight. Active sensors are equipped with light-emitting systems to provide radiation of specific wavebands. One major advantage of active sensors is their ability to capture data independent of changing irradiation conditions (Hatfield *et al.* 2008; Erdle *et al.* 2011). Both active and passive sensors are aimed to measure the amount of light reflected by the crop or object of interest. Some examples of active sensors used for HTP include LiDAR, spectral sensors, and sonar. Examples of passive sensors include digital cameras that collect visible spectral radiation including red, green, blue (RGB) wavebands. Digital cameras have also been modified to capture NIR reflectance (White *et al.* 2012; Busemeyer *et al.* 2013; Andrade-Sanchez *et al.* 2014; Crain *et al.* 2016; Yu *et al.* 2016a; Dobbels and Lorenz 2019). In addition to the visible spectrum, multispectral and hyperspectral cameras have been utilized to capture spectral wavebands throughout the electromagnetic spectrum (Haskett and Sood 1998; Zarco-Tejada *et al.* 2005; Campbell *et al.* 2007; Rodrigues *et al.* 2018). The sensor to use depends on the objective of the research project, with hyperspectral and multispectral cameras costing much more than low cost consumer grade digital cameras. Ultimately, HTP platforms will vary in the spatial, temporal, and spectral resolution of data.

High-throughput phenotyping in soybean breeding programs

Many traits are routinely evaluated in a soybean breeding program that require subjective visual ratings and are very laborious and time consuming to collect. Many of these traits in soybean have been investigated for field-based high-throughput

phenotyping, both with ground based sensing platforms as well as with cameras equipped to unmanned aircraft systems (UAS). Traits that have shown great success include estimating days to plant maturity, quantifying canopy coverage, abiotic and biotic stress detection, and yield estimation, as examples (Singh *et al.* 2016; Yu *et al.* 2016b; Xavier *et al.* 2017; Zhang *et al.* 2017a; Bai *et al.* 2018a; Dobbels and Lorenz 2019; Narayanan *et al.* 2019; Zhou *et al.* 2019).

Chapter 2 – Soybean Iron Deficiency Chlorosis High-Throughput Phenotyping Using an Unmanned Aircraft System

Chapter 2 of this dissertation was published in the Journal of Plant Methods volume 15 article 97.

Citation:
Dobbels, A.A., Lorenz, A.J. Soybean iron deficiency chlorosis high-throughput phenotyping using an unmanned aircraft system. Plant Methods 15, 97 (2019) doi:10.1186/s13007-019-0478-9. (Dobbels and Lorenz 2019)

Author contributions:
Both authors made significant contributions to this research. AD and AL conceived the research ideas and designed the experiments. AD collected the data, conducted the data analysis and wrote the manuscript. AL edited and revised the manuscript. Both authors read and approved the final manuscript.

Summary

Background:

Iron deficiency chlorosis (IDC) is an abiotic stress in soybean [Glycine max (L.) Merr.] that causes significant yield reductions. Symptoms of IDC include interveinal chlorosis and stunting of the plant. While there are management practices that can overcome these drastic yield losses, the preferred way to manage IDC is growing tolerant soybean varieties. To develop varieties tolerant to IDC, breeders may easily phenotype up to thousands of candidate soybean lines every year for severity of symptoms related to IDC, a task traditionally done with a 1–5 visual rating scale. The visual rating scale is subjective and, because it is time consuming and laborious, can typically only be accomplished once or twice during a growing season.

Results:

The goal of this study was to use an unmanned aircraft system (UAS) to improve field screening for tolerance to soybean IDC. During the summer of 2017, 3386 plots were visually scored for IDC stress on two different dates. In addition, images were captured with a DJI Inspire 1 platform equipped with a modified dual camera system which simultaneously captures digital red, green, blue images as well as red, green, near infrared (NIR) images. A pipeline was created for image capture, orthomosaic generation, processing, and analysis. Plant and soil classification was achieved using unsupervised classification resulting in 95% overall classification accuracy. Within the plant classified canopy, the green, yellow, and brown plant pixels were classified and used as features for random forest and neural network models. Overall, the random forest and neural network models achieved similar misclassification rates and classification accuracy, which ranged

from 68 to 77% across rating dates. All 36 trials in the field were analyzed using a linear model for both visual score and UAS image-based scores on both dates. In 32 of the 36 tests on date 1 and 33 of 36 trials on date 2, the LSD associated with UAS image-based scores was lower than the LSD associated with visual scores, indicating the image-based scores provided more precise measurements of IDC severity.

Conclusions:

Overall, the UAS was able to capture differences in IDC stress and may be used for evaluations of candidate breeding lines in a soybean breeding program. This system was both more efficient and precise than traditional scoring methods.

Introduction

Iron deficiency Chlorosis (IDC) is a major soil borne stress in soybean [Glycine max (L.) Merr.] and causes significant yield reductions. In the United States, soybean IDC has been reported to result in yield losses totaling $260 million annually (Hansen *et al.* 2003; Peiffer *et al.* 2012). Soybean IDC is caused by a lack of available iron [Fe(II)] to the plant (Brown *et al.* 1967; Cianzio *et al.* 1979; Silva and Uchida 2000; Hänsch and Mendel 2009). While iron is abundant in almost all soils, deficiencies are caused by several soil chemical factors and their interactions that change the solubility of iron in the soil (Hansen *et al.* 2003; Rogovska *et al.* 2007). Soybean IDC is impacted by soil pH, soil calcium carbonate content, soil moisture content, soil electrical conductivity, iron oxide concentration, and soluble salts (Inskeep and Bloom 1987; Morris *et al.* 1990; Hansen *et al.* 2003; Franzen and Richardson 2008). Deficiency symptoms include interveinal chlorosis and overall stunting of the plant (Jeong and Connolly 2009; Vasconcelos and Grusak 2014). Soybean growers can overcome the drastic yield penalties of IDC by growing tolerant soybean varieties, planting companion crops, reducing other forms of plant stress, and supplementing the soil with iron chelates (Naeve 2006; Kaiser *et al.* 2011).

The preferred method to minimize yield losses caused by IDC is growing a tolerant variety, which is why there is continued interest in the development of IDC tolerant varieties by soybean breeders (Goos and Johnson 2000; Kaiser *et al.* 2011; Lucena and Hernandez-Apaolaza 2017). To accomplish this breeding objective, thousands of potential soybean varieties need to be screened every year for IDC severity. The screening has traditionally been accomplished using a 1-5 visual severity scoring system where a score of 1 is given to tolerant lines and a score of 5 is given to susceptible

lines (Cianzio *et al.* 1979). The visual rating system is labor intensive and typically only done at one time point in the growing season. In addition, intra-rater variability due to the subjectivity of the human eye can result in less accurate phenotypic measurements, and thus, researchers are investigating image-based methods for quantifying IDC severity (Cianzio *et al.* 1979; Naik *et al.* 2017). New automated rating systems hold potential for more objectivity and reliability for phenotyping IDC stress (Singh *et al.* 2016; Naik *et al.* 2017). To date, these phenotyping methods have been implemented from tripods (Naik *et al.* 2017) and push carts (Bai *et al.* 2018a); however, implementation using an unmanned aircraft system (UAS) has not been reported.

High-throughput phenotyping (HTP) refers to the ability for researchers to collect detailed information during a plant life cycle in a non-invasive way (Dhondt *et al.* 2013; Araus and Cairns 2014). This can be done in both controlled and field environments and with a wide array of platforms and sensors including ground based and aerial systems (Araus and Cairns 2014; Singh *et al.* 2016). In recent years, there has been a growing interest in the utilization of aerial HTP platforms, especially for use in germplasm assessment within breeding programs (Haghighattalab *et al.* 2016). While many traits are currently being measured in soybean using these platforms, including plant maturity, canopy coverage, and yield estimation (Yu *et al.* 2016b; Xavier *et al.* 2017), for example, the main goal of this project was to use an unmanned aircraft system (UAS) to improve plant assessments of soybean iron deficiency chlorosis (IDC). The objective of this research was to use images collected from a UAS to measure IDC severity and determine the accuracy and precision of these predictions.

Materials and Methods

Plant material, location, and field design

A series of 36 trials consisting of breeding lines at different stages in the UMN breeding program, ranging from the advanced yield trial stage to the regional trial and commercial testing stage, was used in this study (Figure 2-1). Breeding lines belonged to maturity groups ranging from 00 to II. Individual trials consisted of breeding lines of similar relative maturity. The number of entries in each trial ranged from 16 to 80. Each plot (experimental unit) was planted as a single row 91cm in length and 76.2cm apart. Plots were arranged in a randomized complete block design with two replications. All plots (a total of 3,824) were planted on June 1, 2017.

The location for this study was a field site near Danvers, MN (45.274285, -95.718046) in Swift County. This field has a history of soybean IDC and has been rotated between corn and soybean for several years. Before planting, soil cores were taken and the soil was confirmed to have a pH in the range of 7.5 to 8.2, a range known to induce iron deficiency in soybeans (Inskeep and Bloom 1987; Hansen *et al.* 2003).

A total of nine ground control points (40cm x 20cm cement pavement blocks painted red) were placed in the field (Figure 1). These were placed randomly throughout the field site location in such a way to cover the entire area of interest and remained in the field for the duration of the season. The ground control point coordinates were collected at one time-point during the summer using a Trimble Handheld GPS unit.

Reflectance calibration panels were also created for use in this project. A total of three calibration targets (2 feet by 2 feet matte boards) were made with each target consisting of four levels of grey – 5%, 20%, 40%, and 55% reflectance painted with ‘black’, ‘iron mountain’ ‘flannel gray,’ and ‘silver bullet,’ and for each % reflectance

respectively (BEHR paint brand, Santa Ana, California). Paint was mixed with a 50/50 mix by weight with barium sulfate to ensure a near Lambertian surface. A total of three layers of paint were used on top of one coat of primer. An ASD (Analytical Spectral Devices) Handheld 2: hand held VNIR spectroradiometer was used to measure the reflectance of the panels with the built-in halogen bulb for source lighting.

IDC ground-based phenotyping

Soybean IDC was rated on July 12 and August 1, 2017, herein referred to as date 1 and date 2 respectively. On date 1, soybeans ranged in vegetative growth stages from V3-V6 and on date 2, soybeans ranged in growth stages from V6-R2. Soybeans were rated on both dates with a 1-5 visual rating scale. With this scale, a rating of "1" indicates a plot that is 100% green (no yellowing), a score of "2" indicates slight yellowing with some plants in the plot turning yellow, a score of "3" indicates moderate yellowing with most plants turning yellow in the plot, a score of "4" indicates intense yellowing where all plants are yellow and some are becoming stunted and necrotic, and a score of "5" indicates most severe IDC symptoms where the entire plot is damaged and dying or completely dead (Cianzio *et al.* 1979; Mamidi *et al.* 2014a). Each plot was measured by an expert rater who understands IDC stress symptoms. This ground-based phenotyping served as the reference data in this study for training and validating models. In addition, 252 plots were scored independently by two trained raters for the assessment of inter-rater variability. These plots were chosen because they displayed variation in IDC severity because of their placement in a part of the field with optimal IDC stress for detecting differences between varieties.

UAS platform, sensor, flight plan

In this study, a pipeline was created from image capture to image analysis. Table 2-1 highlights the major steps in this pipeline including (1) UAS image collection, (2) orthomosaic generation, and (3) image processing. In step 1, aerial data were collected on the same dates as ground based data (July 12 and August 1) with a DJI Inspire 1 equipped with a modified dual camera system, "Sentera Double 4K agricultural" (Sentera Inc, Minneapolis, MN). The images were captured in 12.3 mega-pixel (MP) red (650nm x 70nm width), green (548nm x 45nm width), blue (446nm x 60nm width) and 12.3 MP red (650nm x 70nm width), green (548nm x 45nm width), Near Infrared (NIR, 840nm x 20nm width). Each camera has a 60-degree field of view. The UAS was flown using the autonomous flight mission planning of AgVault software. All missions were conducted at an altitude of 60.96 meters with a UAS speed of 5 meters/second and images captured with 70% end lap and side lap. The resulting images had a ground sampling distance of 1.6 cm. All flights were conducted within two hours of solar noon to limit shadow effects.

Image data processing

After image collection, image orthomosaics were generated using Pix4D Desktop (Pix4D, SA). The WGS 84 datum was used with a projected coordinate system of UTM zone 15N. Images captured by the Sentera dual camera system were uploaded into the same project and given group names of "RGB" and "NIR" for the two sets of images respectively. The default processing options template, "Ag RGB," was used for generating geo-referenced orthomosaics. This option generates mosaics from overlapping nadir images and outputs a full resolution GeoTIFF file and merges tiles. In

addition, the “Ag RGB” processing template has faster processing speed and is compatible with RGB cameras.

Pix4D Processing occurs in three major steps including initial processing; point cloud and mesh; and digital surface model, orthomosaic, and index generation. Nine ground control points were input into the Pix4D project directly following the initial processing step using the ray cloud editor.

In step 3, orthomosaics were processed and data extracted from each plot. Orthomosaics were loaded into Erdas Imagine and unsupervised classification using k-means clustering into five classes was done on an indexed map of the ratio of red and green (R-G)/(R+G). After unsupervised classification, the five classes were manually grouped into the “plant” class and the “soil” class based on human observation of the five classes. The classes were recoded, and a mask was set based on the new classification.

Accuracy assessment of the plant and soil classification was conducted using Erdas Imagine software (Hexagon Geospatial, United States). The accuracy assessment toolkit was used to assign 1,000 points across the field of interest. An equalized random sampling scheme was used to set 500 sampling points of soil and 500 of plant classified pixels. The reference data was created by visually assigning each point as plant or soil based on human interpretation of the non-classified original orthomosaic. Class values were hidden during the reference data collection in order to ensure unbiased values. An error matrix was used to compute the overall accuracy, producer accuracy, and user accuracy. The overall classification accuracy was computed by summing the major diagonal numbers (correctly classified) divided by the sum of all sample units in the entire matrix. The producer accuracy was computed by dividing the total number of

correct sample units in each specific category by the total number of the specific sample units of reference data. The user accuracy was computed by dividing the total number of correct sample units in the specific category by the total number of sample units classified as the specific category.

The masked plant canopy was further classified to green, yellow, and brown plant pixels using an additional k-means clustering step. These features were then extracted using QGIS software (QGIS Geographic Information System. Open Source Geospatial Foundation Project. http://qgis.osgeo.org). In QGIS, a polygon shapefile was created where field plot polygons were used to identify each of the 3,824 plots. The zonal statistics plugin was used to extract the proportion of green, yellow, and brown pixels in each plot.

Two modeling algorithms, neural network and random forest, were used to relate these three features to the ground based visual scores (Breiman 2001). Both algorithms are available in the predictive analytics software package within JMP Pro (JMP®, Pro 10, SAS Institute Inc., Cary, NC, 1989-2007). In both cases, the IDC visual score data was treated as a character and 77% of the data, at random, was used to train the models and 33% of the data, at random, was used for validation. The random forest used 100 trees in the forest with 10 minimum splits per tree. The neural network was run using default settings in JMP software. The hidden layer structure used 3 TanH functions and a learning rate of 0.1. Results are reported in a confusion matrix.

Each of the 36 trials in the field were analyzed using a linear model including the IDC score as the response variable, a fixed effect for entry, a fixed effect for block, and a random residual. The least significant difference (LSD) was calculated by multiplying

the square root of the mean square error from the statistical model by the 0.2 t-value for each test. The LSD was calculated for all 36 tests on ground-based UAS scores for both dates of data collection.

Results and Discussion

Ground-based phenotyping

A total of 3,386 plots were assessed for severity to IDC stress on a 1-5 scale on two separate dates (July 12 and August 1, 2017). The distributions of each of the two dates of data, as well as their relationships, can be seen in Figure 2-2. In total, 15%, 45%, 30%, 9%, and 1% were rated 1-5, respectively, on date 1. On date 2 30%, 41%, 18%, 8%, and 3% were rated 1-5, respectively. In total, there was a much higher abundance of entries given a score of "1" on date 2 as compared to date 1. Nevertheless, the overall average score in the field was 2.1 on both dates of visual scoring. The comparison between raters was also investigated on a subset of 252 plots. For these plots, two people independently scored the plots to provide an estimate of inter rater variability in visual scores. The correlation between rater 1 and rater 2 was 0.93.

UAS imagery for IDC phenotyping

In the first step of the image analysis pipeline, plant canopy was masked from the soil using k-means clustering (Figure 2-3), an unsupervised machine learning approach that has been successfully used in many agriculture applications (Bauckhage and Kersting 2013; Wahabzada *et al.* 2015). This approach resulted in an overall classification accuracy of greater than 95%. The user accuracy was 94% and 97% for soil and plant classification, respectively. Table 2-2 is a confusion matrix highlighting the results of the accuracy assessment of this classification.

Previous studies have utilized a variety of techniques to mask plant canopies. In a publication by Yu *et al.* 2016, for example, plant and soil classification was achieved using a random forest model and resulted in an accuracy of 99.9% (Yu *et al.* 2016b). The results here had an accuracy of 95.6%, however, plants under chlorosis or necrosis stress result in spectral properties very similar to that of the soil background. In addition, many misclassification errors occurred at the edges of the canopy where soil and plant canopy pixels were overlapping. One advantage of this study, however, is the ability to classify plant and soil without training data. The unsupervised classification approach using k-means clustering resulted in pixels with similar spectral values being clustered together. This clustering occurs with no former knowledge or input, and can often provide new insights into the data (Singh *et al.* 2016). With supervised approaches such as the random forest, a training data set must be generated by manually interpreting the classes pixels belong to. Other studies have used thresholding approaches to differentiate plants from soil. In these scenarios, the image is often thresholded based on the hue, saturation, value format of the image or based on indices or ratios of different color bands (Karcher and Richardson 2005; Naik *et al.* 2017; Xavier *et al.* 2017).

The percent green, yellow, and brown pixels were also classified using a similar approach as the plant canopy classification (Figure 2-3). These features were used in two different machine learning models (random forest and neural network) to predict IDC severity scores. The confusion matrices for the random forest models for date 1 and date 2 are shown in Tables 2-3 and 2-4 for date 1 and date 2, respectively. Overall, the classification accuracy was 68% for date 1 and 77% for date 2. The increase in

classification accuracy between date 1 and date 2 is likely the result of the size of the plants, with more pixels representing plant material at date 2 than at date 1.

The average canopy coverage of each plot can indicate the overall biomass and light interception of the plots. Canopy coverage was thus calculated as the ratio of "plant classified pixels" to "soil plus plant classified pixels" and compared across the five different severity classes. The average canopy coverage for each IDC class was as follows: class 1 = 0.264, class 2 = 0.246, class 3 = 0.189, class 4 = 0.096, and class 5 = 0.039. Each of these levels was considered significantly different from each other class at the 0.05 probability level using Tukey's honest significant difference, indicating the IDC score explained variation in plot biomass.

UAS imagery is a reliable measure for detecting differences among entries

Another method to test the suitability of the UAS scores is to test if the scores can differentiate between entries in the field. A common procedure for this assessment is to calculate the LSD for comparing performances of breeding lines in typical randomized field trials. For reporting of variety trials, a relaxed significance threshold (e.g., $P < 0.20$) is commonly used for declaring differences among varieties to increase power and reduce type II errors. Based on this, if the LSD is low, the precision of the data is higher, and the researcher is better able determine differences among breeding lines. The LSD values from the ground-based data and the UAS data were compared among the 36 experimental trials, or sets of lines, for both dates of data collection. In 32 of the 36 trials on date 1 and 33 of 36 trials on date 2, the LSD was smaller when using the UAS IDC scores in the linear model compared to the visual scores (Figure 2-4). There was an average 0.15- and 0.20-point reduction in LSD (ranging from 0.35 increase to a 0.50 decrease) with UAS

scores compared to the visual scores for date 1 and date 2 respectively. This reduction in LSD indicates that the UAS data is more precise than visual scores and offers appropriate information for use in a breeding program.

Many previous studies have shown great success and accuracy in collecting phenotypic traits from unmanned aircraft systems both in soybeans and in other crops (Haghighattalab *et al.* 2016; Holman *et al.* 2016; Neely *et al.* 2016; Yu *et al.* 2016b). In addition, previous studies have successfully used image-based methods for classifying and quantifying soybean IDC stress (Naik *et al.* 2017; Zhang *et al.* 2017b). However, to date, no study has demonstrated combining the powers of high-throughput image collection from unmanned aircraft systems with image-based classification for IDC.

UAS imagery compared to other methods for IDC assessment and limitations

Previous studies have tested the use of image analysis procedures to quantify IDC stress (Singh *et al.* 2016; Naik *et al.* 2017; Bai *et al.* 2018a). Their approaches achieved a mean per class accuracy of ~96% and 81%. While the previous studies showed relatively high accuracy, the throughput of taking photos from a tripod or pushcart is much lower in comparison to a UAS. Spatial resolution achieved, however, was much higher (6 pixels/mm from tripod compared to 1.6cm/pixel from the UAS). This decrease in spatial resolution resulted in blending of pixels and thus less resolution to depict subtle changes of individual leaves becoming chlorotic.

For this study, a flight path was chosen to cover a large area within one UAS battery life, and to limit variation in sun positioning and cloud shadows during flight, as these variables are known to present problems with image analysis applications. Future research should be done to test if an increase in spatial resolution through improved

camera sensors or lower flight altitudes would improve predictive abilities. Care should be taken to ensure that flights conducted limit shadowing caused by soybean plots by flying near solar noon, and that the cloud cover during flights be consistent – full cloud cover or no cloud cover is optimum. The system presented in this paper reduced flight time by flying at a higher altitude and will allow researchers to achieve a much higher temporal assessment of IDC severity as well as the ability to rate more plots in any given growing season.

Additionally, the confusion matrices show that many of the misclassified scores are mostly between nearby classes. If a breeder simply wishes to select against scores of 4 or 5, for example, the UAS image-based scores would be very adequate for breeding purposes. To test this, scores of 4 and 5 were binned together as "high stress" and scores of 1, 2, and 3 were binned together as "low stress." The overall accuracy of the random forest model in correctly placing the entries into these two categories was 89%.

A final caution that researchers should consider in employing UAS imagery for IDC detection is that other soybean stresses or field variables may mimic IDC symptoms detected by image analyses. One major biotic factor to soybean production, for example, is soybean cyst nematode. Research plots may experience stunting and chlorosis from nematode presence, which could be rated as IDC susceptible using this system. In addition, healthy weeds in the field would be detected by this system as healthy vegetation, and thus, healthy plots. These cautions were addressed by site selection with limited known off-target stressors and by proper weed control prior to all UAS flights, and should be considered by researchers wishing to employ this technology.

Conclusions

In this study, we achieved high efficiency in collecting data with autonomous UAS flights, greater than 77% accuracy in classifying plots on a 1-5 severity scale, and confidence in this system for IDC assessment through an average reduction in LSD values across a series of experimental trials. This method is high-throughput, objective, and more precise than traditional ground based visual assessments. In addition, it allows researchers to collect information from more plots in a given year and at a much higher temporal frequency than before.

Tables and Figures

Table 2-1. Pipeline for image capture and analysis for iron deficiency chlorosis assessment. The flight path is set up in Pix4D capture with 70% overlap of images. Individual photos are orthomosaiced in Pix4D and K-means clustering is used to mask the plants from the soil background. An additional classification of green, yellow, and brown pixels is performed on the plant objects. In QGIS, plots are defined, and the proportions of green, yellow, and brown pixels are extracted from each plot. Finally, predictions are made to correlate these three features with ground based visual score estimates rated on a one through 5 scoring system.

Category:	Step:	Details:
UAS image collection	Set up UAS	DJI Inspire 1 with Sentera Double 4K sensor
	Prepare flight path	AgVault mobile app or Pix4D capture app
	Fly UAS for data collection	70% image overlap, 61m altitude
Image Orthomosaic using Pix4D	Initial Processing	Key points extraction and matching, camera model optimization, geolocation
	Point Cloud and Mesh	Point densification and 3D textured mesh creation, insert ground control points
	Digital surface model, Orthomosaic, and index	Creation of digital surface model, Orthomosaic, reflectance map, and index map
Image Processing	Plant and soil classification	K-means clustering and recode to plant and soil
	Green, yellow, brown pixel classification	K-means clustering on masked canopy and recode to green, yellow, brown
	Neural Network/Random Forest with ground data	Subset into training and validation sets, ground based data is response variable and green, yellow, brown pixel counts are used as features

Table 2-2. Accuracy Assessment of pixel-based classification method for plant and soil classification. One thousand random points were generated and placed on the orthomosaiced image using the equalized random sampling method. The predicted data was generated from k-means clustering and the reference data was manually created using visual observations of the images. Accuracy assessment results were generated using ERDAS IMAGINE software. An overall classification of 95.6% was achieved

		Reference data			
		Soil	Plant	Row Total	User accuracy (%)
	Soil	**469**	31	500	93.8
Predicted	Plant	13	**487**	500	97.4
data	Column Total	482	518	1,000	
	Producer accuracy (%)	97.3	94.0		
Overall accuracy (%) = 95.6					

Table 2-3. Random forest confusion matrix for date 1 of data collection (July 12). The % green, % yellow, and % brown pixels from each of the research plots were used as features in a random forest model. This confusion matrix shows how well the random forest model predicted the iron deficiency chlorosis (IDC) score from ground-based reference data where each plot was rated on a one through five scale. The overall accuracy was 68%.

		Reference data				
		1	2	3	4	5
Predicted data	1	**76.4%**	22.8%	0%	0.8%	0%
	2	14.3%	**68.2%**	16.1%	1.2%	0.2%
	3	0.8%	19.2%	**65.3%**	14.7%	0%
	4	0%	3.9%	19.7%	**61.9%**	14.5%
	5	0%	0%	0%	100%	**0%**
Overall accuracy (%) = 68%						

Table 2-4. Random forest confusion matrix for date 2 of data collection (August 1). The % green, % yellow, and % brown pixels from each of the research plots were used as features in a random forest model. This confusion matrix shows how well the random forest model predicted the iron deficiency chlorosis (IDC) score from ground-based reference data where each plot was rated on a one through five scale. The overall accuracy was 77%.

		Reference data				
		1	2	3	4	5
Predicted data	1	**85.1%**	14.9%	0%	0%	0%
	2	10.4%	**79.6%**	9.3%	0.5%	0.2%
	3	0.2%	13%	**74%**	12%	0.8%
	4	0%	0.6%	9.9%	**73.6%**	15.9%
	5	0%	0%	3.1%	18.4%	**78.5%**
Overall accuracy (%) = 77%						

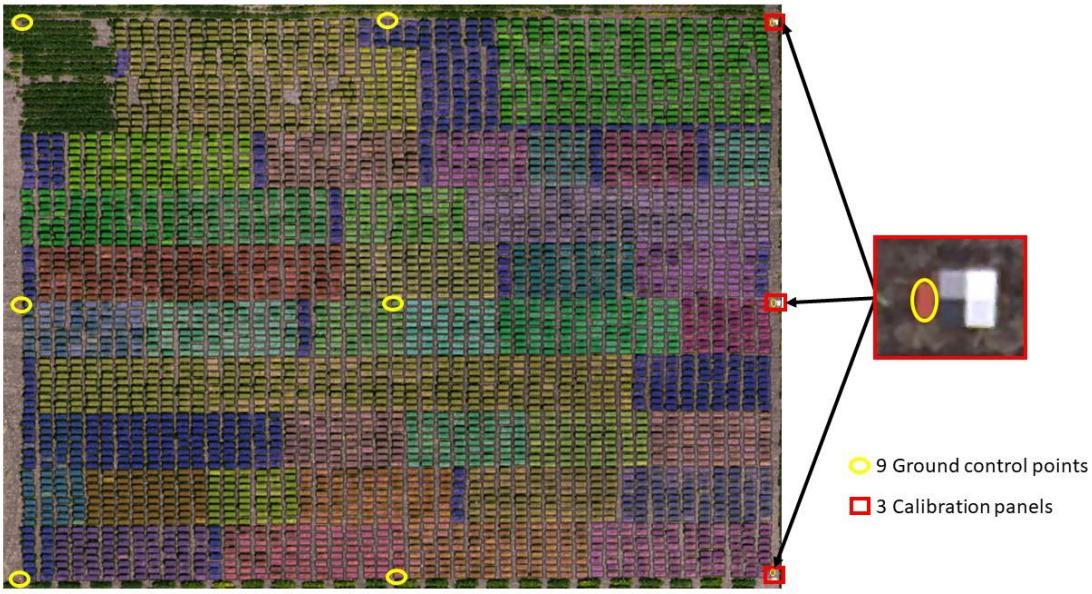

Figure 2-1. Soybean iron deficiency chlorosis testing field site location near Danvers, MN. The field used in this study is located in Six Grove Township, MN (45.274285, -95.718046) in Swift County. The yellow circles highlight the nine ground control points in the field for geometric calibration and the red squares highlight the radiometric calibration panels. These panels were painted with four levels of grey for empirical line method calibration. Overlaid to the field orthomosaic is a vector file delineating the plot boundaries of 3,386 soybean plots. Each plot boundary is colored based on the trial each plot belongs to. A total of 36 trials was grown.

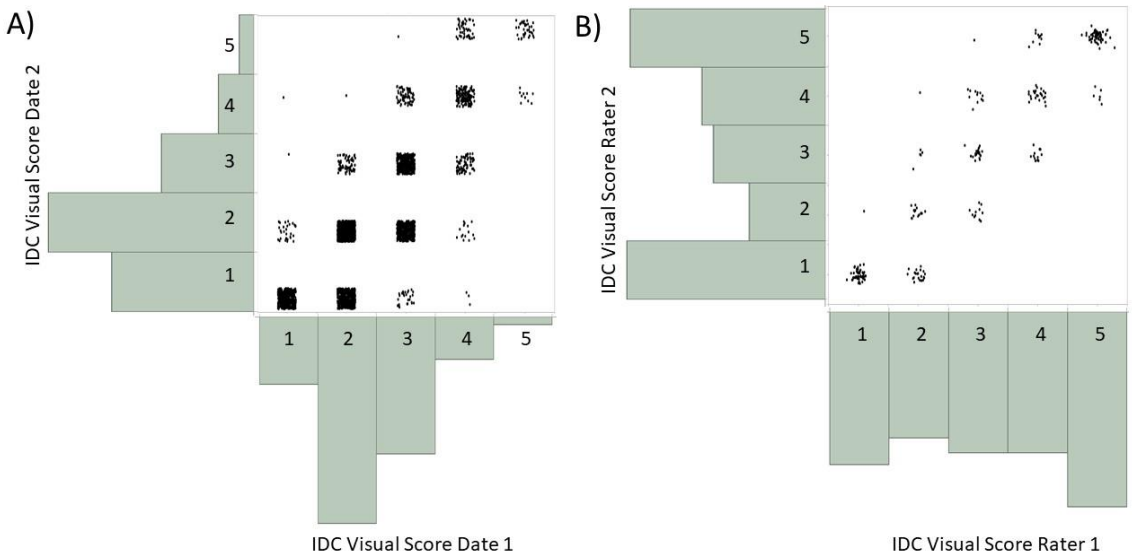

Figure 2-2. Relationships between two dates of iron deficiency chlorosis (IDC) severity (A) and two separate raters scoring plots (B). IDC severity was measured on a total of 3,386 plots on both July 12 and August 01. The correlation of ratings between date 1 and date 2 was found to be 0.80. A subset of 252 plots were measured by two independent raters on date 1. The correlation of ratings between raters was found to be 0.93.

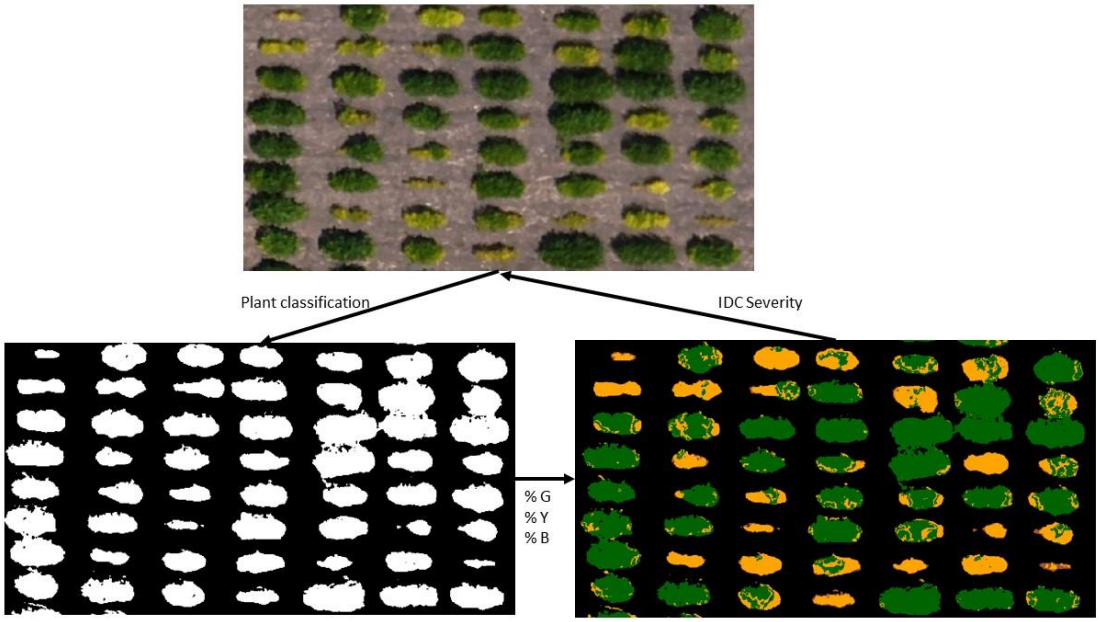

Figure 2-3. Iron deficiency chlorosis classification. The Orthomosaic (top) is first classified into plant and soil pixels (bottom left). The plant pixels are then classified in a second step to green pixels (%G), yellow pixels (%Y), and brown pixels (%B) (bottom right). These features are then related back to ground-based visual scores through random forest and neural network models to classify tolerant and susceptible plots.

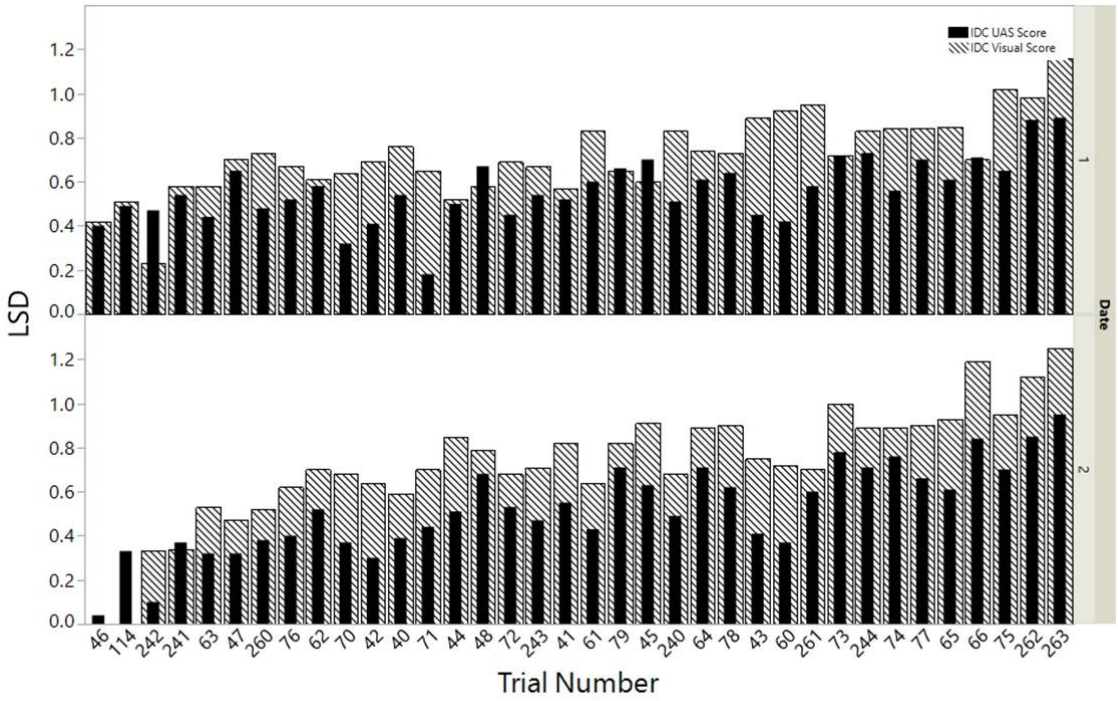

Figure 2-4. A total of 36 trials consisting of soybean breeding lines, each arranged in a randomized complete block design in the field, were analyzed using a linear model for both visual score and unmanned aircraft system (UAS) predicted values on both dates (July 12 and August 01). Bars indicate the least significant difference (LSD) values to separate mean scores of breeding lines for each trial in the field. In 31 of the 36 trials on date 1 (top) and 33 of 36 trials on date 2 (bottom), the LSD was decreased when using the UAS predicted IDC scores (black inside bars in the linear model compared to the visual scores (dashed outside bars).

Chapter 3 - Soybean cyst nematode and iron deficiency chlorosis do not interact to reduce seed yield

Chapter 3 of this dissertation is prepared for the Agronomy Journal

Citation:
Dobbels, A.A., Guimera, V.L., Lorenz, A.J. Naeve, S.L., Soybean cyst nematode and iron deficiency chlorosis do not interact to reduce seed yield, in preparation

Summary

Soybean cyst nematode (SCN) and iron deficiency chlorosis (IDC) are major yield limiting factors to soybean production. In the case of SCN, the nematodes reduce yield by penetrating and feeding on the roots and robbing the plant of energy, whereas with IDC the plants cannot take up what iron is in the soil. Both IDC and SCN are difficult to manage, dynamic, are likely acting together in the field, and a better understanding of their interaction would allow for a more comprehensive management plan for farmers with IDC and SCN stress. The goals of this study were to quantify in season plant stress using remote sensing tools and investigate how IDC and SCN stress interact to impact yield and SCN reproduction. In 2017, 2018, and 2019 a total of nine fields were identified that had documented histories of both IDC and SCN. A range of treatments were added to change the levels of IDC and SCN stress in a randomized complete block factorial design. Results from this three-year study showed that the treatments independently created IDC and SCN severity symptoms and associated differences in normalized difference vegetation index data and yield. Nematode reproduction was significantly impacted by varietal resistance and was not impacted by IDC treatment. An interaction between IDC and SCN treatments was not found for yield, nematode reproduction, or severity symptoms suggesting these stresses act additively.

Introduction

Soybean cyst nematode (SCN, Heterodera glycines Ichinohe) and iron deficiency chlorosis (IDC) are two soil-borne stresses that have a major economic impact on soybean production [Glycine max (L.) Merr.](Clark 1982; Hansen *et al.* 2003; Peiffer *et al.* 2012). Soybean cyst nematode is widely distributed among major soybean growing regions and is the number one yield limiting pathogen of soybean in the United States (Tylka and Marett 2014; Allen *et al.* 2017). In addition to SCN, IDC impacts approximately 1.8 million hectares in the United States (Hansen *et al.* 2003). In the case of SCN, the nematodes penetrate and feed on the roots causing the roots as well as above-ground plant parts to become dwarfed and stunted, or in some cases reducing seed yield without showing aboveground symptoms (Wang *et al.* 2003). On the other hand, IDC is caused by a lack of available iron [Fe(II)] to the plant. While iron is abundant in almost all soils, deficiencies are caused by several factors and their interactions that change the solubility of iron in the soil (Brown *et al.* 1967; Cianzio and Fehr 1980; Silva and Uchida 2000; Hänsch and Mendel 2009).

Management practices for reducing the yield limiting effects of IDC and SCN have been studied previously. Options for managing IDC include growing tolerant soybean cultivars, planting companion crops, reducing other forms of plant stress, and supplementing the soil with iron chelates (Naeve 2006; Kaiser *et al.* 2011). The best option for managing IDC is to grow a tolerant soybean cultivar (Goos and Johnson 2001; Kaiser *et al.* 2014; Chatterjee *et al.* 2017; Martín-Fernández *et al.* 2017). For managing SCN, resistant cultivars with genetic resistant sources including PI 88788 and PI 548402 (often referred to as ‘Peking’) have been widely grown. (Ross and Brim 1957; Concibido

et al. 1997; Chen *et al.* 2001; Zheng *et al.* 2006; Niblack *et al.* 2008; Tylka and Marett 2014; Gardner *et al.* 2017; McCarville *et al.* 2017). Fungicide products with the active ingredient 'fluopyram' have also been studied with variable results on their effect on nematode reproduction and yield (Bissonnette *et al.* 2020).

Identifying IDC or SCN areas within a field is the first step for providing management recommendations. While SCN is present in most fields, the lack of visible symptoms in some cases can make it challenging for producers to know which parts of their fields are infested (Wang *et al.* 2003). Symptoms of IDC also vary spatially within a field and identifying the problematic areas can be laborious. Currently, soil sampling is the recommended approach to determine the presence and density of nematodes and to identify the soil chemical properties associated with IDC (Nutter *et al.* 2002; Naeve and Rehm 2006). Remote sensing offers a method to diagnose and quantify problematic areas with high spatial resolution. Such high spatial resolution of diagnosing problematic areas is an invaluable resource for producers to deploy specific crop management solutions. Detecting both IDC and SCN stress has been reported previously, however, more research is needed to determine how these tools can be used to quantify stress and estimate yield losses for applications in precision agriculture (Nutter *et al.* 2002; Bai *et al.* 2018b; Dobbels and Lorenz 2019).

Studies have shown that IDC and SCN are co-occurring in farmer's fields. One major feature to this phenomena is that high soil pH makes both iron unavailable and increases nematode reproduction (Duggan 1963; Francl 1993; Hansen *et al.* 2004; Rogovska 2006; Rogovska *et al.* 2007, 2009; Pederson *et al.* 2010; Melakeberhan *et al.* 2013; Vasconcelos and Grusak 2014; Assefa *et al.* 2020a). In addition, previous reports

have shown that nematodes are present in all major soybean production regions (Tylka and Marett 2014). The fact that IDC and SCN coexist makes research, breeding efforts, and management recommendations more complicated; and a better understanding of their interaction will help farmers and researchers develop more comprehensive management plans.

Previous research has been conducted to test a range of genotypes resistant and susceptible to both SCN and IDC in a factorial arrangement (Chen *et al.* 2007). In that study, Chen et al. studied the effects of genetic resistance to both SCN and IDC and the corresponding influence on yield, nematode reproduction, and chlorosis symptoms. They found that having resistance to SCN reduced symptoms of IDC, IDC resistance increased SCN reproduction, and resistance to either SCN or IDC increased soybean yield, thus indicating an interaction between these two stressors. It was recommended based on these findings that SCN and IDC management be site specific, but SCN resistance would be preferred if both problems exist in a given field. A major limitation to previous findings was that the treatments were limited to cultivars with varying levels of IDC tolerance and SCN resistance. The previous study did not have gradients of nematode populations or gradients of soil conditions for IDC at each field site, due to difficulty in finding such sites (Chen *et al.* 2007). However, IDC can be induced by adding urea to the soil and IDC can be reduced by adding iron chelates to the soil (Bloom *et al.* 2011b; Gamble *et al.* 2014).

Many factors will alter the levels of both IDC and SCN in a given environment. Management practices determined by the grower such as the decision of what cultivar to plant, what nutrients to apply, planting population, etc. can alter the yield potential in

each field. The objectives of this study, therefore, were to alter IDC and SCN stress in a factorial combination to i) quantify in season plant stress using remote sensing tools and ii) investigate how IDC and SCN stress interact to impact yield and SCN reproduction.

Materials and Methods

Research environments

On-farm experiments were conducted in western Minnesota at three locations per year in 2017, 2018, and 2019 within the counties of Redwood, Swift, Renville, Chippewa, and Yellow Medicine (Table 3-1). Locations were determined based on previous IDC and SCN pressure provided by farmer cooperators and available satellite and soil sampling data. The term environment, herein, refers to a geographically unique environment by year combination, numbered 1-9. Environments 1-3, 4-6, and 6-9 refer to environments in 2017, 2018, and 2019 respectively.

Composite soil samples (0-15cm) were collected prior to planting at each of the locations for common soil chemical factors. Samples were oven oven-dried at 40˚C and analyzed at the research analytical laboratory of the University of Minnesota. Samples were analyzed for available nutrients (K, Mn, Zn, Cu, Fe), soil electrical conductivity (EC), pH, calcium carbonate equivalent (CCE), Olsen-P, and organic matter (OM) according to the Recommended Chemical Soil Test Procedures for the North Central Region (1988). In addition, composite soil samples were collected in each block of the field for nematode egg counts and an *Heterodera glycines* (HG) type test of the nematode populations present in the field according to previously developed procedures (Riggs and Schmitt 1988; Niblack *et al.* 2002). Research plots were planted with a precision research planter when conditions were suitable in either late May or early June for each environment (Table 3-1). Cultivars were seeded in four-row plots 7.9 meters in length

with a 76 cm spacing between each row. The soybeans were planted at 407,407 seeds per hectare.

Weather data including average daily temperatures and accumulated rainfall was gathered from High Plains Regional Climate Center (HPRCC, Lincoln, NE, https://hprcc.unl.edu/). Average daily temperature was plotted by year and accumulated rainfall was plotted by individual environments. Rainfall data is displayed as total rainfall for each month during the growing season.

Experimental treatments and design

Treatments were designed to create a range in both IDC stress and SCN damage so that the main and interaction effects of these two stresses could be studied. Twenty-four treatment combinations were arranged based on a factorial combination of "IDC tolerance, (2 levels)" "SCN resistance, (4 levels)" and "IDC application (3 levels) (Supplemental table 3-1)." Six commercial soybean cultivars, 'S14-J7,' 'PB-1611R2,' 'AG1733,' 'AG14X7,' '7169,' '7186,' were specifically chosen based on both IDC tolerance and SCN resistance as well as having similar maturity group ranges. A description of each cultivar including IDC tolerance rated on a "1-9" scale according to the seed company, IDC tolerance category (tolerant or susceptible), source of resistance to SCN ('Peking', 'PI 88788', Susceptible), and relative maturity can be found in Table 3-1.

Soybean cyst nematode treatments include three levels of SCN varietal resistance including Peking, PI 88788, and Susceptible. In addition, a fourth treatment was included by adding a fungicide (active ingredient, fluopyram) to the Peking sources of resistance with the goal of completely eliminating SCN pressure. Fluopyram was

supplied as Velum Prime (Bayer Crop Science, St. Louis, Missouri) at 0.5 L/ha (0.25 kg Fluopyram/ha) in furrow during planting.

The IDC application treatments were introduced to create a range in IDC stress conditions. It has been shown that NO_{3-} is a causative factor in IDC stress and that iron chelates can remove chlorosis symptoms (Bloom *et al.* 2011a; Gamble *et al.* 2014). These treatments were applied on the furrow directly following planting. Fertilizer nitrogen was supplied as granular urea CH_4N_2O (46–0-0) (Loveland Products, Inc., CO) at 222.2 kg urea/ha (102.2 kg N/ha), ortho-ortho Fe EDDHA was supplied as liquid Soygreen® (West Central, INC, Wilmar, MN) at 3.73 L/ha (0.08 kg chelated iron/ha), and fluopyram was supplied as Velum Prime (Bayer Crop Science, St. Louis, Missouri) at 0.5 L/ha (0.25 kg Fluopyram/ha).

The experimental design for this study was a randomized complete block design with four replications in each environment. A full table of the 24 treatment combinations can be found in supplemental table 3-1.

Data collection

Normalized difference vegetation index (NDVI) measurements were collected on plots every week during the growing season in each environment. The measurements were collected using an active sensor on the ground and NDVI collected from an unmanned aircraft system (UAS).

Ground based NDVI was collected from the second row of each plot using a Crop Circle, model ACS-430 (Holland Scientific, Lincoln, NE). The Crop Circle was run approximately one meter above the canopy to collect approximately 50 spectral

measurements per plot. The individual spectral measurements were averaged for further analysis.

An unmanned aircraft system (UAS) was flown to collect passively sensed NDVI data. A similar platform and data analysis pipeline was used as previously reported (Dobbels and Lorenz 2019). Briefly, flights were conducted using an Inspire 1 UAS equipped with a modified dual camera system (Sentera Double 4K sensor, Sentera, MN) which allowed for the capture of red (R), green (G), blue (B) images along with a second camera modified to capture R, G, near-infrared (NIR) images. Flights were conducted at a 61-meter altitude at a UAS flight speed of 5 m/s. Resulting images had a 1.6 cm ground sample distance. Four ground control points (GCPs) were placed in the corners of each field for geometric calibration, with the known location of each GCP collected with a handheld Garmin device (Garmin eTrex® 20x, Garmin, Lenexa, KS). Orthomosaics were generated for each flight mission using Pix4D desktop (Pix4D, SA). A template provided by the camera manufacturer was used to calculate NDVI values correcting for the quantum efficiency of the sensor. With this sensor, the true red radiance is equal to 0.706*(R – B) and the NIR radiance is equal to the imager blue. The NDVI was then calculated using the final equation: NDVI = (1.706*B - 0.706*R) / (0.294*B + 0.706*R). A shape file was generated to delineate the center two rows of every four-row plot using QGIS. The average NDVI value of every plot was extracted using the zonal statistics plugin of QGIS.

Visual IDC ratings were collected weekly from the center two rows of every plot by an experienced rater who understands IDC conditions according to Supplemental Figure 1. With this scale, a score of one is given to plots showing no signs of yellowing, a score

of two is given to plots with slight yellowing, a score of three is given to plots with moderate yellowing, a score of four is given to plots with intense yellowing and some necrosis, and a score of five is given to plots with severe necrosis and some plant death.

Yield was collected by harvesting the center two rows of each plot with a small-plot combine and adjusted for 13% moisture (Spc 20 in 2017/2018 and Spc40 in 2019, Almaco, Nevada, IA). Grain mass and moisture content were recorded in-field, and a 500-gram subsample was retained for compositional analysis. Protein and oil were analyzed using near-infrared (NIR) spectroscopy at the University of Minnesota NIR Spectroscopy Laboratory (St. Paul, MN) using a Perten DA7200 diode array instrument (Huddinge, Sweden) equipped with calibration equations developed by Perten in cooperation with the University of Minnesota.

Soil sampling for SCN was conducted both at the beginning of the season and at the end of the season to determine the reproduction factor (RF) on each plot, as well as the sample HG type. Prior to planting, a composite soil sample made up of at least 100 cores was collected from each of the four blocks in each environment. At harvest, composite soil samples consisting of ten cores each were collected from the center two rows of every four-row plot in each environment. Soybean cyst nematode egg counts were conducted at the Nematology Lab at the University of Minnesota Southern Research and Outreach Center in Waseca, MN. The RF was calculated by dividing the final SCN eggs/100cc soil by the initial SCN egg/100cc soil. A partial HG test was conducted by calculating the female index (FI) on three differentials [PI 88788, PI 548402 (Peking), and Williams 82 (susceptible)] in a lab test by dividing the mean number of females that developed on each indicator line by the mean number of females on the susceptible check

and multiplied by 100 (Niblack *et al.* 2002). Soil for the partial HG test was collected in the spring of each year from each site.

Data analysis

In season traits of UAS-based NDVI, Crop Circle NDVI, and visual scores were compared to final grain yield using Pearson correlations. Pearson correlations were computed at each time point of data collection for each of the nine environments. The remotely sensed data collected on date seven, final grain yield, and nematode reproduction factor were analyzed for treatment effects. The restricted maximum likelihood (REML) mixed model analysis was performed using JMP PRO version 14.0.0 (SAS Institute Inc., Cary, NC). Analysis of variance (ANOVA) was used to test the fixed effects of the factorial arrangements of IDC treatment, IDC genotype, and SCN resistance level and their corresponding two and three-way interactions. All models included the random effect of block. Environment was first considered a fixed effect in the model to test for variation among sites. Due to a significant treatment by environment interaction and variation across environments, a separate analysis was performed within each environment to test for treatment effects. The three-way interaction term was not significant, and was thus excluded from the model to help evaluate the hypothesis of other fixed effects. Means for all response variables were separated using Fisher's LSD at $p \leq 0.05$. Tukey's honest significant difference was used as a post-hoc test for comparing group means where a significant difference was found. All letters not connected by the same letter were considered statistically different with a p-value less than 0.05.

Results

Research environments

Soil sampling was conducted prior to planting to confirm the presence of SCN eggs, determine SCN HG type, and to measure soil chemical properties in each of the nine environments. Table 3-1 summarizes the research environments in terms of location, soil type, soil chemical properties, initial soybean cyst nematode counts, and HG type test results including the female index on both Peking and PI 88788 indicator lines. While sites with high levels of IDC and large populations of SCN were targeted, there was a range in average yield and nematode reproduction factor (RF) across the nine environments (Figure 3-1a).

Across the nine environments sampled, soil pH averaged 7.6 (range 7.1 – 7.9), calcium carbonate equivalent (CCE) averaged 10% (range 7.5 – 14.3%), EC averaged 1.02 mmhos/cm (range 0.5- 1.38mmhos/cm), and abundance of DTPA-iron averaged 22.3 mg/ kg soil (range 7.8 – 35.3 mg/kg soil). A range of initial SCN egg densities at planting, SCN reproduction, as well as lab test results for HG-type testing were collected and reported (Table 3-1). The average SCN egg density at planting was 1,885 eggs/100cc soil (range 422 - 4,753 eggs/100cc soil). The female index (FI) on indicator line PI 88788 from the in lab test averaged 19.1 (range 6.3 – 58.5) and the FI on indicator line Peking averaged 4.2 (range 0.6 – 14.8). The average RF in the field from the nine environments was 4.3 (range 1.0 – 11.5).

Research environments were monitored for rainfall and temperature. The temperature trends were consistent within a year, while the rainfall was location dependent within a given year (Figure 3-2). Total rainfall accumulation during the

growing season averaged 65.3cm (range 53.7 – 98.3 cm) across the nine environments. All environments had similar trends in terms of average daily temperature (Figure 3-2).

In season field evaluation of plant stress

Data was collected approximately weekly for ten weeks during the growing season of each environment using three different methods including visual severity scores, crop circle NDVI, and NDVI collected from a UAS. Pairwise correlations were performed between yield and data collected from each of these three methods at each of the ten dates of data collection (Figure 3-3). Environment three was excluded from this analysis due to insufficient data collection. Pearson correlation to yield averaged 0.72 for UAS, 0.57 for crop circle, and 0.59 for visual score, on average, across all 9 environments and all 10 dates of data collection. The UAS-NDVI measurements provided the highest correlation to yield, on average, across all dates of data collection.

Previous studies have been conducted to test corresponding yield responses to changes in visual score data (Froechlich and Fehr 1981). In previous reports, it was determined that for every one point increase in IDC severity score, there was an average 20% yield loss. To examine this in our study, the slope coefficient of the linear regression model between visual score and yield was computed. On average across all dates of data collection and all environments, it was determined that for every one point increase in IDC score, there was a 569.1 kg/ha seed yield loss at harvest (range 9kg/ha – 1195 kg/ha). Supplemental table 3-2 shows the slope coefficients for all nine environments for each date of data collection.

Treatment effects on NDVI, yield, and nematode reproduction

Analysis of variance (ANOVA) was used to test the fixed effects of the factorial arrangements of IDC treatment, IDC tolerance, and SCN resistance level and their corresponding two and three-way interactions (Tables 3-3 to 3-5). For UAS-based NDVI, the main effect of IDC treatment (urea, control, Soygreen) was significant in seven of the nine environments; the main effect of SCN resistance (Peking + fluopyram, Peking, PI 88788, susceptible) was significant in one of the nine environments; and the main effect of IDC tolerance (tolerant vs. susceptible) was significant in three of the nine environments. When averaged across all sites, all three main effects had a significant effect on NDVI (Table 3-3). There were no observed significant interactions between IDC treatment and SCN treatment on UAS-based NDVI.

For yield, the main effect of IDC treatment was significant in six of the nine environments; the main effect of SCN resistance was significant in five of the nine environments; and the main effect of IDC tolerance (tolerant vs. susceptible) was significant in three of the nine environments (Table 3-4). When averaged across all environments, all three main effects were significant (Table 3-4, figure 3-1b and 3-1c). A post-hoc test was performed to test mean differences for the IDC application treatments of urea, control, and iron chelates (Table 3-4). Overall, the application of treatments on the furrow at planting successfully created a range in symptoms and seed yield.

Cultivars with varying levels of IDC tolerance were tested in this study in addition to the application treatments of urea and Soygreen (Figure 3-5). The main effect of IDC genetic tolerance on NDVI and yield was significant in three of the nine environments (Tables 3-3 and 3-4). The interaction between IDC tolerance and IDC

application treatment was significant for yield in environments 6,7 and 9 (Table 3-3 and 3-4).

The SCN source of resistance had a significant effect on NDVI in only one environment, but this effect was not significant on average across the range of environments tested (Table 3-3). The SCN source of resistance had a significant effect on yield in five environments, and on average across the range of environments (Table 3-4, Figure 3-6). However, nematode reproduction was significant in all nine environments (Figure 3-5). In three of the five environments, there was a significant effect of yield without showing differences in NDVI values. In four of the nine environments, a significant difference was found for nematode reproduction with no significant difference in yield. In all nine environments, the application of the active ingredient fluopyram, had no significant improvement on yield or nematode reproduction when added on top of the Peking source of resistance. However, there is no evidence in this study to support if that same application of fluopyram would alter levels when applied to a susceptible or PI 88788 source of resistance.

IDC treatments and SCN resistance interactions

A main objective of this study was to test for an interaction between IDC and SCN treatments. In the range of nine environments tested, no interaction was found between these two treatments for NDVI, yield, or nematode reproduction (Tables 3-3, 3-4, 3-5, Figure 3-8). Based on this finding, the two stresses appear to act independently to alter yield and nematode reproduction. In other words, the nematodes reproduce on SCN susceptible soybean plots regardless of the amount of IDC stress occurring on said plots

(Table 3-5). In fact, heavily IDC-stressed soybean plants that are yellow, stunted, and produce low yields will actually support high levels of nematode reproduction.

Discussion

Research environments

Soybean IDC is associated with soil pH, carbonates, ionic strength in the soil measured using electrical conductivity (EC), abundance of extractable iron, soluble salts, and water content (Jessen *et al.* 1988; Silva and Uchida 2000; Hansen *et al.* 2003; Naeve and Rehm 2006). Based on the soil analysis results, we expected and observed moderate to high IDC symptoms in all environments excluding environment three (Hansen *et al.* 2003; Naeve and Rehm 2006). Compared to all other environments, environment three had the lowest soil pH (7.1), the lowest EC value (0.5 mmhos/cm), and the highest amount of plant available iron (35.3 mg/kg soil). Our results confirmed the presence of IDC at all sites and a lack of IDC stress at environment 3 (Table 3-3 and 3-4).

An increased amount of NO_{3-} in the soil has been shown to be associated with an increased level of IDC (Bloom *et al.* 2011b; Kaiser *et al.* 2011). When the soybean plant uptakes NO_{3-} from the soil, it does this in exchange for a bicarbonate ion, which buffers soil pH changes. Bloom et al. (2011) showed that the addition of Fertilizer N, supplied as urea (46–0-0) significantly decreased yield. By adding urea on the furrow at planting, it was hypothesized that the level of chlorosis symptoms would increase, and the resulting yield would significantly decrease. In addition, it has been shown that iron chelates can be added to the soil in the ortho-ortho chelated iron form to reduce the level of chlorosis symptoms, thus resulting in an overall increase in soybean yield (Wiersma 2005; Gamble *et al.* 2014). The effect of adding urea and iron chelates on yield was significant in six of nine environments (Table 3-4). These treatments had only a slight effect on nematode

reproduction in a single environment (Table 3-5). Our results are in agreement with the literature findings on the effects of these treatments (Goos and Johnson 2000; Bloom *et al.* 2011b; Kaiser *et al.* 2014).

Field evaluation of plant stress

Soybean stress was monitored approximately weekly within each environment. Traditional methods of collecting in-season severity notes for IDC or SCN are typically based on subjective visual ratings on a 1-5 scale (Cianzio *et al.* 1979). With recent advances in remote sensing, however, there is growing interest to objectively collect plant health information in a more high-throughput fashion (Nutter *et al.* 2002; Singh *et al.* 2016; Bai *et al.* 2018a; Dobbels and Lorenz 2019).

An unmanned aircraft system (UAS) was deployed in this experiment and compared to a ground based active sensor as well as traditional visual scores. When correlating the three different measurements to yield (an indicator of accumulative plant growth and development), the UAS-based NDVI measurement provided the highest Pearson correlations both across environments and across time (Figure 3-3). Compared to the visual score notes, the UAS measurement is completely objective, and compared to the crop circle, the UAS-based NDVI measurement is capturing both center rows (compared to a single row) and has less variability based on height of sensor and field of view. Finally, the UAS-collected data is the most efficient method for collecting large amounts of remote sensing data over the shortest period of time and can be expanded to larger research trials. Given the efficiency of data collection with the UAS, it would be interesting to test measurements in large scale field operations to identify and diagnose problematic areas for further investigation.

It has also been shown that yield losses from SCN could occur without any visible symptoms in the field (Wang *et al.* 2003). In our study, only one environment showed significant differences in UAS-based NDVI measurements among SCN resistant and SCN susceptible genotypes; however, five environments had significant yield differences and all nine environments had significant RF differences. In a previous study, reflectance values explained up to 60% of the variation in SCN population densities, however, these previous studies showed a much larger range in initial SCN densities with sites having as many as 12,000 eggs/100cc (Nutter *et al.* 2002). It would be interesting to deploy a UAS-based system on larger field settings to flag potential high risk areas for subsequent field scouting or soil sampling. It would also be beneficial to test these measurements across a larger range of SCN densities.

Influence of SCN sources of resistance on yield and nematode reproduction

Soybean cyst nematode sources of resistance had a significant effect on yield, on average, across all environments. There were, however, four environments that did not show a significant SCN treatment effect on yield (Table 3-4). While the field conditions did not have extreme levels of SCN population densities at planting, damage can occur with as low as 10 to 50 eggs/100cc soil (Niblack *et al.* 1992). Chen et al. (2001) also reported significant differences among SCN resistant and SCN susceptible cultivars when the initial egg density was 1,000 eggs/100cc. Yield differences between SCN resistant and susceptible cultivars tend to increase as initial SCN egg counts increase (Niblack *et al.* 1992; Koenning 2000; Chen *et al.* 2001). Environment three had the highest difference between susceptible and resistant genotypes; however, in terms of initial egg counts, it was ranked fifth. The environment with the highest initial egg counts

(environment eight) showed the fourth largest difference between resistant and susceptible cultivars. Our study did not show a strong correlation between initial egg counts and observed yield loss (Supplemental table 3-4).

The female index (FI) on indicator line PI 88788 and Peking was used to determine the HG-type of nematodes present using a lab test of soil samples collected in the spring (Niblack *et al.* 2002). It was determined that environments 1,4,6,7,8, and 9 were HG type 2, environments 2 and 5 were HG type 0, and environment 3 was HG type 1.2 (Table 3-1) according to the 10% rule (Niblack *et al.* 2002). There has been a growing number of fields with increased SCN virulence populations and SCN reproduction on resistant soybean varieties as reported by several surveys conducted in the Midwest and Canada (Zheng *et al.* 2006; Chen *et al.* 2010; Wu and Xue 2010; Acharya *et al.* 2016; McCarville *et al.* 2017). Lab results provided a female index value, however, this data to determine virulence is an imperfect measurement of virulence that would occur on commercial varieties due to the quantitative nature of resistance (Anand 1994; Cook *et al.* 2012). Looking at RF results from the field, 3 of the 4 environments that were HG type 2 from the lab, showed significant reproduction differences between Peking and PI88788 in the field. Environment 5 was determined to be HG type 0 from the lab; however, still showed significant differences in RF between Peking and PI 88788 in the field.

Recommendations based on study results

The two stresses of IDC and SCN appear to act independently to alter yield and nematode reproduction. The nematodes reproduce on SCN susceptible soybean plots regardless of the amount of IDC stress occurring. The lack of interaction between IDC

and SCN on SCN reproduction is actually quite troubling. It would be expected that factors reducing the host plant's health will reduce the ability for the nematodes to reproduce (Chen *et al.* 2007). We did not find this to be the case. This finding may partially support the observation that SCN numbers increase at a much higher rate than expected in high pH soils.

A lack of interaction between SCN and IDC levels suggests that farmers can manage IDC and SCN independently. It is recommended to start by identifying the problem. Soybean IDC will be caused by soil chemical properties including pH, soluble salts, EC, and plant available iron. Previous monitoring of soybean fields will also indicate likely problematic areas for IDC symptoms to occur. Soil sampling for SCN is a required first step. Based on the results of this study, the nematodes are reproducing on susceptible plots even when yield losses are not occurring. For managing IDC, genetic tolerance is the first step, and adding iron chelates will also increase yield in severe IDC environments. Many previous studies have shown that genetic tolerance to IDC is the most important strategy for lessening IDC severity, and our findings support these results (Goos and Johnson 2000; Naeve 2006; Kaiser *et al.* 2014).

Variable rate of application of iron chelates would be recommended if available. Normalized difference vegetation index (NDVI) data collected from a UAS-based or satellite platform from previous seasons could be used to identify regions of the field that are more likely to have IDC stress conditions. For SCN, identification of good SCN resistant varieties based on public variety trial reports, based on seed company advice, or through evaluation of varieties on farm is necessary. Finally, continual monitoring of SCN levels is highly recommended.

Supplemental Material (Chapter 3)

Supplemental Table 3-1: The 24 treatment combinations used to create the factorial arrangement of iron deficiency chlorosis (IDC) application treatment, soybean cyst nematode (SCN) resistance, and IDC tolerance used in this study. Urea, none, and Soygreen were used for the IDC application. Both tolerant and susceptible IDC cultivars (T vs. S) were also evaluated. Finally, SCN genetic sources of resistance include susceptible (SCN susc.), PI 88788 and Peking sources of resistance.

Treatment #	Variety	IDC application	IDC Tolerance	SCN Treatment
1	S14-J7	Urea	T	SCN susc.
2	S14-J7	None	T	SCN susc.
3	S14-J7	Soygreen	T	SCN susc.
4	PB-1611R2	Urea	S	SCN susc.
5	PB-1611R2	None	S	SCN susc.
6	PB-1611R2	Soygreen	S	SCN susc.
7	AG1733	Urea	T	PI 88788
8	AG1733	None	T	PI 88788
9	AG1733	Soygreen	T	PI 88788
10	AG14X7	Urea	S	PI 88788
11	AG14X7	None	S	PI 88788
12	AG14X7	Soygreen	S	PI 88788
13	NuTech 7169	Urea	T	Peking
14	NuTech 7169	None	T	Peking
15	NuTech 7169	Soygreen	T	Peking
16	NuTech7186	Urea	S	Peking
17	NuTech7186	None	S	Peking
18	NuTech7186	Soygreen	S	Peking
19	NuTech 7169	Urea	T	Peking + Fluopyram
20	NuTech 7169	None	T	Peking + Fluopyram
21	NuTech 7169	Soygreen	T	Peking + Fluopyram
22	NuTech7186	Urea	S	Peking + Fluopyram
23	NuTech7186	None	S	Peking + Fluopyram
24	NuTech7186	Soygreen	S	Peking + Fluopyram

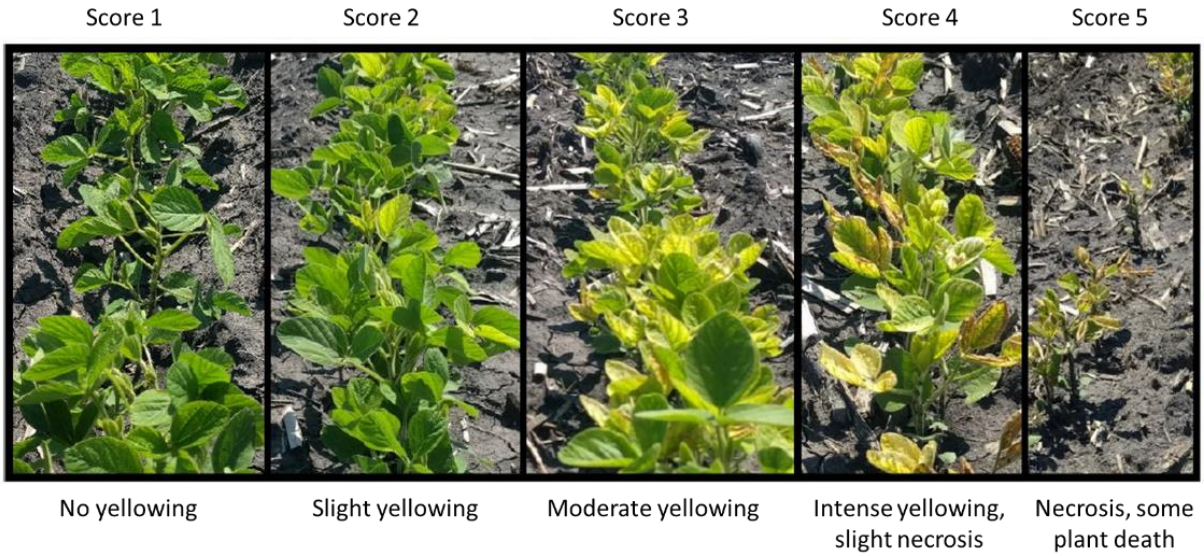

Supplemental Figure 1. Severity rating protocol for visual chlorosis scoring. Visual scores were taken on a 1-5 scale. A score of one is given to plots showing no signs of yellowing, a score of two is given to plots with slight yellowing, a score of three is given to plots with moderate yellowing, a score of four is given to plots with intense yellowing and some necrosis, and a score of five is given to plots with severe necrosis and some plant death.

Supplemental Table 3-2. Slope coefficient for yield by visual severity score across ten dates and nine environments, reported in kg/ha. For every one point increase in visual severity score, there was, on average, a corresponding decrease in yield in kg/ha.

	Environment									
Date	**1**	**2**	**3**	**4**	**5**	**6**	**7**	**8**	**9**	**Average:**
1	-65	-348	-	-654	-738	-642	-322	-344	-400	-390
2	-119	-327	-	-660	-577	-674	-266	-272	-305	-356
3	-65	-301	-	-727	-780	-729	-261	-223	-427	-439
4	-140	-367	-	-822	-950	-826	-275	-302	-433	-514
5	-179	-451	-	-911	-881	-931	-272	-468	-607	-588
6	-185	-503	-	-932	-838	-925	-279	-492	-464	-577
7	-194	-511	-	-1072	-966	-1058	-297	-494	-472	-633
8	-249	-608	-	-902	-1059	-988	-280	-536	-546	-646
9	-18	-616	-	-1066	-1047	-971	-528	-758	-722	-716
10	-9	-706	-	-1112	-1195	-992	--	--	-796	-802

Supplemental Table 3-3. IDC application treatment effect on yield, reproduction factor (RF), protein (P), oil (O), and protein plus oil (P+O). Letters not connected by the same letter were significant at $p<0.05$ using Tukey's Honest Significant Difference.

Treatment	Yield (kg/ha)	SCN reproduction	Protein (db)	Oil	P+O
		Environment 1			
Soygreen	3846.3 a	9.24 a	36.7 b	21.5 a	58.3 b
Control	3787.2 a	8.59 a	37.0 b	21.6 a	58.6 b
Urea	3642.2 a	9.08 a	37.6 a	21.5 a	59.1 a
P>F	0.264	0.95	<0.0001	0.0814	0.0002
		Environment 2			
Soygreen	4554.5 a	5.31 a	37.5 ab	21.5 a	59.0 b
Control	4462 a	5.93 a	37.4 b	21.6 a	59.0 b
Urea	3741.4 b	4.54 a	37.9 a	21.6 a	59.4 a
P>F	<0.0001	0.32	0.0204	0.65	0.0029
		Environment 3			
Soygreen	3824.6 a	9.75 a	40.2 b	20.9 a	61.1 b
Control	3797.5 a	10.92 a	40.3 b	20.9 a	61.2 ab
Urea	3742.9 a	13.7 a	40.7 a	20.8 a	61.5 a
P>F	0.8	0.08	0.0071	0.66	0.0082
		Environment 4			
Soygreen	4309.9 a	1.78 a	38.1 a	21.8 a	59.9 a
Control	3389.7 b	1.49 a	35.6 a	20.6 a	56.2 a
Urea	3200.4 b	1.31 a	36.1 a	20.3 a	56.4 a
P>F	0.0005	0.087	0.36	0.29	0.34
		Environment 5			
Soygreen	4643.4 a	4.44 a	37.7 b	21.5 a	59.2 b
Control	4008.0 b	4.35 a	37.8 b	21.3 a	59.1 b
Urea	3741.1 b	2.30 a	38.6 a	21.2 a	59.8 a
P>F	0.001	0.031	0.0005	0.15	<0.0001
		Environment 6			
Soygreen	4428.8 a	2.96 a	37.2 a	21.0 a	58.2 a
Control	3493.4 b	2.94 a	39.0 a	21.5 a	60.5 a
Urea	2060.3 c	2.23 a	32.1 b	17.3 b	49.4 b
P>F	<0.0001	0.37	0.0043	0.0004	<.0001
		Environment 7			
Soygreen	2847.1 a	2.94 a	38.0 b	21.3 a	59.3 ab
Control	2746.4 a	3.02 a	37.9 b	21.2 ab	59.1 b
Urea	1977.0 b	2.23 a	38.6 a	20.9 b	59.6 a
P>F	<0.0001	0.066	<0.0001	0.012	0.031
		Environment 8			
Soygreen	3700.7 a	1.06 a	37.8 b	20.8 a	58.6 ab
Control	3607.1 ab	1.05 a	37.8 b	21.0 a	58.8 a
Urea	3358.3 b	0.93 a	38.4 a	20.7 a	59.2 b
P>F	0.0067	0.43	<0.0001	0.083	0.0004
		Environment 9			
Soygreen	3840.1 a	1.04 a	38.4 a	21.0 a	59.5 a
Control	3807.0 a	0.88 a	38.4 a	21.1 a	59.5 ab
Urea	3714.1 a	1.23 a	38.1 b	21.1 a	59.2 b
P>F	0.58	0.19	0.008	0.82	0.023

Supplemental Table 3-4. SCN treatment effect on yield, reproduction factor (RF), protein (P), oil (O), and protein plus oil (P+O). Letters not connected by the same letter were significant at $p<0.05$ using Tukey's Honest Significant Difference.

Treatment	Yield (kg/ha	SCN reproduction	Protein (db)	Oil	P+O
			Environment 1		
Peking + Ilevo	3726.2 a	3.47 c	36.4 b	21.9 a	58.4 b
Peking	3776.6 a	3.26 c	36.3 b	21.8 a	58.2 b
PI 88788	3679.7 a	10.1 b	37.7 a	21.3 b	59.0 a
Susceptible	3851.7 a	19.0 a	38.1 a	21.0 c	59.2 a
P>F	0.68	<0.0001	<0.0001	<0.0001	<0.0001
			Environment 2		
Peking + Ilevo	4476.0 a	1.73 c	37.2 b	21.9 a	59.1 a
Peking	4227.2 a	2.60 c	37.0 b	21.9 a	59.0 a
PI 88788	4126.9 a	5.68 b	38.1 a	21.3 b	59.4 a
Susceptible	4180.4 a	11.0 a	38.0 a	21.0 c	59.0 a
P>F	0.28	<0.0001	<0.0001	<0.0001	0.066
			Environment 3		
Peking + Ilevo	4601.0 a	3.74 c	39.1 b	21.4 a	60.5 b
Peking	4384.4 a	4.13 c	39.2 b	21.4 a	60.6 b
PI 88788	3592.6 b	15.7 b	41.7 a	20.3 b	62.1 a
Susceptible	2575.4 c	22.3 a	41.3 a	20.3 b	61.7 a
P>F	<0.0001	<0.0001	<0.0001	<0.0001	<0.0001
			Environment 4		
Peking + Ilevo	3693.5 ab	1.11 b	36.1 a	21.2 ab	57.3 a
Peking	3656.8 ab	1.35 b	37.7 a	22.2 a	59.9 a
PI 88788	4134.8 a	1.15 b	38.9 a	21.5 ab	60.4 a
Susceptible	3048.5 b	2.50 a	33.6 a	18.7 b	52.2 a
P>F	0.0179	<0.0001	0.073	0.015	0.052
			Environment 5		
Peking + Ilevo	4494.7 a	0.508 b	37.0 b	22.0 a	59.0 bc
Peking	4017.6 ab	0.326 b	37.3 b	21.6 a	58.9 c
PI 88788	4432.4 a	1.60 b	39.2 a	20.9 b	60.2 a
Susceptible	3578.7 b	12.4 a	38.5 a	20.8 b	59.3 b
P>F	0.0042	<0.0001	<0.0001	<0.0001	<0.0001
			Environment 6		
Peking + Ilevo	3473.7 a	0.49 b	36.3 ab	21.1 a	57.5 a
Peking	3141.5 a	0.51 b	35.0 ab	20.0 ab	55.0 a
PI 88788	3152.1 a	1.71 b	33.2 b	17.7 b	50.9 a
Susceptible	3542.6 a	8.13 a	39.7 a	20.8 ab	60.5 a
P>F	0.27	<0.0001	0.063	0.037	0.072
			Environment 7		
Peking + Ilevo	2652.3 a	1.26 bc	37.8 b	21.4 a	59.2 b
Peking	2425.6 a	1.08 c	37.9 b	21.3 a	59.2 b
PI 88788	2636.4 a	2.32 b	39.1 a	20.9 b	60.0 a
Susceptible	2379.9 a	6.25 a	37.9 b	20.9 b	58.9 b
P>F	0.043	<0.0001	<0.0001	0.0005	<0.0001
			Environment 8		
Peking + Ilevo	3769.2 a	0.33 c	37.5 c	21.1 a	58.7 b
Peking	3608.2 a	0.44 c	37.6 c	21.1 a	58.7 b
PI 88788	3655.0 a	1.39 b	38.7 a	20.6 b	59.3 a
Susceptible	3189.0 b	1.89 a	38.1 b	20.6 b	58.7 b
P>F	<0.0001	<0.0001	<0.0001	<0.0001	<0.0001
			Environment 9		
Peking + Ilevo	3871.4 a	0.40 c	37.4 c	21.6 a	58.9 c
Peking	3762.7 a	0.38 c	37.9 b	21.4 a	59.4 b
PI 88788	3810.0 a	1.31 b	38.9 a	20.8 b	59.8 a
Susceptible	3704.2 a	2.10 a	38.9 a	20.4 c	59.3 b
P>F	0.7	<0.0001	<0.0001	<0.0001	<0.0001

Supplemental Table 3-5. Yield differences between Peking and Susceptible (Susc.) plots along with initial SCN egg counts. Environments are sorted by nematode count in ascending order.

Environment	Nematodes (eggs/100CC)	Peking yield (kg/ha)	Susc. Yield (kg/ha)	Difference
1	422	3776.6	3851.7	-75.1
5	756	4017.6	3578.7	438.9
7	935	2425.6	2379.9	45.7
6	1269	3473.7	3542.6	-68.9
3	1619	4384.4	2575.4	1809
2	1700	4227.2	4180.4	46.8
4	2169	3656.8	3048.5	608.3
9	3338	3762.7	3704.2	58.5
8	4753	3608.2	3189	419.2

References

Acharya K., C. Tande, and E. Byamukama, 2016 Determination of heterodera glycines virulence phenotypes occurring in South Dakota. Plant Dis. 100. https://doi.org/10.1094/PDIS-04-16-0572-RE

Allen T. W., C. A. Bradley, A. J. Sisson, E. Byamukama, M. I. Chilvers, *et al.*, 2017 Soybean yield loss estimates due to diseases in the United States and Ontario, Canada, from 2010 to 2014. Plant Heal. Prog. 18: 19–27. https://doi.org/10.1094/PHP-RS-16-0066

Anand S. C., 1994 Genetic diversity for resistance to Heterodera glycines race 5 in soybean. J. Nematol. 26: 76–79.

Andrade-Sanchez P., M. A. Gore, J. T. Heun, K. R. Thorp, A. E. Carmo-Silva, *et al.*, 2014 Development and evaluation of a field-based high-throughput phenotyping platform. Funct. Plant Biol. 41: 68–79. https://doi.org/10.1071/FP13126

Araus J. L., and J. E. Cairns, 2014 Field high-throughput phenotyping: The new crop breeding frontier. Trends Plant Science. 19: 52–61. https://doi.org/10.1016/j.tplants.2013.09.008

Araus J. L., S. C. Kefauver, J. Atieno, Y. Li, P. Langridge, *et al.*, 2015 Breeding to adapt agriculture to climate change: affordable phenotyping solutions. Current Opinion in Plant Biology. 45: 93–99. https://doi.org/10.1016/j.pbi.2018.05.003

Assefa T., J. Zhang, A. N. M. Lauter, A. Singh, J. A. O. Rourke, *et al.*, 2020 Deconstructing the genetic architecture of iron deficiency chlorosis in soybean using genome-wide approaches. 1–13.

Bai G., S. Jenkins, W. Yuan, G. L. Graef, and Y. Ge, 2018a Field-based scoring of soybean iron deficiency chlorosis using RGB imaging and statistical learning. Front. Plant Sci. 9: 1–12. https://doi.org/10.3389/fpls.2018.01002

Bai G., S. Jenkins, W. Yuan, G. L. Graef, and Y. Ge, 2018b Field-Based Scoring of Soybean Iron Deficiency Chlorosis Using RGB Imaging and Statistical Learning. 9: 1–12. https://doi.org/10.3389/fpls.2018.01002

Bandillo N., D. Jarquin, Q. Song, R. Nelson, P. Cregan, *et al.*, 2015 A Population Structure and Genome-Wide Association Analysis on the USDA Soybean Germplasm Collection. Plant Genome 8: plantgenome2015.04.0024. https://doi.org/10.3835/plantgenome2015.04.0024

Bauckhage C., and K. Kersting, 2013 Data mining and pattern recognition in agriculture. Künstl Intell 27: 313–324. https://doi.org/10.1007/s13218-013-0273-0

Bissonnette K. M., C. Christopher, P. Mark, D. Gregory, M. Peter, *et al.*, 2020 Effects of ILeVO seed treatment on Heterodera glycines reproduction and soybean yield in small-plot and strip-trial experiments in Iowa. Plant Dis. 1–34.

Bloom P. R., G. W. Rehm, J. A. Lamb, and A. J. Scobbie, 2011 Soil Nitrate is a Causative Factor in Iron Deficiency Chlorosis in Soybeans. Soil Sci. Soc. Am. J. 75: 2233. https://doi.org/10.2136/sssaj2010.0391

Breiman L., 2001 Random forests. Mach. Learn. 45: 5–32. https://doi.org/10.1023/A:1010933404324

Brown J. C., C. R. Weber, and B. E. Caldwell, 1967 Efficient and inefficient use of iron by two soybean genotypes and their isolines. Agron. J. 59: 459–462.

Busemeyer L., D. Mentrup, K. Möller, E. Wunder, K. Alheit, *et al.*, 2013 Breedvision - A multi-sensor platform for non-destructive field-based phenotyping in plant breeding. Sensors (Switzerland) 13: 2830–2847. https://doi.org/10.3390/s130302830

Campbell P. K. E., E. M. Middleton, J. E. McMurtrey, L. A. Corp, and E. W. Chappelle, 2007 Assessment of Vegetation Stress Using Reflectance or Fluorescence Measurements. J. Environ. Qual. 36: 832–845. https://doi.org/10.2134/jeq2005.0396

Charlson D. V., T. B. Bailey, S. R. Cianzio, and R. C. Shoemaker, 2005 Molecular marker Satt481 is associated with iron-deficiency chlorosis resistance in a soybean breeding population. Crop Sci. 45: 2394–2399. https://doi.org/10.2135/cropsci2004.0510

Chatterjee A., S. Lovas, H. Rasmussena, and R. J. Goos, 2017 Foliar Application of Iron Fertilizers to Control Iron Deficiency Chlorosis of Soybean. Crop. Forage Turfgrass Manag. 3: 1–7. https://doi.org/10.2134/cftm2017.05.0037

Chen S. Y., P. M. Porter, J. H. Orf, C. D. Reese, W. C. Stienstra, *et al.*, 2001 Soybean cyst nematode population development and associated soybean yields of resistant and susceptible cultivars in Minnesota. Plant Dis. 85: 760–766. https://doi.org/10.1094/PDIS.2001.85.7.760

Chen S., J. E. Kurle, S. R. Stetina, G. A. Nelson, and N. C. Hansen, 2007 Interactions between iron-deficiency chlorosis and soybean cyst nematode in Minnesota soybean fields. 131–139. https://doi.org/10.1007/s11104-007-9370-x

Chen S. Y., B. Potter, and J. H. Orf, 2010 Virulence of the soybean cyst nematode has increased over years in Minnesota. Jorunal Nematology. 42: 238–238.

Chen D., K. Neumann, S. Friedel, B. Kilian, M. Chen, *et al.*, 2014 Dissecting the phenotypic components of crop plant growthand drought responses based on high-throughput image analysis w open. Plant Cell 26: 4636–4655. https://doi.org/10.1105/tpc.114.129601

Cheverud J. M., 2001 A simple correction for multiple comparisons in interval mapping genome scans. Heredity. 87: 52–58. https://doi.org/10.1046/j.1365-2540.2001.00901.x

Cianzio S. R. De, W. R. Fehr, and I. C. Anderson, 1979 (1979) Genotypic evaluation for iron deficiency chlorosis in soybeans by visual scores and chlorophyll concentration. Crop Sci. 19: 644–646.

Cianzio S. R., and W. R. Fehr, 1980 Genetic control of iron deficiency chlorosis in soybeans. Iowa State J. Res. 54: 367–375.

Cianzio S. R., and W. R. Fehr, 1982 Variation in the inheritance of resistance to iron deficiency chlorosis in soybeans. Crop Sci. 22: 433–434.

Clark R. B., 1982 Iron deficiency in plants grown in the Great Plains of the United States. J. Plant Nutrition. 5.

Concibido V. C., D. A. Lange, R. L. Denny, J. H. Orf, and N. D. Young, 1997 Genome mapping of soybean cyst nematode resistance genes in “Peking”, PI 90763, and PI 88788 using DNA markers. Crop Sci. 37: 258–264. https://doi.org/10.2135/cropsci1997.0011183X003700010046x

Cook D. E., T. G. Lee, X. Guo, S. Melito, K. Wang, *et al.*, 2012 Copy number variation of multiple genes at Rhg1 mediates nematode resistance in soybean. Science. 338: 1206–1209. https://doi.org/10.1126/science.1228746

Coppens F., N. Wuyts, D. Inzé, and S. Dhondt, 2017 Unlocking the potential of plant phenotyping data through integration and data-driven approaches. Curr. Opin. Syst. Biol. 4: 58–63. https://doi.org/10.1016/j.coisb.2017.07.002

Crain J. L., Y. Wei, J. Barker, S. M. Thompson, P. D. Alderman, *et al.*, 2016 Development and deployment of a portable field phenotyping platform. Crop Sci. 56: 965–975. https://doi.org/10.2135/cropsci2015.05.0290

Crossa J., P. Pérez, J. Hickey, J. Burgueño, L. Ornella, *et al.*, 2014 Genomic prediction in CIMMYT maize and wheat breeding programs. Heredity (Edinb). 112: 48–60. https://doi.org/10.1038/hdy.2013.16

Currie I., and M. Durban, 2002 Flexible smoothing with P -splines : a unified approach. 333–349.

Dhondt S., N. Wuyts, and D. Inzé, 2013 Cell to whole-plant phenotyping: The best is yet to come. Trends Plant Sci. 18: 428–439. https://doi.org/10.1016/j.tplants.2013.04.008

Diers B. W., S. R. Cianzio, and R. C. Shoemaker, 1992 Possible identification of quantitative trait loci affecting iron efficiency in soybean. J. Plant Nutr. 15: 2127–2136. https://doi.org/10.1080/01904169209364462

Dobbels A. A., and A. J. Lorenz, 2019 Soybean iron deficiency chlorosis high throughput phenotyping using an unmanned aircraft system. Plant Methods 15: 1–9. https://doi.org/10.1186/s13007-019-0478-9

Duggan J. J ., 1963 Relationship between Intensity of Cereal Root Eelworm (Heterodera avenae Wollenweber 1924) Infestation and pH Value of Soil. Irish J. Agric. Res. 2: 105–110.

Endelman J. B., 2011 Ridge Regression and Other Kernels for Genomic Selection with R Package rrBLUP. Plant Genome 4: 250–255. https://doi.org/10.3835/plantgenome2011.08.0024

Erdle K., B. Mistele, and U. Schmidhalter, 2011 Comparison of active and passive spectral sensors in discriminating biomass parameters and nitrogen status in wheat cultivars. F. Crop. Res. 124: 74–84. https://doi.org/10.1016/j.fcr.2011.06.007

Eskridge K. ., S. G. Gilmour, R. Mead, N. . Butler, and D. A. Travnicek, 2006 Large supersaturated designs. J. Stat. Comput. Simul. 74: 525–542.

Fahlgren N., M. A. Gehan, and I. Baxter, 2015 Lights, camera, action: High-throughput plant phenotyping is ready for a close-up. Curr. Opin. Plant Biol. 24: 93–99. https://doi.org/10.1016/j.pbi.2015.02.006

Fehr W. R., 1982 Control of iron-deficiency chlorosis in soybeans by plant breeding. J. Plant Nutr. 5.

Fiorani F., and U. Schurr, 2013 Future Scenarios for Plant Phenotyping. Annu. Rev. Plant Biol. 64: 267–291. https://doi.org/10.1146/annurev-arplant-050312-120137

Francl L. J., 1993 Multivariate Analysis of Selected Edaphic Factors and Their Relationship to Heterodera glycines Population Density. J. Nematol. 25: 270–276.

Franzen D. W., and J. L. Richardson, 2008 Soil factors affecting iron chlorosis of soybean in the red river valley of North Dakota and Minnesota. J. Plant Nutr. 23: 67–78. https://doi.org/10.1080/01904160009381998

Froechlich D. M., and W. R. Fehr, 1981 Agronomic Performance of Soybeans with Differing Levels of Iron Deficiency Chlorosis on Calcareous Soil. Crop Sci. 21: 438–441. https://doi.org/10.2135/cropsci1981.0011183x002100030021x

Furbank R. T., and M. Tester, 2011 Phenomics - technologies to relieve the phenotyping bottleneck. Trends Plant Sci. 16: 635–644. https://doi.org/10.1016/j.tplants.2011.09.005

Gamble A. V., J. A. Howe, D. Delaney, E. van Santen, and R. Yates, 2014 Iron chelates alleviate iron chlorosis in soybean on high pH soils. Agron. J. 106: 1251–1257. https://doi.org/10.2134/agronj13.0474

Gardner M., R. Heinz, J. Wang, and M. G. Mitchum, 2017 Genetics and adaptation of soybean cyst nematode to broad spectrum soybean resistance. G3 Genes, Genomes, Genet. 7: 835–841. https://doi.org/10.1534/g3.116.035964

Godwin I. D., J. Rutkoski, R. K. Varshney, and L. T. Hickey, 2019 Technological perspectives for plant breeding. Theor. Appl. Genet. 132: 555–557. https://doi.org/10.1007/s00122-019-03321-4

Goos R. J., and B. E. Johnson, 2000 A comparison of three methods for reducing iron-deficiency chlorosis in soybean. Agron. J. 92: 1135–1139. https://doi.org/10.2134/agronj2000.9261135x

Goos R. J., and B. Johnson, 2001 Seed Treatment, Seeding Rate, and Cultivar Effects on Iron Deficiency Chlorosis of Soybean. J. Plant Nutr. 24: 1255–1268. https://doi.org/10.1081/PLN-100106980

Goos R. J., B. E. Johnson, R. J. Goos, B. E. Johnson, S. Science, *et al.*, 2009 Evaluation of Soybean Cultivars for Resistance to Iron Deficiency Chlorosis in Rows Versus Hills. 4167: 105–114. https://doi.org/10.1080/01904160903392550

Haghighattalab A., L. González Pérez, S. Mondal, D. Singh, D. Schinstock, *et al.*, 2016 Application of unmanned aerial systems for high throughput phenotyping of large wheat breeding nurseries. Plant Methods 12–35. https://doi.org/10.1186/s13007-016-0134-6

Hänsch R., and R. R. Mendel, 2009 Physiological functions of mineral micronutrients (Cu, Zn, Mn, Fe, Ni, Mo, B, Cl). Curr. Opin. Plant Biol. 12: 259–266. https://doi.org/10.1016/j.pbi.2009.05.006

Hansen N. C., M. A. Schmitt, J. E. Andersen, and J. S. Strock, 2003 Iron Deficiency of Soybean in the Upper Midwest and Associated Soil Properties. Agron. J. 95: 1595–1601. https://doi.org/10.2134/agronj2003.1595

Hansen N. C., V. D. Jolley, S. L. Naeve, and R. J. Goos, 2004 Iron deficiency of soybean in the North Central U.S. and associated soil properties. Soil Sci. Plant Nutr. 50: 983–987. https://doi.org/10.1080/00380768.2004.10408564

Haskett H. T., and A. K. Sood, 1998 Trade-off studies of detection performance versus the number of reflective spectral bands in hyperspectral imagery. 3372: 26–42. https://doi.org/10.1117/12.312606

Hatfield J. L., A. A. Gitelson, J. S. Schepers, and C. L. Walthall, 2008 Application of spectral remote sensing for agronomic decisions. Agron. J. 100: 117–131. https://doi.org/10.2134/agronj2006.0370c

Heffner E. L., A. J. Lorenz, J. L. Jannink, and M. E. Sorrells, 2010 Plant breeding with Genomic selection: Gain per unit time and cost. Crop Sci. 50: 1681–1690. https://doi.org/10.2135/cropsci2009.11.0662

Helms T. C., R. A. Scott, W. T. Schapaugh, R. J. Goos, D. W. Franzen, *et al.*, 2010 Soybean iron-deficiency chlorosis tolerance and yield decrease on calcareous soils. Agron. J. 102: 492–498. https://doi.org/10.2134/agronj2009.0317

Holman F. H., A. B. Riche, A. Michalski, M. Castle, M. J. Wooster, *et al.*, 2016 High throughput field phenotyping of wheat plant height and growth rate in field plot trials using UAV based remote sensing. Remote Sens. Environ. 8: 1–24. https://doi.org/10.3390/rs8121031

Inskeep W. P., and P. R. Bloom, 1987 Soil chemical factors associated with soybean chlorosis in Calciaquolls of Western Minnesota. Agron J. 79: 779–786.

Jannink J. L., A. J. Lorenz, and H. Iwata, 2010 Genomic selection in plant breeding: From theory to practice. Briefings Funct. Genomics Proteomics 9: 166–177. https://doi.org/10.1093/bfgp/elq001

Jeong J., and E. L. Connolly, 2009 Iron uptake mechanisms in plants: functions of the FRO family of ferric reductases. Plant Sci. 176: 709–714. https://doi.org/10.1016/j.plantsci.2009.02.011

Jessen H. ., R. W. Dragonuk, Hintz, and W. R. Fehr, 1988 Alternative breeding strategies for the improvement of iron efficiency in soybean. J. Plant Nutr. 11: 717–726.

Kaiser D. E., J. A. Lamb, and P. R. Bloom, 2011 Managing Iron Deficiency Chlorosis in Soybean. Univ. Minnesota Ext.

Kaiser D. E., J. A. Lamb, P. R. Bloom, and J. A. Hernandez, 2014 Comparison of field management strategies for preventing iron deficiency chlorosis in soybean. Agron. J. 106: 1963–1974. https://doi.org/10.2134/agronj13.0296

Karcher D. E., and M. D. Richardson, 2005 Batch analysis of digital images to evaluate turfgrass characteristics. Crop Sci. 45: 1536–1539. https://doi.org/10.2135/cropsci2004.0562

King K. E., G. A. Peiffer, M. Reddy, N. Lauter, S. F. Lin, *et al.*, 2013 Mapping of Iron and Zinc Quantitative Trait Loci in Soybean for Association To Iron Deficiency Chlorosis Resistance. J. Plant Nutr. 36: 2132–2153. https://doi.org/10.1080/01904167.2013.766804

Koenning S. R., 2000 Density-Dependent Yield of Heterodera glycines-Resistant and -Susceptible Cultivars. J. Nematol. 32: 502–7.

Li J., and L. Ji, 2005 Adjusting multiple testing in multilocus analyses using the eigenvalues of a correlation matrix. Heredity (Edinb). 95: 221–227. https://doi.org/10.1038/sj.hdy.6800717

Liesch A. M., D. A. Ruiz Diaz, K. L. Martin, B. L. Olson, D. B. Mengel, *et al.*, 2011 Management strategies for increasing soybean yield on soils susceptible to iron deficiency. Agron. J. 103: 1870–1877. https://doi.org/10.2134/agronj2011.0191

Lin S., S. Cianzio, and R. Shoemaker, 1997a Mapping genetic loci for iron deficiency chlorosis in soybean. Mol. Breed. 3: 219–229. https://doi.org/10.1023/A:1009637320805

Lin S., S. Cianzio, and R. Shoemaker, 1997b Mapping genetic loci for iron deficiency chlorosis in soybean. Mol. Breed. 3: 219–229. https://doi.org/10.1023/A:1009637320805

Lin S. F., D. Grant, S. Cianzio, and R. Shoemaker, 2000 Molecular characterization of iron deficiency chlorosis in soybean. J. Plant Nutr. 23: 1929–1939. https://doi.org/10.1080/01904160009382154

Lorenz A. J., 2013 Resource allocation for maximizing prediction accuracy and genetic gain of genomic selection in plant breeding: A simulation experiment. G3 Genes, Genomes, Genet. 3: 481–491. https://doi.org/10.1534/g3.112.004911

Lucena J. J., and L. Hernandez-Apaolaza, 2017 Iron nutrition in plants: an overview. Plant Soil 418: 1–4. https://doi.org/10.1007/s11104-017-3316-8

Mamidi S., S. Chikara, R. J. Goos, D. L. Hyten, D. Annam, *et al.*, 2011 Genome-Wide Association Analysis Identifies Candidate Genes Associated with Iron Deficiency Chlorosis in Soybean. Plant Genome J. 4: 154. https://doi.org/10.3835/plantgenome2011.04.0011

Mamidi S., R. K. Lee, J. R. Goos, and P. E. McClean, 2014a Genome-wide association studies identifies seven major regions responsible for iron deficiency chlorosis in soybean (Glycine max). PLoS One 9: 1–13. https://doi.org/10.1371/journal.pone.0107469

Mamidi S., R. K. Lee, J. R. Goos, and P. E. McClean, 2014b Genome-wide association studies identifies seven major regions responsible for iron deficiency chlorosis in soybean (Glycine max). PLoS One 9: e107469. https://doi.org/10.1371/journal.pone.0107469

Mansur L., 1992 Resistance to Iron-Deficiency Chlorosis in PI 437654 Soybean. Crop Sci. 32: 1137. https://doi.org/10.2135/cropsci1992.0011183x003200050014x

Martín-Fernández C., Á. Solti, V. Czech, K. Kovács, F. Fodor, *et al.*, 2017 Response of soybean plants to the application of synthetic and biodegradable Fe chelates and Fe complexes. Plant Physiol. Biochem. 118: 579–588. https://doi.org/10.1016/j.plaphy.2017.07.028

McCarville M. T., C. C.Marett, M. P.Mullaney, G. D. Gebhart, and G. L. Tylka, 2017 Increase in soybean cyst nematode virulence and reproduction on resistant soybean varieties in Iowa from 2001 to 2015 and the effects on soybean yields. Plant Heal. Prog. 18: 146–155. https://doi.org/10.1094/PHP-RS-16-0062

Melakeberhan H., J. D. Ey, V. C. B. Aligar, T. E. C. A. J. R, I. B. Unit, *et al.*, 2013 Effect of soil pH on the pathogenesis of Heterodera glycines and Meloidogyne incognita on Glycine max genotypes. 6: 585–592.

Merry R., K. Butenhoff, B. W. Campbell, J.-M. Michno, D. Wang, *et al.*, 2019 Identification and Fine-Mapping of a Soybean Quantitative Trait Locus on Chromosome 5 Conferring Tolerance to Iron Deficiency Chlorosis. Plant Genome 12: 3. https://doi.org/10.3835/plantgenome2019.01.0007

Meuwissen T. H. E., B. J. Hayes, and M. E. Goddard, 2001 Prediction of total genetic value using genome-wide dense marker maps. Genetics 157: 1819–1829.

Moran Lauter A. N., G. A. Peiffer, T. Yin, S. A. Whitham, D. Cook, *et al.*, 2014 Identification of candidate genes involved in early iron deficiency chlorosis signaling in soybean (Glycine max) roots and leaves. BMC Genomics 15: 1–25. https://doi.org/10.1186/1471-2164-15-702

Moreira F. F., H. R. Oliveira, J. J. Volenec, K. M. Rainey, and L. F. Brito, 2020 Integrating High-Throughput Phenotyping and Statistical Genomic Methods to Genetically Improve Longitudinal Traits in Crops. 11: 1–18. https://doi.org/10.3389/fpls.2020.00681

Morris D. R., R. H. Loeppert, and T. J. Moore, 1990 Indigenous soil factors influencing iron chlorosis of soybean in calcareous soils. Soil Sci. Soc. Am. J. 54: 1329–1336.

Mourtzinis S., and S. P. Conley, 2017 Delineating soybean maturity groups across the United States. Agron. J. 109: 1397–1403. https://doi.org/10.2134/agronj2016.10.0581

Naeve S. L., 2006 Iron deficiency chlorosis in soybean: Soybean seeding rate and companion crop effects. Agron. J. 98: 1575–1581. https://doi.org/10.2134/agronj2006.0096

Naeve S. L., and G. W. Rehm, 2006 Genotype x environment interactions within iron deficiency chlorosis-tolerant soybean genotypes. 98: 808–814. https://doi.org/10.2134/agronj2005.0281

Naik H. S., J. Zhang, A. Lofquist, T. Assefa, S. Sarkar, *et al.*, 2017 A real - time phenotyping framework using machine learning for plant stress severity rating in soybean. Plant Methods 13–23. https://doi.org/10.1186/s13007-017-0173-7

Narayanan B., B. Floyd, K. Tu, L. Ries, and N. Hausmann, 2019 Improving soybean breeding using UAS measurements of physiological maturity. Proc. SPIE 27. https://doi.org/10.1117/12.2519072

Neely L., A. Rana, M. V Bagavathiannan, J. Henrickson, E. B. Putman, *et al.*, 2016 Unmanned aerial vehicles for high- throughput phenotyping and agronomic research. PLoS One 7: 1–26. https://doi.org/10.5061/dryad.65m87

Neilson E. H., A. M. Edwards, C. K. Blomstedt, B. Berger, B. L. Møller, *et al.*, 2015 Utilization of a high-throughput shoot imaging system to examine the dynamic phenotypic responses of a C4 cereal crop plant to nitrogen and water deficiency over time. J. Exp. Bot. 66: 1817–1832. https://doi.org/10.1093/jxb/eru526

Niblack T. L., N. K. Baker, and D. C. Norton, 1992 Yield losses due to Heterodera glycines in Iowa. Plant Dis. 76: 943–948.

Niblack T. L., P. R. Arelli, G. R. Noel, C. H. Opperman, J. H. Orf, *et al.*, 2002 A revised classification scheme for genetically diverse populations of Heterodera glycines. J. Nematol. 34: 279–288.

Niblack T. L., A. L. Colgrove, K. Colgrove, and J. P. Bond, 2008 Shift in Virulence of Soybean Cyst Nematode is Associated with Use of Resistance from PI 88788. Plant Heal. Prog. 9: 29. https://doi.org/10.1094/php-2008-0118-01-rs

Nutter F. W., G. L. Tylka, J. Guan, A. J. D. Moreira, C. . C. Marett, *et al.*, 2002 Use of Remote Sensing to Detect Soybean Cyst Nematode-Induced Plant Stress. 34: 222–231.

O'Rourke J. A., D. V. Charlson, D. O. Gonzalez, L. O. Vodkin, M. A. Graham, *et al.*, 2007a Microarray analysis of iron deficiency chlorosis in near-isogenic soybean lines. BMC Genomics 8: 1–13. https://doi.org/10.1186/1471-2164-8-476

O'Rourke J. A., M. A. Graham, L. Vodkin, D. O. Gonzalez, S. R. Cianzio, *et al.*, 2007b Recovering from iron deficiency chlorosis in near-isogenic soybeans: A microarray study. Plant Physiol. Biochem. 45: 287–292. https://doi.org/10.1016/j.plaphy.2007.03.008

O'Rourke J. A., R. T. Nelson, D. Grant, J. Schmutz, J. Grimwood, *et al.*, 2009 Integrating microarray analysis and the soybean genome to understand the soybeans iron deficiency response. BMC Genomics 10: 1–17. https://doi.org/10.1186/1471-2164-10-376

Pauli D., P. Andrade-Sanchez, A. E. Carmo-Silva, E. Gazave, A. N. French, *et al.*, 2016a Field-based high-throughput plant phenotyping reveals the temporal patterns of quantitative trait loci associated with stress-responsive traits in cotton. G3 Genes, Genomes, Genet. 6: 865–879. https://doi.org/10.1534/g3.115.023515

Pauli D., S. C. Chapman, R. Bart, C. N. Topp, C. J. Lawrence-Dill, *et al.*, 2016b The quest for understanding phenotypic variation via integrated approaches in the field environment. Plant Physiol. 172: 622–634. https://doi.org/10.1104/pp.16.00592

Pauli D., S. C. Chapman, R. Bart, C. N. Topp, C. J. Lawrence-Dill, *et al.*, 2016c The quest for understanding phenotypic variation via integrated approaches in the field

environment. Plant Physiol. 4: pp.00592.2016. https://doi.org/10.1104/pp.16.00592

Pederson P., G. L. Tylka, A. P. Mallarino, A. E. Macguidwin, N. C. Koval, *et al.*, 2010 Correlation between Soil pH, Heterodera glycines Population Densities, and Soybean Yield. Crop Sci. 50: 1458–1464.

Peiffer G. A., K. E. King, A. J. Severin, G. D. May, S. R. Cianzio, *et al.*, 2012 Identification of candidate genes underlying an iron efficiency quantitative trait locus in soybean. 158: 1745–1754. https://doi.org/10.1104/pp.111.189860

Reynolds D., F. Baret, C. Welcker, A. Bostrom, J. Ball, *et al.*, 2019 What is cost-efficient phenotyping? Optimizing costs for different scenarios. Plant Sci. 282: 14–22. https://doi.org/10.1016/j.plantsci.2018.06.015

Reynolds M., S. Chapman, L. Crespo-Herrera, G. Molero, S. Mondal, *et al.*, 2020 Breeder friendly phenotyping. Plant Sci. 110396. https://doi.org/10.1016/j.plantsci.2019.110396

Riggs R. D., and D. P. Schmitt, 1988 Complete Characterization of the Race Scheme for Heterodera glycines. J. Nematol. 20: 392–5.

Rodrigues F. A., G. Blasch, P. Defourny, J. I. Ortiz-Monasterio, U. Schulthess, *et al.*, 2018 Multi-temporal and spectral analysis of high-resolution hyperspectral airborne imagery for precision agriculture: Assessment of wheat grain yield and grain protein content. Remote Sens. 10. https://doi.org/10.3390/rs10060930

Rodríguez-Álvarez M. X., D. J. Lee, T. Kneib, M. Durbán, and P. Eilers, 2015 Fast smoothing parameter separation in multidimensional generalized P-splines: the SAP algorithm. Stat. Comput. 25: 941–957. https://doi.org/10.1007/s11222-014-9464-2

Rogovska N., 2006 Use of precision agriculture technologies in studying the relationships among soil pH , calcium carbonate equivalent , soybean cyst nematode population density , and soybean yield

Rogovska N. P., A. M. Blackmer, and A. P. Mallarino, 2007 Relationships between soybean yield , soil pH , and soil carbonate concentration. 71: 1251–1256. https://doi.org/10.2136/sssaj2006.0235

Rogovska N. P., A. M. Blackmer, and G. L. Tylka, 2009 Soybean Yield and Soybean Cyst Nematode Densities Related to Soil pH, Soil Carbonate Concentrations, and Alkalinity Stress Index. 1019–1026. https://doi.org/10.2134/agronj2008.0086x

Roitsch T., L. Cabrera-Bosquet, A. Fournier, K. Ghamkhar, J. Jiménez-Berni, *et al.*, 2019 Review: New sensors and data-driven approaches—A path to next generation phenomics. Plant Sci. 282: 2–10. https://doi.org/10.1016/j.plantsci.2019.01.011

Ross J. P., and C. A. Brim, 1957 Resistance of soybeans to the soybean cyst nematode as determined by a double-row method. Plant Dis. 41: 923–924.

Sagan V., M. Maimaitijiang, P. Sidike, K. Eblimit, K. T. Peterson, *et al.*, 2019 UAV-based high resolution thermal imaging for vegetation monitoring, and plant phenotyping using ICI 8640 P, FLIR Vue Pro R 640, and thermomap cameras. Remote Sens. 11. https://doi.org/10.3390/rs11030330

Severin A. J., G. A. Peiffer, W. W. Xu, D. L. Hyten, B. Bucciarelli, *et al.*, 2010 An integrative approach to genomic introgression mapping. Plant Physiol. 154: 3–12. https://doi.org/10.1104/pp.110.158949

Silva J., and R. Uchida, 2000 Essential nutrients for plant growth: nutrient functions and deficiency symptoms, pp. 31–55 in *Plant Nutrient Management in Hawaii's Soils, Approaches for Tropical and Subtropical Agriculture*,.

Singh A., B. Ganapathysubramanian, A. K. Singh, and S. Sarkar, 2016 Machine learning for high-throughput stress phenotyping in plants. Trends Plant Sci. 21: 110–124. https://doi.org/10.1016/j.tplants.2015.10.015

Song Q., D. L. Hyten, G. Jia, C. V. Quigley, E. W. Fickus, *et al.*, 2013 Development and Evaluation of SoySNP50K, a High-Density Genotyping Array for Soybean. PLoS One 8: 1–12. https://doi.org/10.1371/journal.pone.0054985

Song Q., J. Jenkins, G. Jia, D. L. Hyten, V. Pantalone, *et al.*, 2016 Construction of high resolution genetic linkage maps to improve the soybean genome sequence assembly Glyma1.01. BMC Genomics 17: 33. https://doi.org/10.1186/s12864-015-2344-0

Soybase.org, SoyBase and the Soybean Breeder's Toolbox

Sun J., J. E. Rutkoski, J. A. Poland, J. Crossa, J.-L. Jannink, *et al.*, 2017 Multitrait, Random Regression, or Simple Repeatability Model in High-Throughput Phenotyping Data Improve Genomic Prediction for Wheat Grain Yield. Plant Genome 10: plantgenome2016.11.0111. https://doi.org/10.3835/plantgenome2016.11.0111

Tardieu F., L. Cabrera-Bosquet, T. Pridmore, and M. Bennett, 2017 Plant Phenomics, From Sensors to Knowledge. Curr. Biol. 27: R770–R783. https://doi.org/10.1016/j.cub.2017.05.055

Tylka G. L., and C. C. Marett, 2014 Distribution of the Soybean Cyst Nematode , Heterodera glycines , in the United States and Canada : 1954 to 2014. Plant Heal. Br. 15: 85–87. https://doi.org/10.1094/PHP-BR-14-0006.The

Vasconcelos M. W., and M. A. Grusak, 2014 Morpho-physiological parameters affecting iron deficiency chlorosis in soybean (Glycine max L .). Plant Soil 374: 161–172. https://doi.org/10.1007/s11104-013-1842-6

Velazco J. G., M. X. Rodríguez-Álvarez, M. P. Boer, D. R. Jordan, P. H. C. Eilers, *et al.*, 2017 Modelling spatial trends in sorghum breeding field trials using a two-dimensional P-spline mixed model. Theor. Appl. Genet. 130: 1375–1392. https://doi.org/10.1007/s00122-017-2894-4

Wahabzada M., A. Mahlein, C. Bauckhage, and U. Steiner, 2015 Metro maps of plant disease dynamics — automated mining of differences using hyperspectral images. PLoS One 1–20. https://doi.org/10.1371/journal.pone.0116902

Wang J., T. L. Niblack, P. Microbiology, J. A. Tremain, W. J. Wiebold, *et al.*, 2003 Soybean Cyst Nematode Reduces Soybean Yield Without Causing Obvious Aboveground Symptoms

Wang J., P. E. McClean, R. Lee, R. J. Goos, and T. Helms, 2008 Association mapping of

iron deficiency chlorosis loci in soybean (Glycine max L. Merr.) advanced breeding lines. Theor. Appl. Genet. 116: 777–787. https://doi.org/10.1007/s00122-008-0710-x

Weiss M. G., 1943 Inheritance and Physiology of Efficiency in Iron Utilization in Soybeans. Genetics 28: 253–68.

White J. W., P. Andrade-Sanchez, M. A. Gore, K. F. Bronson, T. A. Coffelt, *et al.*, 2012 Field-based phenomics for plant genetics research. F. Crop. Res. 133: 101–112. https://doi.org/10.1016/j.fcr.2012.04.003

White J. W., and M. M. Conley, 2013 A flexible, low-cost cart for proximal sensing. Crop Sci. 53: 1646–1649. https://doi.org/10.2135/cropsci2013.01.0054

Wiersma J. V, 2005 Partial Solutions to Iron Deficiency in Soybean. 934: 924–934. https://doi.org/10.2134/agronj2004.0309

Wu R., C. X. Ma, M. Lin, Z. Wang, and G. Casella, 2004 Functional mapping of quantitative trait loci underlying growth trajectories using a transform-both-sides logistic model. Biometrics 60: 729–738. https://doi.org/10.1111/j.0006-341X.2004.00223.x

Wu G. Z., and H. W. Xue, 2010 Arabidopsis beta-Ketoacyl-[Acyl Carrier Protein] Synthase I Is Crucial for Fatty Acid Synthesis and Plays a Role in Chloroplast Division and Embryo Development. Plant Cell 22: 3726–3744. https://doi.org/10.1105/tpc.110.075564

Xavier A., B. Hall, A. A. Hearst, K. A. Cherkauer, and K. M. Rainey, 2017 Genetic architecture of phenomic-enabled canopy coverage in glycine max. Genetics 206: 1081–1089. https://doi.org/10.1534/genetics.116.198713/-/DC1.1

Yu N., L. Li, N. Schmitz, L. F. Tian, J. A. Greenberg, *et al.*, 2016a Development of methods to improve soybean yield estimation and predict plant maturity with an unmanned aerial vehicle based platform. Remote Sens. Environ. 187: 91–101. https://doi.org/10.1016/j.rse.2016.10.005

Yu N., L. Li, N. Schmitz, L. F. Tian, J. A. Greenberg, *et al.*, 2016b Development of methods to improve soybean yield estimation and predict plant maturity with an unmanned aerial vehicle based platform. Remote Sens. Environ. 187: 91–101. https://doi.org/10.1016/j.rse.2016.10.005

Zarco-Tejada P. J., S. L. Ustin, and M. L. Whiting, 2005 Temporal and spatial relationships between within-field yield variability in cotton and high-spatial hyperspectral remote sensing imagery. Agron. J. 97: 641–653. https://doi.org/10.2134/agronj2003.0257

Zhang J., H. S. Naik, T. Assefa, S. Sarkar, and R. V. C. Reddy, 2017 Computer vision and machine learning for robust phenotyping in genome-wide studies. Sci. Rep. 7: 1–11. https://doi.org/10.1038/srep44048

Zheng J., Y. Li, and S. Chen, 2006 Characterization of the virulence phenotypes of Heterodera glycines in Minnesota. J. Nematol. 38: 383–390.

Zhou J., D. Yungbluth, C. N. Vong, A. Scaboo, and J. Zhou, 2019 Estimation of the

maturity date of soybean breeding lines using UAV-based multispectral imagery. Remote Sens. 11. https://doi.org/10.3390/rs11182075

Figures

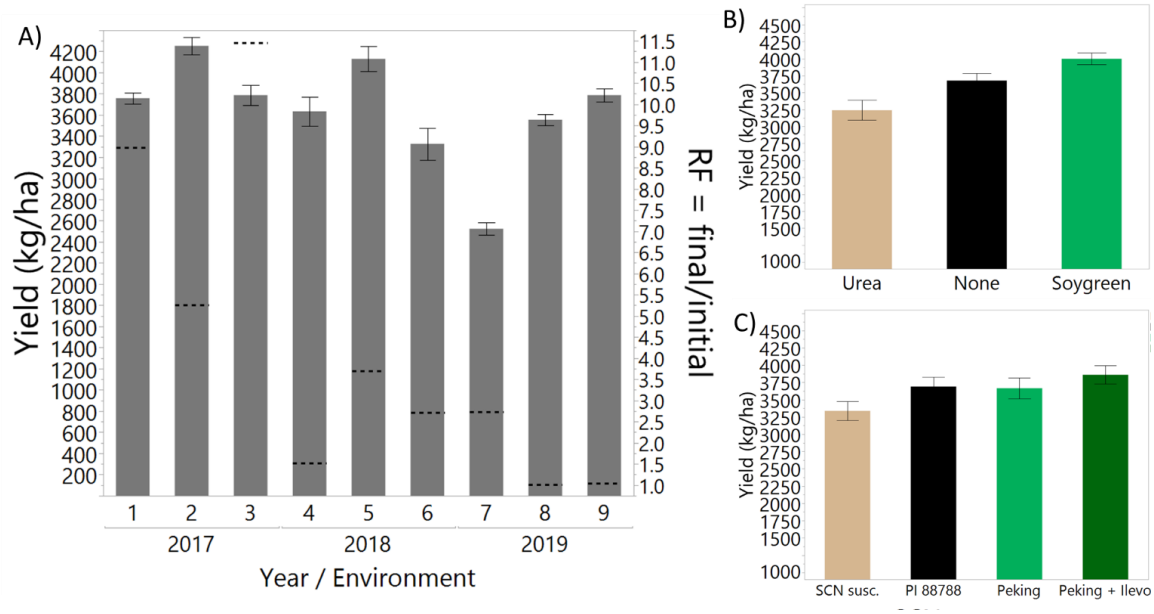

Figure 3-1. A) Yield (left) and reproduction factor (RF) (right) across nine environments. The mean yield (kg/ha) is represented by bars with corresponding standard error bars. The dashed line for each environment is the average RF of soybean cyst nematode (SCN) computed as the final egg count divided by the initial egg count. B) Yield by IDC application treatments of urea, no application, and soygreen averaged across all environments. C) Yield by SCN treatment of SCN susceptible, Peking resistance, PI 88788 resistance, and Peking resistance plus Ilevo treatment.

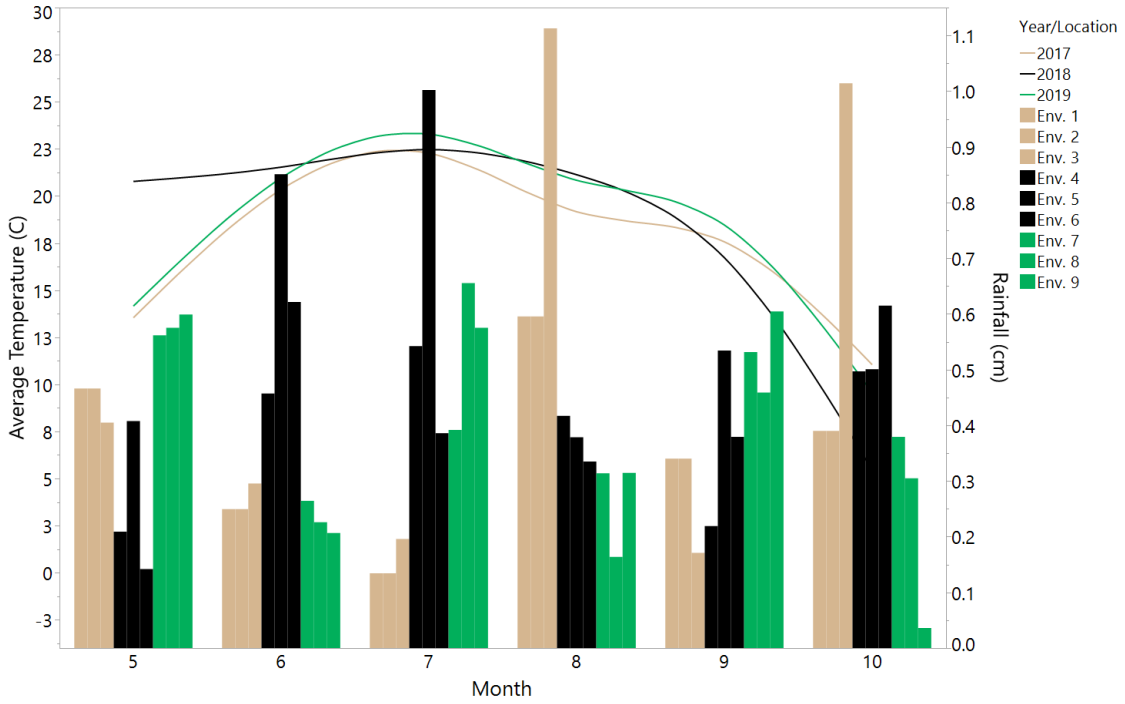

Figure 3-2. Rainfall and daily average temperatures for nine environments. Rainfall is represented as a sum of daily rainfall for each month (May – October, 5-10) for each of the nine environments signified by the bar charts. Daily mean temperature is represented for each of the three years as a smooth line fit across the same time period.

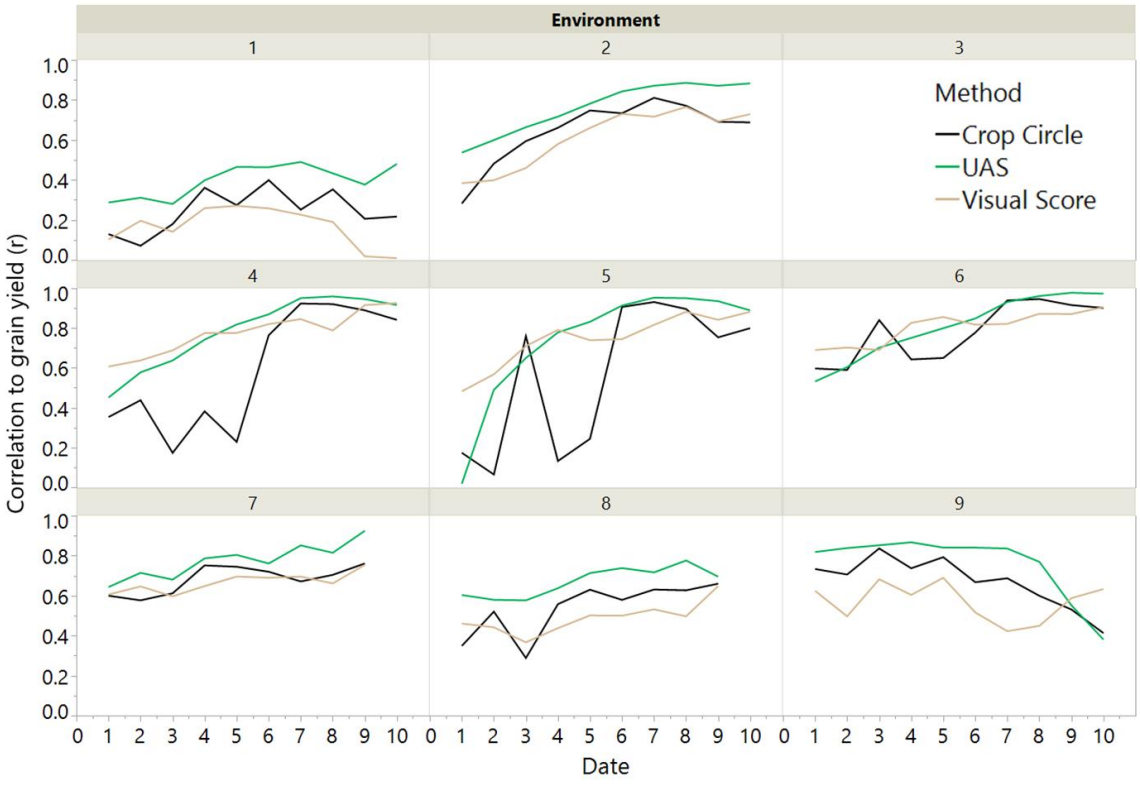

Figure 3-3. Pearson correlations between data collected approximately weekly and grain yield. Data was collected with an unmanned aircraft system (UAS) for passively sensed normalized difference vegetation indix (NDVI), Crop Circle for ground based actively sensed NDVI, and by visual scores taken on a 1-5 scale.

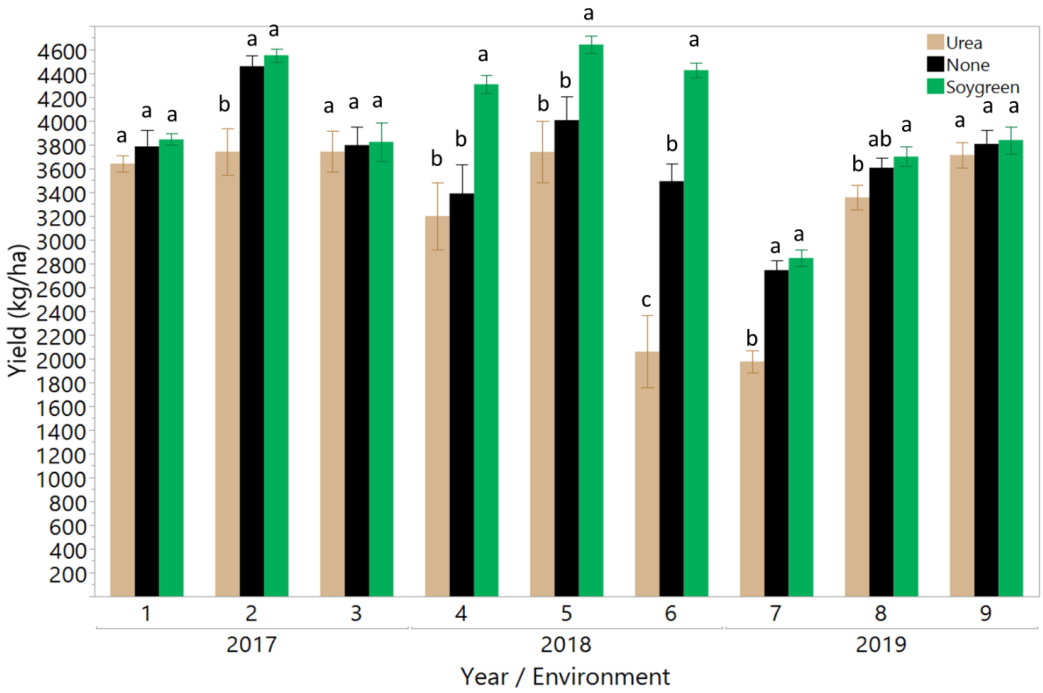

Figure 3-4. Yield differences by IDC application treatment across nine environments over the course of three years. Bars indicate the average yield for the three treatments of urea (tan bars), no application (black bars), and soygreen (green bars) as well as corresponding standard error bars. Letters not connected by the same letter are significantly different at $p<0.05$.

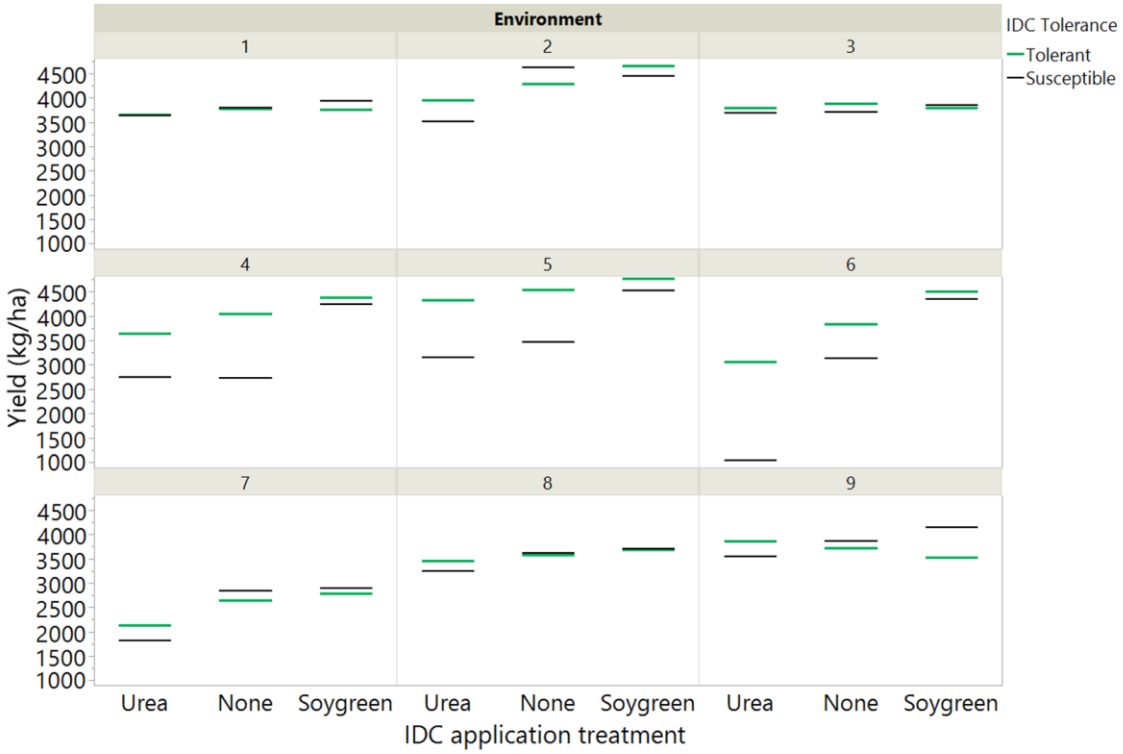

Figure 3-5. Iron deficiency chlorosis (IDC) genetic tolerance to IDC impact on yield. Green lines indicate the average yield among IDC tolerant soybean cultivars in each of the nine environments for each of the three treatments of urea, none, and Soygreen. Black lines indicate the average yield among IDC susceptible cultivars in each of the nine environments for each of the three treatments of urea, none, and Soygreen.

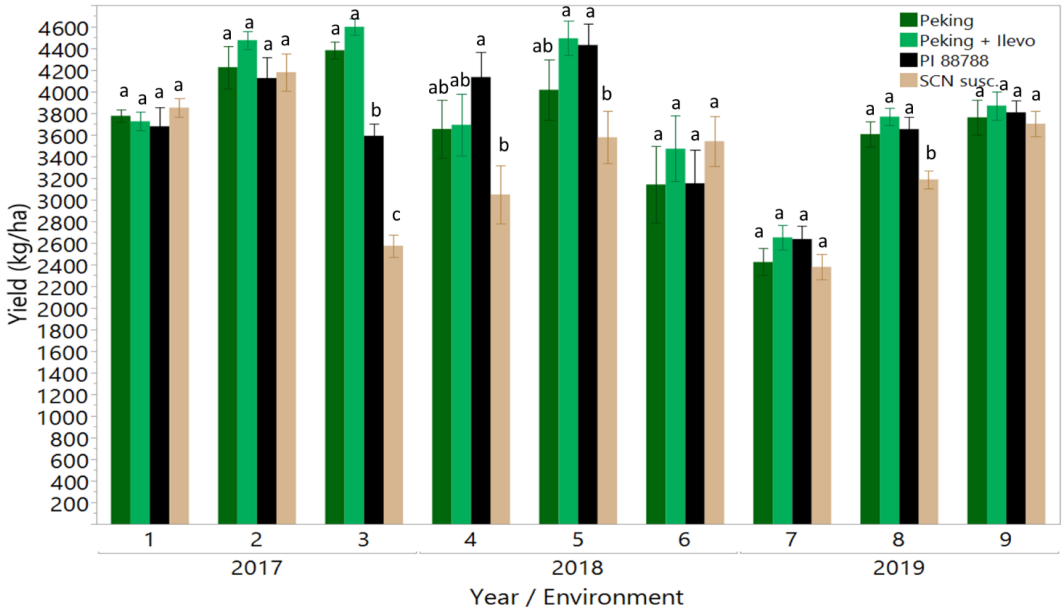

Figure 3-6. Yield differences by soybean cyst nematode (SCN) treatment. Soybean cyst nematode treatments include three levels of SCN varietal resistance including Peking, PI 88788, and Susceptible. In addition, a fourth treatment was included by adding a fungicide (active ingredient fluopyram) to the Peking sources of resistance with the goal of completely eliminating SCN pressure

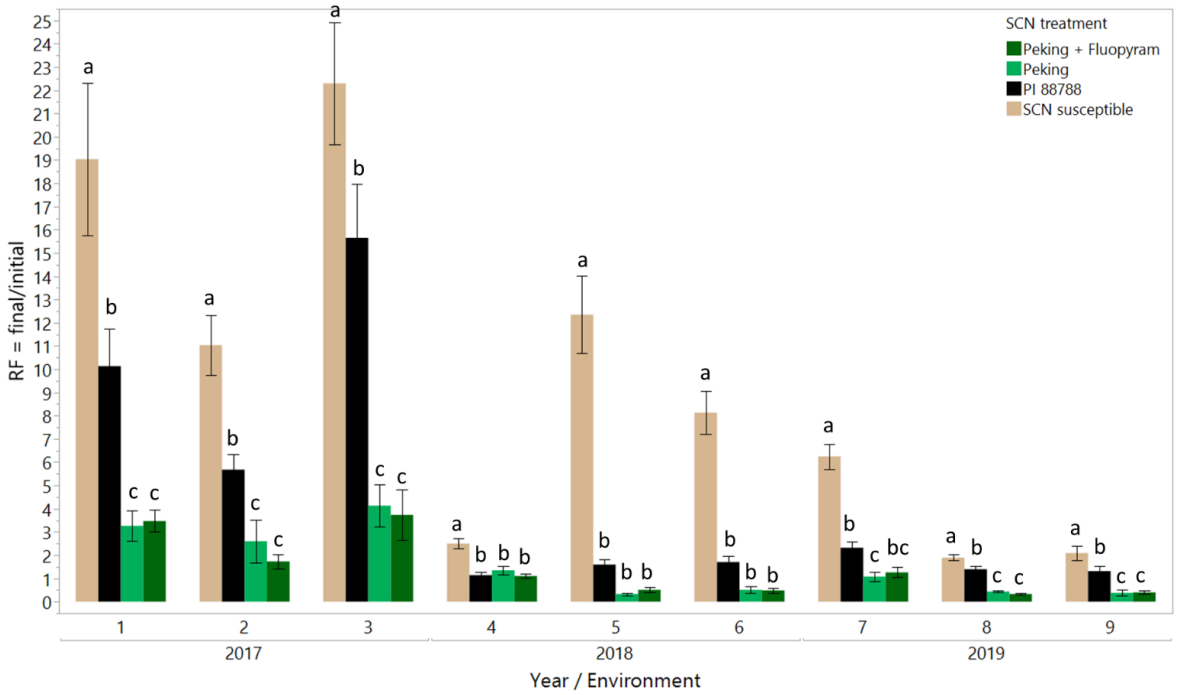

Figure 3-7. Reproduction factor (RF) differences by soybean cyst nematode (SCN) treatment across nine environments in three years. Soybean cyst nematode treatments include three levels of SCN varietal resistance including Peking, PI 88788, and Susceptible. In addition, a fourth treatment was included by adding a fungicide (active ingredient fluopyram) to the Peking sources of resistance with the goal of completely eliminating SCN pressure

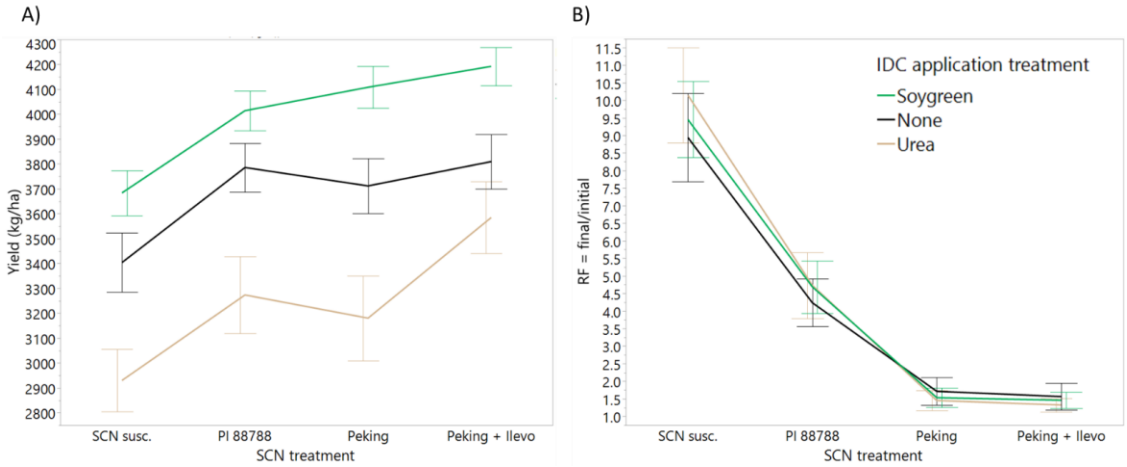

Figure 3-8. IDC and SCN interaction graph for yield (A) and reproduction factor (RF, B). The three levels of IDC application include Soygreen (green bars), no application (black bars), and urea (tan bars). The four levels of SCN treatment include SCN susceptible (SCN susc.), PI 88788 source of resistance, Peking source of resistance, and Peking + ILeVo.

Tables

Table 3-1. Soil chemical properties and SCN beginning of season counts. A total of nine environments (env.) were used in this study distributed throughout 6 different counties in Minnesota. The soils series and taxonomic class information of each field was collected using the Web soil survey. Soil pH, available nutrients, electrical conductivity, calcium carbonate equivalent, and organic matter were analyzed in a soil testing lab. Nematode egg counts per 100 CC of soil reported below consist of the average of four replications of initial season egg counts at each of the nine environments. Soil samples were also analyzed for HG type using Peking and PI 88788 indicator lines. The female index (FI) was calculated by dividing the mean number of females that developed on a indicator line by the mean number of females on the susceptible check multiplied by 100.

Env.	County	Soil Series	Taxonomic class	Planting Date	pH	Fe (mg/kg soil)	EC (mmhos/cm)	CCE (%)	OM	Olsen-P (mg/kg soil)	K (mg/kg soil)	Mn (mg/kg soil)	Zn (mg/kg soil)	Cu (mg/kg soil)	Nematodes (eggs/100CC)	Peking FI (±)	PI 88788 FI (*, ±)
1	Swift	Quam silty clay loam	Fine-silty	06/02/17	7.9	8.1	0.5	NA	6.8	16	189	5.5	1.3	1.4	422	1.7	18.7*
2	Swift	Bearden-Quam	Fine-silty	06/02/17	7.7	7.8	1.4	NA	4.9	25	432	10.6	4.9	1.6	1,700	3.9	6.3
3	Redwood	Normania loam	Fine-loamy	05/16/17	7.1	35.3	0.5	NA	5.6	NA	228	21.5	2.9	1.1	1,619	14.8±	13.6±
4	Swift	Bearden-Quam	Fine-silty	05/22/18	7.7	8.5	1.0	7.53	6.1	7	360	9.5	4.2	1.1	2,169	3.9	10.9*
5	Renville	Harps clay loam	Fine-loamy	05/24/18	7.8	9.3	1.3	14.3	6.1	16.5	181	10.1	2.5	1.4	756	0.6	8.4
6	Chippewa	Bearden-Quam	Fine-silty	05/16/18	7.7	8.5	1.4	8.41	7.4	20	288	8.6	2.7	1.5	1,269	2.1	22.7*
7	Redwood	Canisteo	Fine-loamy	06/08/19	7.7	11.53	2.3	13.6	5.4	NA	254	5.49	3.58	1.16	935	6.2	16.5*
8	Yellow Medicine	Canisteo	Fine-loamy	06/04/19	7.6	15.59	2.1	5.4	4.4	NA	267	3.25	5.06	1.11	4,753	1.9	58.5*
9	Swift	Bearden-Quam	Fine-silty	06/02/19	7.7	12.64	1.2	2.65	4.1	15	227	4.67	6.28	1.16	3,338	2.6	16.5*

* = female index greater than 10 on PI 88788, HG type 2

± = female index greater than 10 on both Peking and PI 88788, HG type 1.2

Table 3-2. Cultivar descriptions. A total of six cultivars were used in this study. Iron deficiency chlorosis (IDC) tolerance, soybean cyst nematode (SCN) resistance, and maturity group data was provided by the seed company.

Cultivar	Seed Company	IDC Tolerance Rating	IDC Tolerance Class	SCN Resistance	Maturity Group
S14-J7	Syngenta	2	Tolerant	Susceptible	1.4
PB-1611R2	Prairiebrand	5	Susceptible	Susceptible	1.6
AG1733	Asgrow	2	Tolerant	PI 88788	1.7
AG14X7	Asgrow	5	Susceptible	PI 88788	1.4
NuTech 7169	NuTech seed	4	Tolerant	Peking	1.6
NuTech 7186	NuTech seed	6	Susceptible	Peking	1.8

Table 3-3. Analysis of variance (ANOVA) for UAS-based NDVI. The ANOVA was used to test the fixed effects of the factorial arrangements of IDC treatment, IDC genotype, and SCN resistance level and their corresponding two and three-way interactions. All models included the random effect of block. A separate analysis was done for each environment as well as an across environment analysis (All sites)

	Environment									
Source	**1**	**2**	**3**	**4**	**5**	**6**	**7**	**8**	**9**	**All sites**
IDC application treatment	***	***	NA	***	***	***	***	***	NS	***
IDC Tolerance	NS	NS	NA	***	***	***	NS	NS	NS	***
IDC application treatment*IDC Tolerance	NS	*	NA	NS	NS	**	*	NS	***	***
SCN treatment	NS	NS	NA	NS	NS	***	NS	NS	NS	NS
IDC application treatment*SCN treatment	NS	NS	NA	NS	NS	NS	NS	NS	NS	NS
IDC Tolerance*SCN treatment	NS	NS	NA	NS	NS	***	NS	NS	*	NS

*= significant at $p < 0.05$
**= significant at $p<0.01$
***=significant at $p<0.001$

Table 3-4. Analysis of variance (ANOVA) for yield. The ANOVA was used to test the fixed effects of the factorial arrangements of IDC treatment, IDC genotype, and SCN resistance level and their corresponding two and three-way interactions. All models included the random effect of block. A separate analysis was done for each environment as well as an across environment analysis (All sites)

Source	Environment									All Sites
	1	2	3	4	5	6	7	8	9	
IDC treatment	NS	***	NS	***	***	***	***	**	NS	***
IDC tolerance	NS	NS	NS	***	***	***	NS	NS	NS	***
IDC treatment*IDC tolerance	NS	NS	NS	NS	NS	***	*	NS	***	***
SCN treatment	NS	NS	***	*	***	NS	*	***	NS	***
IDC treatment*SCN treatment	NS	NS	NS	NS	NS	NS	NS	NS	NS	NS
IDC Tolerance*SCN treatment	***	*	NS	NS	NS	**	NS	**	*	NS

*= significant at $p < 0.05$
**= significant at $p<0.01$
***=significant at $p<0.001$

Table 3-5. Analysis of variance (ANOVA) for reproduction factor. The ANOVA was used to test the fixed effects of the factorial arrangements of IDC treatment, IDC genotype, and SCN resistance level and their corresponding two and three-way interactions. All models included the random effect of block. A separate analysis was done for each environment as well as an across environment analysis (All sites)

	Environment									
Source	**1**	**2**	**3**	**4**	**5**	**6**	**7**	**8**	**9**	**All Sites**
IDC treatment	NS	NS	NS	NS	*	NS	NS	NS	NS	NS
IDC tolerance	NS	NS	NS	NS	NS	NS	NS	NS	*	NS
IDC treatment*IDC tolerance	NS	NS	NS	NS	NS	NS	NS	NS	NS	NS
SCN treatment	***	***	***	***	***	***	***	***	***	***
IDC treatment*SCN treatment	NS	NS	NS	NS	***	NS	NS	NS	NS	NS
IDC tolerance*SCN treatment	NS	NS	NS	NS	NS	*	NS	NS	NS	NS

*= significant at $p < 0.05$
**= significant at $p<0.01$
***=significant at $p<0.001$

Chapter 4 – Soybean Iron Deficiency Chlorosis Genome-wide Association Analysis of Temporal Changes in Chlorosis Severity

Summary

Iron deficiency chlorosis (IDC) is a major soil borne stress that causes significant yield reduction to soybean [Glycine max (L.) Merr.] in the Midwest. Iron deficiency chlorosis is a complex trait that varies both spatially and temporally, complicating screening of soybean lines for tolerance to IDC. Previous studies have successfully identified quantitative trait loci (QTL) associated with iron defficiency in soybean. To improve genome-wide association studies, more precise image-based phenotyping methods have proven successful in identifying smaller effect QTL that would otherwise be missed using visual scoring. With recent advancements in high-throughput phenotyping and the ability to capture data on thousands of plots more efficiently, the genetic control of traits that are expressed throughout a crops lifecycle can be studied more thoroughly. The goals of this study were 1) to determine the genetic basis of IDC tolerance using UAS- and ground-based phenotypes, 2) to determine if genetic variation exists for rate of recovery of IDC symptoms, and 3) discover QTL associated with rate of recovery. A panel of 348 soybean plant accessions was evaluated in five environments using both visual and UAS-based estimates of IDC severity. Using both phenotyping approaches, three significant QTL were found to be associated with IDC tolerance. Rate of recovery of IDC symptoms was measured and seven additional novel QTL were identified. Overall UAS estimates of IDC prove to be a valuable tool to reliably measure phenotypes at a higher temporal resolution than ever before. To date, this is the first ever genetic analysis performed on the rate of recovery to IDC stress.

Introduction

Iron deficiency chlorosis (IDC) is a major abiotic stress causing significant yield reduction to soybean [Glycine max (L.) Merr.]. An estimated 1.8 million hectares are impacted in the upper Midwest and losses due to IDC can add up to 260 million dollars annually (Hansen *et al.* 2004; Peiffer *et al.* 2012). Iron is abundant in almost all soils; however, deficiencies are caused by several soil chemical factors and their interactions that change the solubility of iron in the soil (Hansen *et al.* 2003). While there are several strategies to manage IDC, growing a soybean variety tolerant to IDC is preferred (Goos and Johnson 2000; Hansen *et al.* 2004; Goos *et al.* 2009; Liesch *et al.* 2011).

Soybean varieties show a range in response to IDC, with some being very tolerant to the stress, while others are highly sensitive. It has been shown, however, that no cultivar exists that is completely tolerant to IDC (Fehr 1982). Many studies have been conducted to identify quantitative trait loci (QTL) controlling IDC tolerance. The first study on the genetics of IDC in soybean, conducted in 1943, concluded that IDC tolerance is controlled by a single recessive gene (Weiss 1943). Many follow up studies, however, have shown that varietal IDC tolerance is a polygenic trait (Charlson *et al.* 2005; Wang *et al.* 2008; Mamidi *et al.* 2014b; Moran Lauter *et al.* 2014; Merry *et al.* 2019; Assefa *et al.* 2020b). A QTL on chromosome 03 has been reported as a major effect QTL in several coarse and fine mapping studies (Lin *et al.* 1997a, 2000; O'Rourke *et al.* 2007b, 2009; Severin *et al.* 2010; Mamidi *et al.* 2011, 2014b; Peiffer *et al.* 2012; Zhang *et al.* 2017b; Merry *et al.* 2019; Assefa *et al.* 2020a). In addition, several QTL

have been found throughout the soybean genome including QTL on *Gm*05/*Gm*06 (Merry *et al.* 2019), *Gm*20 (King *et al.* 2013), *Gm*05/*Gm*07/*Gm*16/*Gm*17/*Gm*18/ *Gm*19 (Mamidi *et al.* 2014), and *Gm*18/*Gm*20 (Zhang *et al.* 2017).

Screening of soybean lines for tolerance to IDC is a difficult task for plant breeders and researchers (Fehr 1982; Diers *et al.* 1992; Helms *et al.* 2010). Iron deficiency chlorosis is a complex trait that varies both spatially and temporally. Within a field site, symptoms can vary from non-existent in one area to very severe just meters away due to variations in soil properties (Rogovska *et al.* 2007). In addition, chlorotic symptoms will vary from one year to the next and within a given growing season, all in relatively unpredictable manner (Naeve and Rehm 2006; Bloom *et al.* 2011). It has been shown that the relative genotypic tolerance to IDC is not affected by the date of severity note recording, however, this was only studied with relatively few genotypes (Naeve and Rehm 2006). Given the time requirements to acquire reliable phenotype data on IDC symptoms, no studies to our knowledge have studied the temporal changes in IDC severity, often only relying on individual or very few time points of data collection (Mamidi *et al.* 2011; Merry *et al.* 2019; Assefa *et al.* 2020b).

The genetic control of traits that are expressed throughout a crops lifecycle have been reported in several systems. The genetic architecture of traits such as drought stress response, leaf area, biomass, height, plant volume, canopy coverage, and others have been studied (Wu *et al.* 2004; Chen *et al.* 2014; Neilson *et al.* 2015; Sun *et al.* 2017; Xavier *et al.* 2017; Sagan *et al.* 2019; Moreira *et al.* 2020). In a greenhouse experiment

for sorghum, for example, high-throughput phenotyping (HTP) data collected through the plant's growth cycle was used identify individuals with traits contributing to stress tolerance (Neilson *et al.* 2015). In soybeans, an unmanned aircraft system was used to study the genetic architecture of canopy coverage at different plant growth stages, suggesting that average canopy coverage is a highly heritable trait that could be used for indirect selection of yield (Xavier *et al.* 2017). In cotton, a field based HTP system was used to study the genetic basis of stress-adaptive traits taken at different time points (Pauli *et al.* 2016a).

Image-based scoring of IDC via an unmanned aircraft system (UAS) can provide researchers the opportunity to study the dynamic response of IDC at a high temporal resolution (Dobbels and Lorenz 2019). The goals of this study, therefore, were 1) to determine the genetic basis of IDC tolerance using UAS- and ground-based phenotypes, 2) to determine if genetic variation exists for rate of recovery of IDC symptoms, and 3) discover QTL associated with rate of recovery.

Materials and Methods

Plant material

A diverse panel of soybean accessions was assembled from the USDA Germplasm Collection as described by Virdi et. al. (2021). Briefly, from the 14,430 unique soybean accessions in the USDA Soybean Germplasm Collection, 1271 belong to soybean maturity group 1 (MG1) (Bandillo et al., 2015). Of the 1271 accessions of MG1, a set of 400 was sampled to maximize the genetic variation in the MG1 accessions

using a supersaturated design (Eskridge *et al.* 2006) as implemented by Jarquin et al. (2021). This panel of 400 lines was previously used to study traits such as canopy architecture, shoot architecture, and branch angle (Virdi et al., 2021). A subset of 348 lines from the panel of 400 was selected and used in this study based on seed availability.

Research environments

Four research environments over two years were used for field evaluation of IDC severity. The locations for this study included a field site near Danvers, MN (45.274285, -95.718046) in Swift County during the 2018 and 2019 growing season; a field site near Glyndon, MN (46.900237, -96.528783) in Clay County in 2019; and a field site near Eldred, MN (47.695160, -96.807550) in Polk County in 2019. Field environments herein will be referred to as DA18, DA19, EL19, and GL19 for the four environments of Danvers, 2018; Danvers, 2019; Eldred, 2019; and Glyndon, 2019 respectively. All fields were reported as having a history of soybean IDC stress based on farmer cooperator knowledge and soil tests conducted previously at each site to confirm the presence of IDC symptoms. All sites were rotated between corn and soybean crops for several previous years.

Each soybean accession was planted as a single row 91cm in length at DA18 and DA19, 61cm in length at EL19, and as hill plots at GL19. All plots at each location were planted 76.2 cm apart. Plot sizes ranged in length due to available equipment with cooperators. Plots were arranged in a randomized complete block design with two replications for DA18 and were planted as randomized single replication trials in all 2019

locations. Plots were planted on May 22 for DA18; May 30 for DA19; July 13 for EL19; and July 22 for GL19. Accumulated rainfall data was downloaded from the High Plains Regional Climate Center for each environment (HPRCC, Lincoln, NE, https://hprcc.unl.edu/).

Field evaluation of iron deficiency chlorosis

Soybeans were visually scored for IDC symptoms using a 1-5 visual rating scale. A rating of "1" is given to a plot that is 100% green (no yellowing), a score of "2" indicates slight yellowing with some plants in the plot turning yellow, a score of "3" indicates moderate yellowing with most plants turning yellow in the plot, a score of "4" indicates intense yellowing where all plants are yellow and some are becoming stunted and necrotic, and a score of "5" indicates most severe IDC symptoms where the entire plot is damaged and dying or completely dead (Cianzio *et al.* 1979; Mamidi *et al.* 2014a). Each plot was measured by an expert rater who understands IDC stress symptoms.

An unmanned aircraft system (UAS) was used to measure IDC severity symptoms according to previously published procedures (Dobbels and Lorenz 2019). Red, green, blue (RGB) images were captured using cameras equipped to a UAS. Based on each environment, flights were performed on different dates with a target frequency of one flight per week (Table 4-1). In DA18 and DA19, flights were performed approximately weekly for nine weeks starting in early June. For EL19 and GL19, only four flights were conducted at each location (Table 4-1). In addition, RGB images were captured with different cameras and aircraft systems. An Inspire 1 (SZ DJI Technology Co., Ltd,

Shenzhen, China) UAS equipped with a Sentera Double 4k sensor (Sentera, Minneapolis, MN) was flown at the DA18 and DA19; an Inspire 1 UAS equipped with a Zenmuse X3 camera was used at GL19; and a Phantom 4 professional drone was used at EL19. Flights were conducted at various altitudes to ensure sufficient ground sample distances (GSD) for corresponding plot sizes (Table 4-1). Flights were programmed using autonomous flight paths with 80% side and end lap using the Pix4D capture application downloaded on an Apple iPad device.

Image analysis was performed similar to Dobbels and Lorenz (2019). Raw images were first processed using Pix4D Desktop (Pix4D, SA) to generate orthomosaics with a UTM zone 15N projected coordinate system. Ground control points were input into the Pix4D projects to ensure proper geometric accuracy. Ground control points were manually identified in the basic editor of Pix4D software prior to initial processing.

To estimate IDC severity, the orthomosaics were processed in Erdas Imagine software (Hexagon Geospatial, United States). First, pixels were classified into "plant" and "soil" classes using k-means clustering, followed by the classification of green, yellow, and brown plant pixels within the plant classified canopy. In QGIS software (QGIS Geographic Information System. Open Source Geospatial Foundation Project, http://qgis.osego.org), a polygon shapefile was created to delineate the region of interest around each plot. In order to mimic how researchers rate IDC severity, the proportions of green, yellow, and brown pixels were extracted from the region of interest using the zonal statistics plugin of QGIS (Dobbels and Lorenz 2019).

The UAS-based estimate of IDC severity was calculated using the random forest algorithm (Breiman 2001). The visual score data was treated as a character and 67% of the data, at random were used to train the model, while the remaining 33% of the data were used for validation. For flights where ground notes were not obtained, visual score data were generated from visual observations of drone imagery on a computer. Random forest was implemented using the predictive analytics software package within JMP Pro (JMP®, Pro 13, SAS Institute Inc., Cary, NC, 1989-2007).

In order to create a continuous severity score, output of the random forest model was used. Since a visual score of a "one" would indicate 0% severity and a visual score of a "five" would indicate 100% severity, the following equation was used to estimate IDC severity based on the random forest output.

$$\textit{IDC Severity Score} = 25\times P(y=2) + 50\times P(y=3) + 75\times P(y=4) + 100\times P(y=5) \quad (1)$$

where y represents the IDC score on a 1-5 scale as described above, and $P(y=k)$ represent the probability a plot was given a score of k according to the random forest model. Using equation 1, a IDC severity score ranging from zero to 100 was calculated for each plot.

Phenotypic data analysis

Spatial analysis on all IDC scores was performed in each of the four environments using P-spline mixed models (Currie and Durban 2002; Rodríguez-Álvarez *et al.* 2015; Velazco *et al.* 2017). The SpATS R package (Velazco *et al.* 2017) was used with genotype, plot row, and plot column each fitted as a random effect. Using the SpATS

model, trends in field spatial variation of iron deficiency chlorosis severity were modelled by a smooth bivariate function of the spatial coordinates (row and column) represented by 2D P-splines (Velazco *et al.* 2017). The output of the SpATS model was a spatially adjusted IDC score for each plot.

Two critical time-points were identified in each environment: 1) the initial onset of IDC severity (approximately 30-40 days after planting) as well as 2) the recovery of IDC severity defined as a separate independent scoring of IDC approximately 14 days after the initial IDC assessment. These two ratings, herein, will be referred to as "flash IDC score" and "recovery IDC score" and the dates of these scores in each environment are indicated in Table 4-1 by the "†" and "‡" symbols for flash and recovery, respectively.

To determine if there was genetic variation for rate of recovery, a subset of environments and a subset of soybean accessions were used from the entire dataset. First, DA18 rep 2 was omitted from the dataset as this environment showed a lack of chlorosis symptoms based on field spatial variability. Second, the research locations of EL19 and GL19 were omitted as they were planted in the middle of a typical growing season. Accessions that were scored as a "one" or a "five" during the flash IDC score evaluation for any plot were omitted as these plots, by definition, cannot display any rate of recovery. These were excluded so that limitations in scale did not confound the genetic analysis. The final dataset for testing rate of recovery consisted of 96 soybean accessions measured approximately weekly in two environments – DA18 and DA19. Temporal

trends of IDC severity were analyzed using all UAS missions within each of these two remaining environments. A linear relationship between IDC score and days after planting was modeled for every plot within each environment on the sub. The slope coefficient for each linear model fitted to each plot was extracted. This slope coefficient, herein, will be referred to as the "rate of recovery."

In order to calculate the reliability of accessions means, variance components were estimated using the following model:

$$y_{ij} = \mu + g_i + e_j + \varepsilon_{ij} \quad (2)$$

where y_{ij} is the response variable (flash IDC, recovery IDC scores from ground and UAS estimates, and rate of recovery), μ is the overall mean, g_i is the effect of the i^{th} soybean accession, e_j is the effect of the j^{th} environment, and ε_{ij} is the residual. To calculate reliability, all effects were considered to be random except for the effect of environment. Variance components from (2) were used to estimate reliability for each trait as:

$$i^2 = \frac{Vg}{Vp} = \frac{Vg}{Vg + V\epsilon/loc} \quad (3)$$

where i^2 is the reliability estimate, V_g is the variance component due to soybean accession and V_p is the variance component due to environments also defined as V_g + residual variance divided by number of locations. All analyses were performed in R version 3.6.3 and the lme4 package (R Core Team, 2013, Vienna, Austria).

Genome-wide association analysis

All soybean accessions were genotyped using the Illumina Infinium SoySNP50K BeadChip described previously (Song *et al.* 2013). Single nucleotide polymorphism data was obtained from Soybase (https://soybase.org/snps/) and converted to marker scores of -1, 0, and 1 for aa, Aa, and AA, respectively. Additionally, markers with a minor-allele frequency of less than 0.025 and markers with a threshold of 0.025 missingness were removed. All genomic positions of markers reference the Wm82.a2.v2 genome assembly (Song *et al.* 2016). Genome-wide association analysis was conducted using the *GWAS* function within the *rrBLUP* package version 4.6; (Endelman, 2011). The P3D option was set to "TRUE" so that variance components were estimated by REML only once. The number of principal components to account for population structure and to be included as fixed effects in the model was repeated with five different levels. No changes in associations across different numbers of principal components was observed and therefore the final number of principal components was set to three, which is similar to previous studies (Merry *et al.* 2019). Genome-wide association analyses were performed using spatially-adjusted IDC scores averaged across environments for UAS IDC severity, ground-based visual assessments, and rate of IDC recovery.

To declare statistically significant associations between SNPs and phenotypes, a genome-wide significance threshold was determined based on the 'effective number' (M_{eff}) of independent tests (Cheverud 2001; Li and Ji 2005; Bandillo *et al.* 2015). Briefly, the correlation matrix and eigenvalue decomposition among filtered SNPs

(32,910) were calculated to determine M_{eff}. M_{eff} was calculated to be 520. Using the experiment-wise error rate (α_e) of 0.05, the marker significance threshold was calculated as $-\log_{10}(1-(1-\alpha_e)^{\wedge 1/Meff}) = 4.00$. Quantitative trait loci (QTL) were defined by a 500 kilobase (kb) window to define SNPs tagging a locus, similar to previous studies (Bandillo *et al.* 2015).

Results

Phenotyping results and spatial trends

A total of four environments were used to evaluate the IDC severity of 348 diverse MG1 soybean accessions. IDC symptoms were measured using both visual scores on a 1-5 rating scale as well as IDC severity measured on a continuous 0-100 scale using a UAS image-based rating system. The range in flash IDC score across environments as well as the coefficient of determination between UAS estimates and ground visual measurements can be found in Figure 4-1. The coefficient of determination between UAS estimates and visual assessments varied from 0.45 to 0.75 among the four environments, with an average coefficient of determination of 0.60. In addition, the environments exhibited a range in severity symptoms. The average UAS severity for flash IDC score was 6.6%, 36.9%, 39.3%, and 50.4% for DA18; GL19; DA19; and EL19; respectively.

For all environments, there existed spatial trends in both flash IDC scores and recovery IDC scores. Figure 4-2 shows a graphical representation of the flash IDC score fitted spatial trend for each of the five environments, as obtained from the SpATS

package. Reliability (i^2) was calculated for flash and recovery IDC scores for both UAS and visual ratings. In addition, i^2 was assessed before and after using spatially-adjusted scores from the SpATS output (Table 4-2). Reliability was increased for all measurements when using spatially-adjusted scores compared to those not spatially adjusted. Based on this finding spatially-adjusted plot scores were used for all downstream analyses.

Temporal dynamics of iron deficiency chlorosis severity

Soybean IDC ratings were taken at multiple time points within each environment to assess the temporal dynamics of IDC severity symptoms (Table 4-1). The average IDC score of the 348 plant introgression lines in each environment was plotted against days after planting to examine changes in symptoms over time (Figure 4-3). In addition, precipitation patterns were overlaid as bars to provide insight into the influence of this factor on variation in IDC scores across time.

The temporal dynamics of IDC stress was also assessed by examining the progression of severity for each of the five classes of IDC flash scores (Figure 4-4). By breaking the analysis into groups based on flash IDC score, we can better delineate IDC severity changes across time (days after planting). Figure 4-4 shows that plots with initial ratings of "5" tended to remain severely stressed, with the exception of the Glyndon, 2019 location. In addition, the plots rated as healthy early in the season tended to remain healthy, with the exception of the Eldred, 2019 location.

The relationship between IDC score and days after planting was modeled for every plot within each environment using a simple linear model. A subset of these environments and a subset of the soybean accessions were used to test for genetic variation in the rate of recovery to IDC stress. The average rate of recovery in DA18 was 0.008 units decrease in IDC score per day, and the average rate of recovery in DA19 was 0.023 units decrease in IDC score per day. The range in rate of recovery was -0.08 to 0.06 in DA18, and -.06 to 0.017 in DA19. A significant difference among soybean accessions was found for rate of recovery ($p<0.05$) and the reliability (i^2) for rate of recovery across these environments was 0.41.

Significant QTL for iron deficiency chlorosis tolerance and rate of recovery

Genome-wide association analysis was performed using the mean IDC score across environments both for UAS IDC severity and ground-based visual assessments of the spatially adjusted values. Table 4-3 highlights the significant SNPs associated with IDC tolerance along with their associated SNP ID, chromosome, position (bp), and association ($-\log_{10}(p)$ values) for spatially adjusted UAS flash and recovery scores as well as spatially-adjusted visual flash and recovery scores. In order to declare significantly associated SNPs, a genome-wide significance threshold was set to 4.00 based on the effective number of independent tests (Li and Ji 2005).

Significant SNPs were identified using all four measurements of IDC. A total of ten, eight, fourteen, and nine QTL were declared significantly associated with UAS flash score, UAS recovery score, visual flash score, and visual recovery score, respectively

(Table 4-3). The most prominent SNP, *Gm03* (SNP ss715585469), was consistent for each assessment of IDC. In addition, significant QTL were identified on *Gm09* (ss715604418) and *Gm05* (ss715592610). A total of ten overlapping SNPs were identified for UAS and visual flash score estimates, and eight overlapping QTL for recovery IDC score. It is worth noting, however, that for the flash stage of measurements, the QTL on *Gm05* using visual score measurements that was not detected using the UAS-based measures of IDC symptoms. It is also interesting to note that flash and recovery measurements identified similar QTL, however, the recovery measurement identified one less QTL compared to the flash score.

For rate of recovery, five QTL were declared significant [-log(p) > 4.00] (Table 4-4). These QTL are located on five chromosomes (*Gm02*, *Gm14*, *Gm16*, *Gm18*, and *Gm19*) and none of these QTL correspond with the QTL identified in either the flash or recovery IDC scores. Within the genomic regions of interest, the genes and descriptions based on the Williams 82 reference genome are listed (Table 4-5). From this table, no gene was found that has an obvious indication of being related to soybean IDC or rate of recovery. In addition, none of these genes appear in previous QTL mapping studies for IDC tolerance.

Further investigation was conducted to explore the temporal trends in IDC score of the groups of lines containing the "+1" and "-1" alleles at each of the significant SNP positions (Figure 4-5). The five panels in Figure 4-5 represent the *Gm02*, *Gm14*, *Gm16*, *Gm18*, and *Gm19* alleles for the A, B, C, D, and E panels, respectively. Green lines

indicate the "-1" allele for each SNP and the tan lines represent the "+1" allele for each SNP. From this figure and from the analysis of rate of recovery, certain genotypes recover at a faster rate than other genotypes. In some cases, accessions that are rated as more severe compared to other accessions early in the season actually recover to the extent of being less severe by the end of the season.

Discussion

Iron deficiency chlorosis is an important problem to soybean production in the Midwest, impacting an estimated 1.8 million acres (Hansen *et al.* 2004). While growers have several options for managing IDC, the best option is to plant soybean cultivars with varietal genetic tolerance (Goos and Johnson 2000). Many studies have been conducted to increase our understanding of the genetics underlying IDC, however, these studies have relied on individual or only a few measurements during the growing season (O'Rourke *et al.* 2007b; Mamidi *et al.* 2011, 2014a; Zhang *et al.* 2017b; Merry *et al.* 2019). With recent advances in high-throughput phenotyping (HTP), researchers are now able to study the temporal variation in chlorosis symptoms to increase our understanding of QTL underlying tolerance at different time points of stress, as well as the variation in the rate at which different soybean accessions recover to IDC stress (Dobbels and Lorenz 2019). This study set out to examine the genetics underlying IDC tolerance and to test for genetic variation of the rate of recovery from stress conditions.

Genetics of flash and recovery severity symptoms:

Genome-wide association analysis on a diverse panel of 348 soybean plant accessions identified significant QTL on *Gm03*, *Gm05*, and *Gm09* of the soybean genome. The SNP with the highest association to IDC scores was found on *Gm03*. Several previous studies have also identified this QTL for IDC tolerance (Lin *et al.* 1997, 2000; O'Rourke *et al.* 2007, 2009; Severin *et al.* 2010; Mamidi *et al.* 2011, 2014b; Peiffer *et al.* 2012; Zhang *et al.* 2017; Merry *et al.* 2019; Assefa *et al.* 2020). Since Lin *et al.* (1997), several fine mapping, genome-wide association analyses, genome-wide epistatic analyses, hydroponic studies, and others have been used to identify the underlying mechanism for this QTL (O'Rourke *et al.* 2007b, 2009; Severin *et al.* 2010; Mamidi *et al.* 2011, 2014b; Peiffer *et al.* 2012; Zhang *et al.* 2017b; Merry *et al.* 2019; Assefa *et al.* 2020a). In a recent study, researchers dissected the QTL on *Gm03* into four distinct genomic intervals harboring multiple candidate genes (Assefa *et al.* 2020a). In our study, this historical QTL on *Gm03* was identified in all environments, even in Danvers, 2018 when very few symptoms were apparent in the IDC nursery. The *Gm03* QTL was also identified at multiple time points through the growing season. While this QTL is of high importance to genetic studies and for researchers to gain a better understanding of the underlying gene networks and pathways involved in IDC tolerance, it was shown that this QTL is not an important source of genetic variation among elite breeding lines (Merry *et al.* 2019).

Additional QTL were also identified during the flash and recovery scoring of IDC on *Gm05* and *Gm09* (Table 4-3). The QTL identified on *Gm05* corresponds with previous studies on IDC in which the QTL was identified in both a plant introduction panel and in the USDA Northern Regional Trials panel of soybean genotypes (Merry *et al.* 2019). In addition, this QTL was fine mapped in a Fiskeby III x Mandarin (Ottawa) population and the final mapped interval of this QTL resides between 0 and 137,207bp on *Gm05* which contains 17 putative gene models (Merry *et al.* 2019). The other significant QTL, to knowledge, has not been identified in IDC tolerance. While it has not yet been studied, the ss715604418 SNP at 43614074 bp on Gm09 resides on a gene model (Glyma.09g212100.Wm82.a2.v1). The homolog of this gene in Arabidopsis (AT4G19040.1) is known to be involved in enhanced disease resistance to pathogenic fungi (Soybase.org). This QTL may warrant further investigation.

Genetic variation for rate of recovery:

Temporal variation within each environment was also apparent. In three of the four environments tested, there was an average decrease in severity symptoms as the days after planting increased. In one environment (EL19), however, the severity increased over the four time points of data collection. Soil water content influences iron in solution due to changes in aeration and carbon dioxide concentrations (Clark 1982; Rogovska *et al.* 2007). In addition, rainfall patterns have been useful in modeling IDC severity (Kaiser *et al.* 2014). We hypothesized that increases in rainfall would thus drive an

increase in IDC severity. It appears that the EL19 may have experienced consecutive rainfall events that may have been associated with an increase in IDC symptoms.

Soybean IDC is also impacted by the amount of NO_{3-} in the soil (Bloom *et al.* 2011b; Kaiser *et al.* 2011). When a plant uptakes NO_{3-}, it does this in exchange of a bicarbonate ion which neutralizes the soil pH. This soil NO_{3-} impact on soybean IDC may explain why wheel tracks in a soybean field are green and also explains why companion crops can be used to reduce IDC by using excess nitrogen build up in the soil (Naeve 2006; Kaiser *et al.* 2014). It may be the case that the growth or lack of growth of soybean roots and plant biomass could cause in-season variation to IDC symptoms, however, it appears that few studies have actually analyzed the temporal dynamics of the rates of IDC recovery. Perhaps this could be an avenue of future research to better select varieties tolerant to IDC stress.

Recent advances in remote sensing and high-throughput phenotyping (HTP) affords researchers the opportunity to collect data more frequently during the span of the growing season (Dobbels and Lorenz 2019). In the case of IDC, studies have shown that symptoms tend to decrease towards the end of the growing season, indicating a recovery from IDC symptoms (Naeve and Rehm 2006). No studies, however, have quantified rates of IDC recovery nor the genetics of the rate of recovery. The study presented here aimed to quantify the rate of recovery as the linear relationship between IDC severity and days after planting and test if genetic variation exists for this trait.

The rate of recovery was initially studied using all available genotypes and environments, however, sub-setting the data was necessary to find a genetic signal for this phenotype. The sub-setting was mainly performed to exclude environments that showed no symptoms of IDC and to exclude environments where not enough temporal information was collected. The environments at EL19 and GL19 were planted extremely late (July 13/July 22) and excluding these environments to examine temporal effect of IDC was appropriate as they don't reflect typical soybean planting dates. In addition, soybean plots that were very healthy during the flash score (score = one) or plots that were very stressed during the flash score (score = five) showed no changes in IDC severity and were also excluded for this analysis (Figure 4-4).

The reliability estimate of rate of recovery was estimated to be 0.41. When comparing this estimate to both the flash and recovery ratings individually, it appears this traits has a slightly lower reliability. However, significant differences among soybean accessions were found for the rate of recovery (p value <0.05). In addition, GWAS identified seven SNPs on five chromosomes that were significantly associated with rate of recovery (Table 4-4).

The seven SNPs for rate of recovery were found on *Gm02*, *Gm14*, *Gm16*, *Gm18*, and *Gm19* (Table 4-4). None of these QTL overlapped with significant QTL identified at individual time points of flash or recovery score. In addition, it appears that none of these QTL have been identified in previous QTL mapping studies for IDC. Further investigation was performed to look at soybean accessions carrying the homozygous

alleles ("+1" and "-1") by investigating the temporal patterns of these accessions (Figure 4-5). While researchers have investigated IDC severity early in the season, it is worth pointing out that certain genotypes recover at a faster rate than other genotypes. In the case of the *Gm18* allele (Panel D, figure 4-5), for example, the soybean accessions carrying the "-1" allele recovered to the extent that by the end of the growing season, lines carrying this allele had lower severity symptoms compared to lines carrying the "+1" allele, on average. It would be worth investigating the effect this phenomena would have on seed yield, however, no yield data was collected for these small research plots.

Limitations and future directions:

The results of this study provides insights on the use of modelling temporal trends combined with HTP data to improve GWAS related to soybean iron deficiency chlorosis. In this study, QTL were identified for both flash and recovery IDC scores as well as new QTL for the rate of recovery. The results of this study provides insights on possible future research studies that could be conducted. To start, the success of the UAS-based measurements of IDC affords many possibilities. Future research could be conducted in more environments with more replications within each environment.

The rate of recovery phenotype in this study was based on a linear relationship between IDC score and days. It would be interesting to also test other quadratic or non-linear models for rate of recovery. Finally, none of these research trials were harvested for grain yield. It would be interesting to see the relationships between the flash IDC score, the recovery IDC score, the rate of recovery, and grain yield. The research plots

were not harvested because all plots were planted as small plots to reduce field space requirements. A subset of soybean accessions, however, could be tested in larger plots in future research studies.

Conclusions

The goals of this study were to 1) to determine the genetic basis of IDC tolerance using UAS- and ground-based phenotypes, 2) to determine if genetic variation exists for rate of recovery of IDC symptoms, and 3) discover QTL associated with rate of recovery. A total ten SNPs were identified and overlapping between both UAS-based and visual estimates of IDC stress and both of these phenotypes provided estimates with similar reliability. Second, genetic variation was found for the rate of recovery. It was found in this study that some genotypes recover from IDC symptoms more rapidly than other genotypes. Based on this genetic variation for rate of recovery, five additional QTL were identified. These additional QTL may serve as candidates for further investigation to confirm their effect on both IDC tolerance and seed yield.

Tables and Figures (Chapter 4 IDC GWAS)

Table 4- 1. Environments and unmanned aircraft system (UAS) flight dates and flight parameters. Four locations were used to assess iron deficiency chlorosis (IDC) tolerance of 348 soybean accessions. To quantify temporal patterns of IDC stress, flight missions were conducted across nine dates for Danvers in 2018 and 2019, and across four dates for Eldred and Glyndon in 2019. In addition, three separate UAS's were used in this study and flight altitudes were adjusted based on UAS camera and plot size of each location.

Env.	Drone/camera	Flight alt.	GSD (cm)	Planting date	1	2	3	4	5	6	7
DA18	Inspire 1/Sentera Double 4K	61 m	1.76	5/22	6/21	6/27	7/05†	7/12	7/17‡	7/26	7/31
DA19	Inspire 1/Sentera Double 4K	61 m	1.76	5/30	6/19	7/1	7/15†	7/22	7/29‡	8/06	8/13
EL19	Phantom 4 Pro	46 m	1.22	7/13	8/9	8/14†	8/19	8/26‡			
GL19	Inspire 1 Zenmuse X3	18 m	0.83	7/22	8/9	8/14†	8/20	8/25‡			

†Date of flash score
‡Date of recovery Score

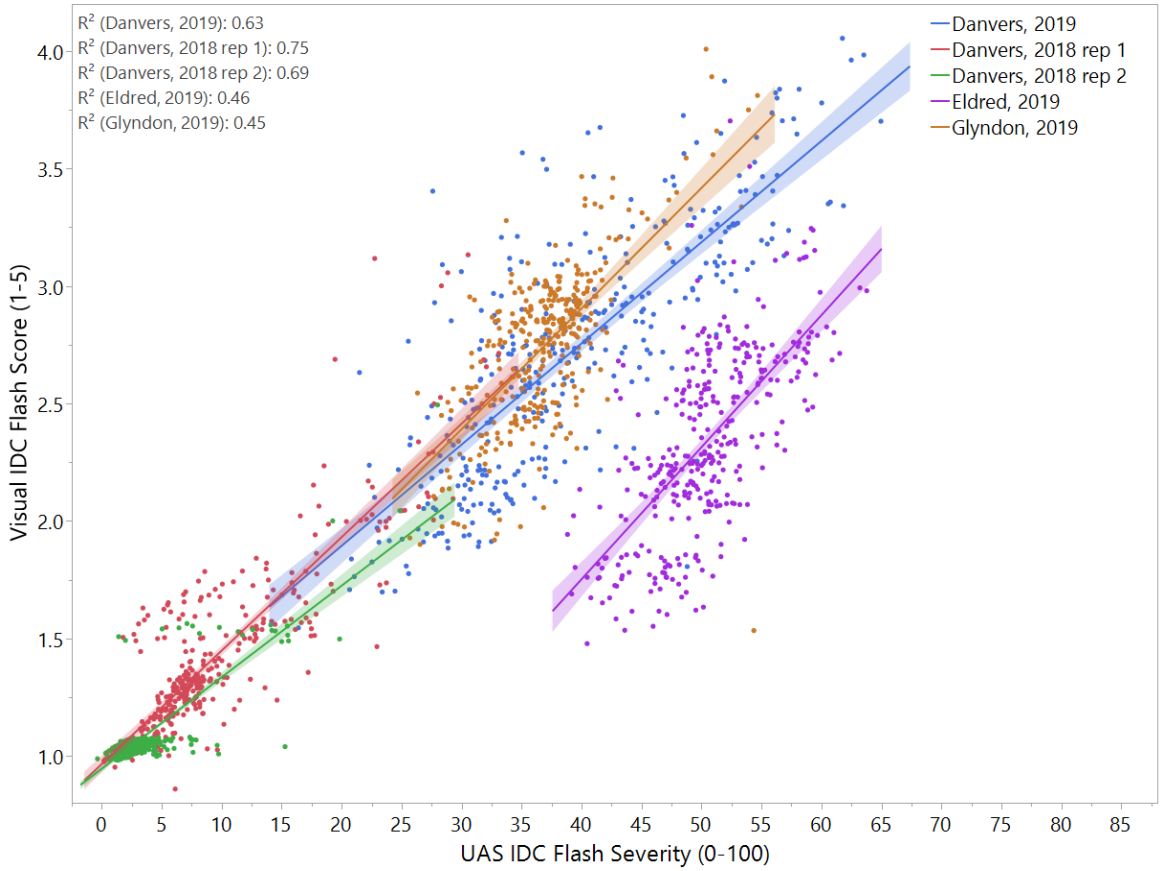

Figure 4-1. Flash IDC visual score vs. flash UAS severity score. A total of five trials (Four single replication environments plus one two replication environment) are indicated by the marker/fitted line color and were evaluated for IDC using two methods: visual assessment taken on a 1-5 scale (y-axis) and UAS severity score (0-100, x-axis). The coefficient of determination (R^2) was also determined for the linear regression model between visual and UAS estimates.

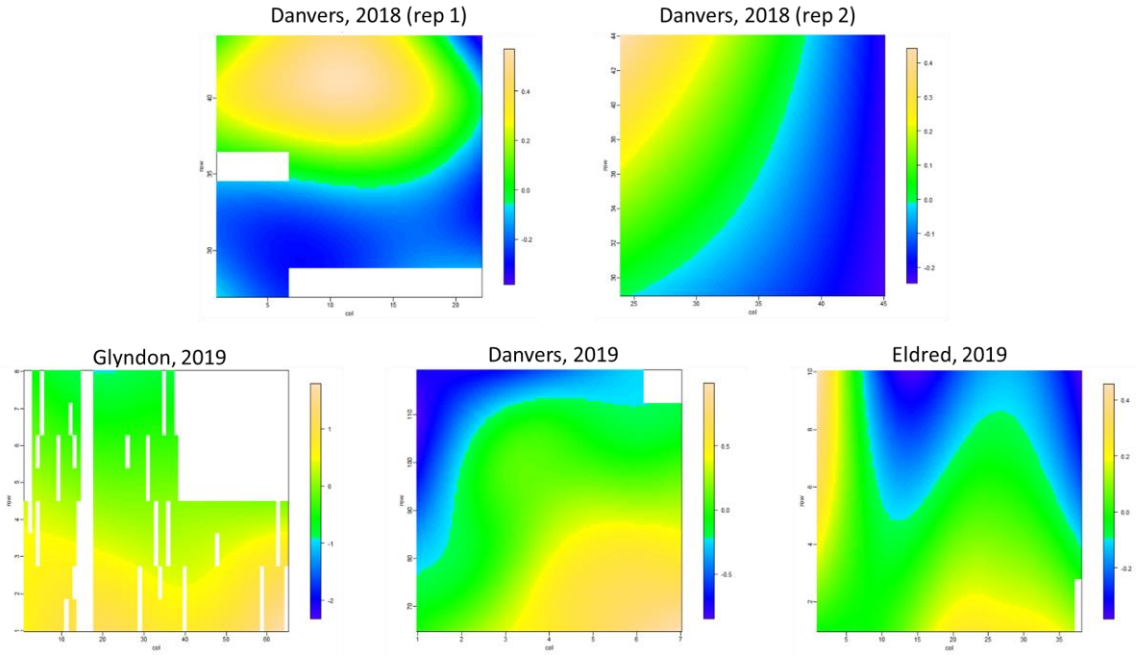

Figure 4-2. Spatial patterns at each of the five environments. Spatially adjusted means for all iron deficiency chlorosis measurements were estimated in each of the five environments using P-spline mixed models. The fitted spatial trends are shown for each of the five environments. White colored pixels indicate missing plots.

Table 4-2. Reliability estimates of accession means for IDC flash and recovery scores. The reliability estimates were calculated before and after fitting spatially adjusted means from the SpATS package. In addition, reliability was estimated for both visual scores and UAS scores during the flash and recovery assessments of chlorosis symptoms.

	No spatial adjustment		**With Spatial Adjustment**	
	Flash	Recovery	Flash	Recovery
Visual Score	0.49	0.45	0.54	0.54
UAS Severity	0.47	0.44	0.56	0.52

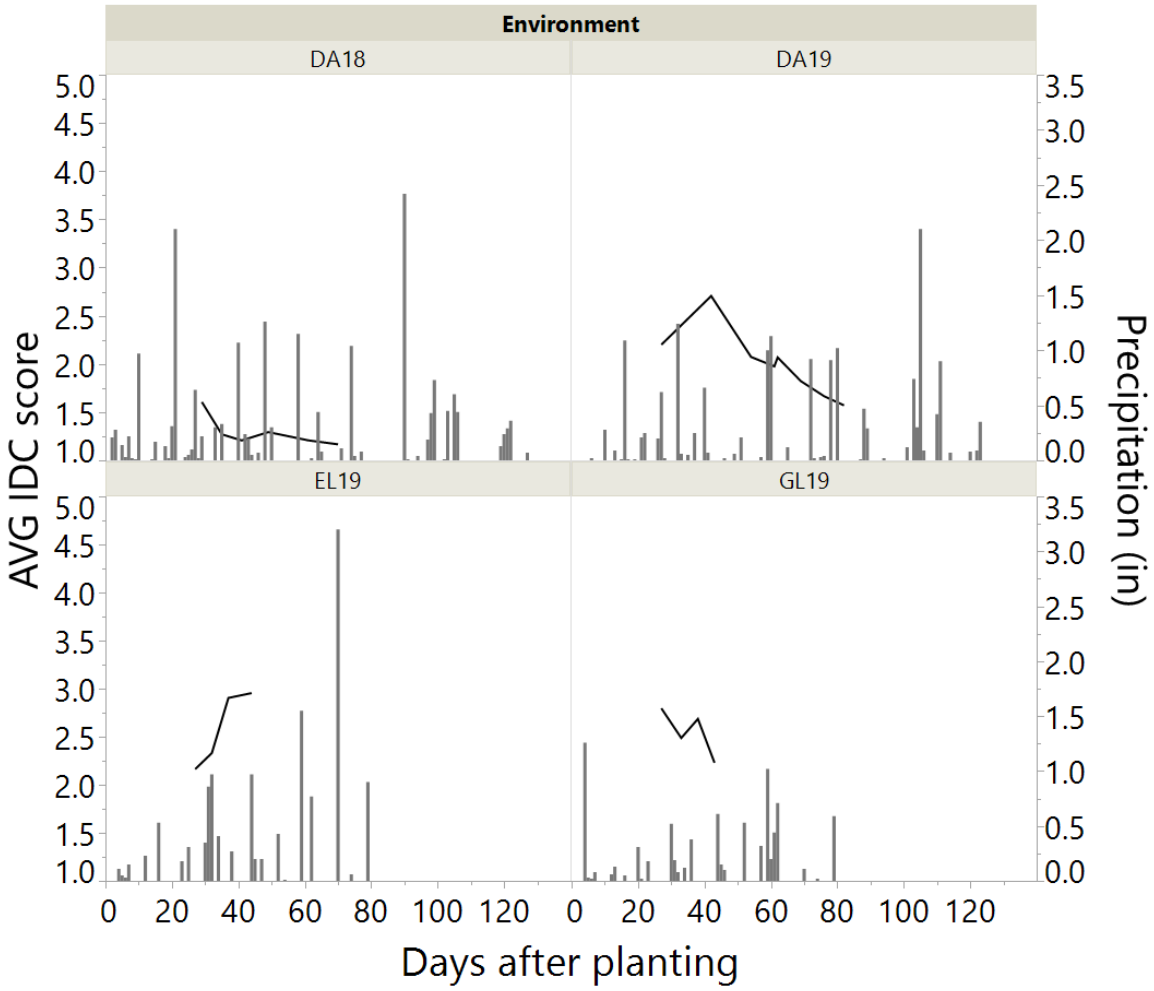

Figure 4-3. Average iron deficiency chlorosis (IDC) scores across multiple flights for each of the four environments. The average IDC score is the mean of all 358 plant introgression lines at each environment (lines). The precipitation (bars) is the rainfall (inches) at each time point of a rainfall event according to the High Plains Regional Climate Center data. DA18 represents Danvers, 2018 location; DA19 represents the Danvers, 2019 location; EL19 represents the Eldred, 2019 location; and GL19 represents the Glyndon, 2019 location.

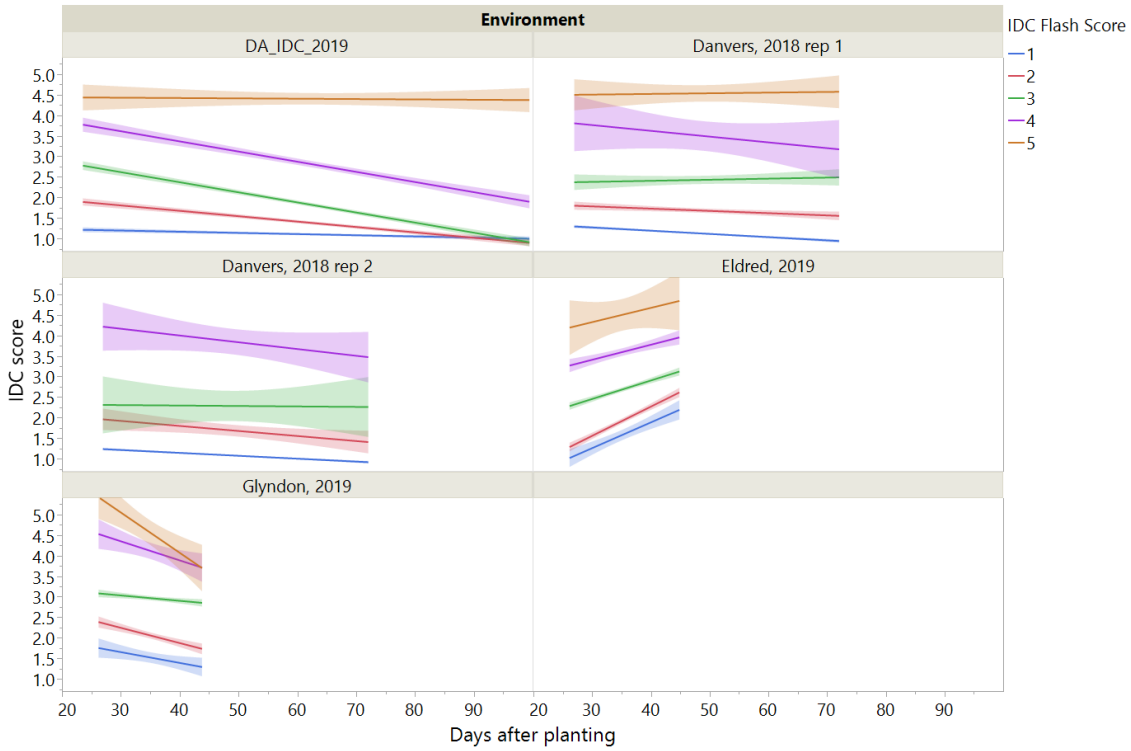

Figure 4-4. Soybean IDC spatially adjusted visual score (y-axis) across time (x-axis) in each of the four environments plus a second replication in Danvers, 2018. The colored lines indicate the five classes of IDC as defined by initial IDC severity scores. A score of a "1" indicates no chlorosis symptoms and a "5" indicates severe symptoms and necrosis.

Table 4-3. Significant single nucleotide polymorphisms (SNPs) associated with iron deficiency chlorosis (IDC) tolerance and their associated SNP I.D., chromosome number, position in base pairs (bp), and significance of association (–log10(p)) values for unmanned aircraft system (UAS) flash and recovery scores as well as visual (VS) flash and recovery scores.

SNP	Chromosome #	Position (bp)	UAS IDC Flash -log(p)*	UAS IDC Recovery -log(p)*	VS IDC Flash -log(p)*	VS IDC Recovery -log(p)*
ss715585469	3	34532040	9.962*	8.366*	9.521*	10.251*
ss715585425	3	34243241	5.976*	5.208*	7.781*	5.272*
ss715585427	3	34245545	5.800*	5.303*	7.686*	5.221*
ss715585451	3	34400542	6.212*	5.010*	6.986*	4.961*
ss715585450	3	34399757	6.015*	4.882*	6.832*	4.729*
ss715585452	3	34403919	5.398*		6.011*	
ss715585444	3	34374076	5.617*	4.510*	5.635*	4.176*
ss715585486	3	34612476	5.921*	5.207*	5.246*	5.566*
ss715585442	3	34364354	4.560*	4.415*	5.019*	4.140*
ss715585473	3	34547382			4.811*	4.229*
ss715604418	9	43614074	4.494*		4.732*	
ss715592610	5	201448			4.566*	
ss715585472	3	34545549			4.362*	
ss715604389	9	43375648			4.009*	

**= above significance threshold of 4.00*

Table 4-4. Significant single nucleotide polymorphisms (SNPs) associated with iron deficiency chlorosis (IDC) rate of recovery and their associated SNP I.D., chromosome number, position in base pairs (bp), and association (–log10(p)) values for UAS flash and recovery scores as well as visual flash and recovery scores.

SNP	Chromosome #	Position (bp)	Rate of Recovery -log(p)*
ss715632703	Chr18	7917371	4.76139*
ss715635025	Chr19	40683950	4.52203*
ss715635026	Chr19	40685025	4.52203*
ss715624771	Chr16	35646769	4.47839*
ss715635029	Chr19	40701199	4.352907*
ss715619536	Chr14	48597275	4.338533*
ss715582750	Chr02	41382652	4.14603*

**= above significance threshold of 4.00*

Table 4-5. Identification of nearest non-significant SNPs flanking the significant SNP were identified to delineate genomic regions of interest. The SNPs were declared significant based on a –log(p) value greater than 4.00 for the association to the rate of recovery of IDC severity. The Williams 82 (WM 82) reference genome was used to identify genes within the genomic regions of interest. Annotations are based on the WM 82 reference genome.

SNP ID	Chromosome #	SNP Status	WM 82 Gene identifier	Annotation
ss715632702	Chr18	Flanking	Glyma.18g081700	RNA-binding (RRM/RBD/RNP motifs) family protein)
ss715632703	Chr18	Significant		
ss715632704	Chr18	Flanking		
ss715635024	Chr19	Flanking	Glyma.19g146000	squamosa promoter binding protein-like 9
ss715635025	Chr19	Significant	Glyma.19g146100	NA
ss715635026	Chr19	Significant		
ss715635029	Chr19	Significant		
ss715635030	Chr19	Flanking		
ss715624770	Chr16	Flanking	Glyma.16g194300	NA
ss715624771	Chr16	Significant		
ss715624772	Chr16	Flanking		
ss715619537	Chr14	Flanking	Glyma.14g220900	GDSL-like Lipase/Acylhydrolase superfamily protein)
ss715619536	Chr14	Significant	Glyma.14g221000	ZINC FINGER FYVE DOMAIN CONTAINING PROTEIN
ss715619535	Chr14	Flanking	Glyma.14g221100	winged-helix DNA-binding transcription factor family protein)
ss715582748	Chr02	Flanking	Glyma.02g226600	(pfkB-like carbohydrate kinase family protein)
ss715582750	Chr02	Significant	Glyma.02g226700	NA
ss715582751	Chr02	Flanking	Glyma.02g226800	(phospholipase C 2)

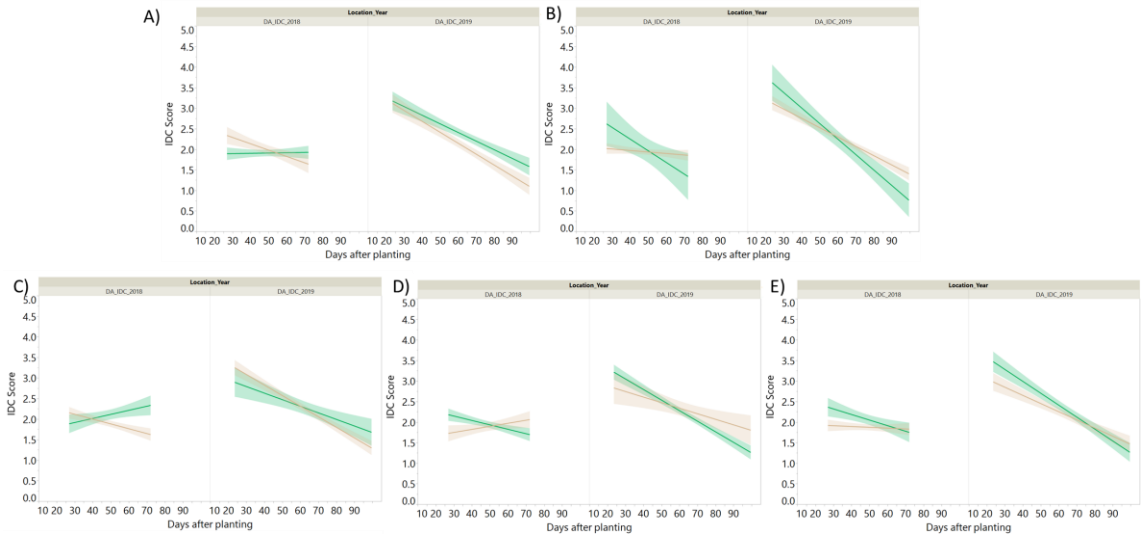

Figure 4-5. Temporal patterns of IDC score (y-axis) by days after planting (x-axis) of five significantly associated alleles (panels A-E) to the rate of recovery phenotype in two environments (Danvers, 2018 left; and Danvers, 2019 right) within each panel. The five panels represent the Gm02, Gm14, Gm16, Gm18, and Gm19 significant alleles for A, B, C, D, E, respectively. Green lines indicate the "-1" allele for each SNP and the tan lines represent the "+1" allele for each SNP.

Literature cited

Acharya K., C. Tande, and E. Byamukama, 2016 Determination of heterodera glycines virulence phenotypes occurring in South Dakota. Plant Dis. 100. https://doi.org/10.1094/PDIS-04-16-0572-RE

Allen T. W., C. A. Bradley, A. J. Sisson, E. Byamukama, M. I. Chilvers, *et al.*, 2017 Soybean yield loss estimates due to diseases in the United States and Ontario, Canada, from 2010 to 2014. Plant Heal. Prog. 18: 19–27. https://doi.org/10.1094/PHP-RS-16-0066

Anand S. C., 1994 Genetic diversity for resistance to Heterodera glycines race 5 in soybean. J. Nematol. 26: 76–79.

Andrade-Sanchez P., M. A. Gore, J. T. Heun, K. R. Thorp, A. E. Carmo-Silva, *et al.*, 2014 Development and evaluation of a field-based high-throughput phenotyping platform. Funct. Plant Biol. 41: 68–79. https://doi.org/10.1071/FP13126

Araus J. L., and J. E. Cairns, 2014 Field high-throughput phenotyping: The new crop breeding frontier. Trends Plant Sci. 19: 52–61. https://doi.org/10.1016/j.tplants.2013.09.008

Araus J. L., S. C. Kefauver, J. Atieno, Y. Li, P. Langridge, *et al.*, 2015 Breeding to adapt agriculture to climate change: affordable phenotyping solutions. Curr. Opin. Plant Biol. 45: 93–99. https://doi.org/10.1016/j.pbi.2018.05.003

Assefa T., J. Zhang, A. N. M. Lauter, A. Singh, J. A. O. Rourke, *et al.*, 2020a Deconstructing the genetic architecture of iron deficiency chlorosis in soybean using genome-wide approaches. 1–13.

Assefa T., J. Zhang, R. V. Chowda-Reddy, A. N. Moran Lauter, A. Singh, *et al.*, 2020b Deconstructing the genetic architecture of iron deficiency chlorosis in soybean using genome-wide approaches. BMC Plant Biol. 20: 1–13. https://doi.org/10.1186/s12870-020-2237-5

Bai G., S. Jenkins, W. Yuan, G. L. Graef, and Y. Ge, 2018a Field-based scoring of soybean iron deficiency chlorosis using RGB imaging and statistical learning. Front. Plant Sci. 9: 1–12. https://doi.org/10.3389/fpls.2018.01002

Bai G., S. Jenkins, W. Yuan, G. L. Graef, and Y. Ge, 2018b Field-Based Scoring of Soybean Iron Deficiency Chlorosis Using RGB Imaging and Statistical Learning. 9: 1–12. https://doi.org/10.3389/fpls.2018.01002

Bandillo N., D. Jarquin, Q. Song, R. Nelson, P. Cregan, *et al.*, 2015 A Population Structure and Genome-Wide Association Analysis on the USDA Soybean Germplasm Collection. Plant Genome. https://doi.org/10.3835/plantgenome2015.04.0024

Bauckhage C., and K. Kersting, 2013 Data mining and pattern recognition in agriculture. Künstl Intell 27: 313–324. https://doi.org/10.1007/s13218-013-0273-0

Bissonnette K. M., C. Christopher, P. Mark, D. Gregory, M. Peter, *et al.*, 2020 Effects of ILeVO seed treatment on Heterodera glycines reproduction and soybean yield in small-plot and strip-trial experiments in Iowa. Plant Dis. 1–34.

Bloom P. R., G. W. Rehm, J. A. Lamb, and A. J. Scobbie, 2011a Soil Nitrate is a Causative Factor in Iron Deficiency Chlorosis in Soybeans. Soil Sci. Soc. Am. J. 75: 2233. https://doi.org/10.2136/sssaj2010.0391

Bloom P. R., G. W. Rehm, J. A. Lamb, and A. J. Scobbie, 2011b Soil Nitrate is a Causative Factor in Iron Defi ciency Chlorosis in Soybeans. 75: 2233–2241. https://doi.org/10.2136/sssaj2010.0391

Breiman L., 2001 Random forests. Mach. Learn. 45: 5–32. https://doi.org/10.1023/A:1010933404324

Brown J. C., C. R. Weber, and B. E. Caldwell, 1967 Efficient and inefficient use of iron by two soybean genotypes and their isolines. Agron. J. 59: 459–462.

Busemeyer L., D. Mentrup, K. Möller, E. Wunder, K. Alheit, *et al.*, 2013 Breedvision - A multi-sensor platform for non-destructive field-based phenotyping in plant breeding. Sensors (Switzerland) 13: 2830–2847. https://doi.org/10.3390/s130302830

Campbell P. K. E., E. M. Middleton, J. E. McMurtrey, L. A. Corp, and E. W. Chappelle, 2007 Assessment of Vegetation Stress Using Reflectance or Fluorescence Measurements. J. Environ. Qual. 36: 832–845. https://doi.org/10.2134/jeq2005.0396

Charlson D. V., T. B. Bailey, S. R. Cianzio, and R. C. Shoemaker, 2005 Molecular marker Satt481 is associated with iron-deficiency chlorosis resistance in a soybean breeding population. Crop Sci. 45: 2394–2399. https://doi.org/10.2135/cropsci2004.0510

Chatterjee A., S. Lovas, H. Rasmussena, and R. J. Goos, 2017 Foliar Application of Iron Fertilizers to Control Iron Deficiency Chlorosis of Soybean. Crop. Forage Turfgrass Manag. 3: 1–7. https://doi.org/10.2134/cftm2017.05.0037

Chen S. Y., P. M. Porter, J. H. Orf, C. D. Reese, W. C. Stienstra, *et al.*, 2001 Soybean cyst nematode population development and associated soybean yields of resistant and susceptible cultivars in Minnesota. Plant Dis. 85: 760–766. https://doi.org/10.1094/PDIS.2001.85.7.760

Chen S., J. E. Kurle, S. R. Stetina, G. A. Nelson, and N. C. Hansen, 2007 Interactions between iron-deficiency chlorosis and soybean cyst nematode in Minnesota soybean fields. 131–139. https://doi.org/10.1007/s11104-007-9370-x

Chen S. Y., B. Potter, and J. H. Orf, 2010 Virulence of the soybean cyst nematode has increased over years in Minnesota. Jorunal Nematol. 42: 238–238.

Chen D., K. Neumann, S. Friedel, B. Kilian, M. Chen, *et al.*, 2014 Dissecting the phenotypic components of crop plant growthand drought responses based on high-throughput image analysis w open. Plant Cell 26: 4636–4655. https://doi.org/10.1105/tpc.114.129601

Cheverud J. M., 2001 A simple correction for multiple comparisons in interval mapping genome scans. Heredity (Edinb). 87: 52–58. https://doi.org/10.1046/j.1365-2540.2001.00901.x

Cianzio S. R. De, W. R. Fehr, and I. C. Anderson, 1979 (1979) Genotypic evaluation for iron deficiency chlorosis in soybeans by visual scores and chlorophyll concentration. Crop Sci. 19: 644–646.

Cianzio S. R., and W. R. Fehr, 1980 Genetic control of iron deficiency chlorosis in soybeans. Iowa State J. Res. 54: 367–375.
Cianzio S. R., and W. R. Fehr, 1982 Variation in the inheritance of resistance to iron deficiency chlorosis in soybeans. Crop Sci. 22: 433–434.
Clark R. B., 1982 Iron deficiency in plants grown in the Great Plains of the United States. J. Plant Nutr. 5.
Concibido V. C., D. A. Lange, R. L. Denny, J. H. Orf, and N. D. Young, 1997 Genome mapping of soybean cyst nematode resistance genes in "Peking", PI 90763, and PI 88788 using DNA markers. Crop Sci. 37: 258–264. https://doi.org/10.2135/cropsci1997.0011183X003700010046x
Cook D. E., T. G. Lee, X. Guo, S. Melito, K. Wang, *et al.*, 2012 Copy number variation of multiple genes at Rhg1 mediates nematode resistance in soybean. Science. 338: 1206–1209. https://doi.org/10.1126/science.1228746
Coppens F., N. Wuyts, D. Inzé, and S. Dhondt, 2017 Unlocking the potential of plant phenotyping data through integration and data-driven approaches. Curr. Opin. Syst. Biol. 4: 58–63. https://doi.org/10.1016/j.coisb.2017.07.002
Crain J. L., Y. Wei, J. Barker, S. M. Thompson, P. D. Alderman, *et al.*, 2016 Development and deployment of a portable field phenotyping platform. Crop Sci. 56: 965–975. https://doi.org/10.2135/cropsci2015.05.0290
Crossa J., P. Pérez, J. Hickey, J. Burgueño, L. Ornella, *et al.*, 2014 Genomic prediction in CIMMYT maize and wheat breeding programs. Heredity (Edinb). 112: 48–60. https://doi.org/10.1038/hdy.2013.16
Currie I., and M. Durban, 2002 Flexible smoothing with P -splines : a unified approach. 333–349.
Dhondt S., N. Wuyts, and D. Inzé, 2013 Cell to whole-plant phenotyping: The best is yet to come. Trends Plant Sci. 18: 428–439. https://doi.org/10.1016/j.tplants.2013.04.008
Diers B. W., S. R. Cianzio, and R. C. Shoemaker, 1992 Possible identification of quantitative trait loci affecting iron efficiency in soybean. J. Plant Nutr. 15: 2127–2136. https://doi.org/10.1080/01904169209364462
Dobbels A. A., and A. J. Lorenz, 2019 Soybean iron deficiency chlorosis high throughput phenotyping using an unmanned aircraft system. Plant Methods 15: 1–9. https://doi.org/10.1186/s13007-019-0478-9
Duggan J. . J. ., 1963 Relationship between Intensity of Cereal Root Eelworm (Heterodera avenae Wollenweber 1924) Infestation and pH Value of Soil. Irish J. Agric. Res. 2: 105–110.
Endelman J. B., 2011 Ridge Regression and Other Kernels for Genomic Selection with R Package rrBLUP. Plant Genome 4: 250–255. https://doi.org/10.3835/plantgenome2011.08.0024
Erdle K., B. Mistele, and U. Schmidhalter, 2011 Comparison of active and passive spectral sensors in discriminating biomass parameters and nitrogen status in wheat cultivars. F. Crop. Res. 124: 74–84. https://doi.org/10.1016/j.fcr.2011.06.007
Eskridge K. ., S. G. Gilmour, R. Mead, N. . Butler, and D. A. Travnicek, 2006 Large

supersaturated designs. J. Stat. Comput. Simul. 74: 525–542.
Fahlgren N., M. A. Gehan, and I. Baxter, 2015 Lights, camera, action: High-throughput plant phenotyping is ready for a close-up. Curr. Opin. Plant Biol. 24: 93–99. https://doi.org/10.1016/j.pbi.2015.02.006
Fehr W. R., 1982 Control of iron-deficiency chlorosis in soybeans by plant breeding. J. Plant Nutr. 5.
Fiorani F., and U. Schurr, 2013 Future Scenarios for Plant Phenotyping. Annu. Rev. Plant Biol. 64: 267–291. https://doi.org/10.1146/annurev-arplant-050312-120137
Francl L. J., 1993 Multivariate Analysis of Selected Edaphic Factors and Their Relationship to Heterodera glycines Population Density. J. Nematol. 25: 270–276.
Franzen D. W., and J. L. Richardson, 2008 Soil factors affecting iron chlorosis of soybean in the red river valley of North Dakota and Minnesota. J. Plant Nutr. 23: 67–78. https://doi.org/10.1080/01904160009381998
Froechlich D. M., and W. R. Fehr, 1981 Agronomic Performance of Soybeans with Differing Levels of Iron Deficiency Chlorosis on Calcareous Soil 1 . Crop Sci. 21: 438–441. https://doi.org/10.2135/cropsci1981.0011183x002100030021x
Furbank R. T., and M. Tester, 2011 Phenomics - technologies to relieve the phenotyping bottleneck. Trends Plant Sci. 16: 635–644. https://doi.org/10.1016/j.tplants.2011.09.005
Gamble A. V., J. A. Howe, D. Delaney, E. van Santen, and R. Yates, 2014 Iron chelates alleviate iron chlorosis in soybean on high pH soils. Agron. J. 106: 1251–1257. https://doi.org/10.2134/agronj13.0474
Gardner M., R. Heinz, J. Wang, and M. G. Mitchum, 2017 Genetics and adaptation of soybean cyst nematode to broad spectrum soybean resistance. G3 Genes, Genomes, Genet. 7: 835–841. https://doi.org/10.1534/g3.116.035964
Godwin I. D., J. Rutkoski, R. K. Varshney, and L. T. Hickey, 2019 Technological perspectives for plant breeding. Theor. Appl. Genet. 132: 555–557. https://doi.org/10.1007/s00122-019-03321-4
Goos R. J., and B. E. Johnson, 2000 A comparison of three methods for reducing iron-deficiency chlorosis in soybean. Agron. J. 92: 1135–1139. https://doi.org/10.2134/agronj2000.9261135x
Goos R. J., and B. Johnson, 2001 Seed Treatment, Seeding Rate, and Cultivar Effects on Iron Deficiency Chlorosis of Soybean. J. Plant Nutr. 24: 1255–1268. https://doi.org/10.1081/PLN-100106980
Goos R. J., B. E. Johnson, R. J. Goos, B. E. Johnson, S. Science, *et al.*, 2009 Evaluation of soybean cultivars for resistance to iron deficiency chlorosis in rows versus hills. 4167: 105–114. https://doi.org/10.1080/01904160903392550
Haghighattalab A., L. González Pérez, S. Mondal, D. Singh, D. Schinstock, *et al.*, 2016 Application of unmanned aerial systems for high throughput phenotyping of large wheat breeding nurseries. Plant Methods 12–35. https://doi.org/10.1186/s13007-016-0134-6
Hänsch R., and R. R. Mendel, 2009 Physiological functions of mineral micronutrients

(Cu, Zn, Mn, Fe, Ni, Mo, B, Cl). Curr. Opin. Plant Biol. 12: 259–266. https://doi.org/10.1016/j.pbi.2009.05.006
Hansen N. C., M. A. Schmitt, J. E. Andersen, and J. S. Strock, 2003 Iron Deficiency of Soybean in the Upper Midwest and Associated Soil Properties. Agron. J. 95: 1595–1601. https://doi.org/10.2134/agronj2003.1595
Hansen N. C., V. D. Jolley, S. L. Naeve, and R. J. Goos, 2004 Iron deficiency of soybean in the North Central U.S. and associated soil properties. Soil Sci. Plant Nutr. 50: 983–987. https://doi.org/10.1080/00380768.2004.10408564
Haskett H. T., and A. K. Sood, 1998 Trade-off studies of detection performance versus the number of reflective spectral bands in hyperspectral imagery. 3372: 26–42. https://doi.org/10.1117/12.312606
Hatfield J. L., A. A. Gitelson, J. S. Schepers, and C. L. Walthall, 2008 Application of spectral remote sensing for agronomic decisions. Agron. J. 100: 117–131. https://doi.org/10.2134/agronj2006.0370c
Heffner E. L., A. J. Lorenz, J. L. Jannink, and M. E. Sorrells, 2010 Plant breeding with Genomic selection: Gain per unit time and cost. Crop Sci. 50: 1681–1690. https://doi.org/10.2135/cropsci2009.11.0662
Helms T. C., R. A. Scott, W. T. Schapaugh, R. J. Goos, D. W. Franzen, *et al.*, 2010 Soybean iron-deficiency chlorosis tolerance and yield decrease on calcareous soils. Agron. J. 102: 492–498. https://doi.org/10.2134/agronj2009.0317
Holman F. H., A. B. Riche, A. Michalski, M. Castle, M. J. Wooster, *et al.*, 2016 High throughput field phenotyping of wheat plant height and growth rate in field plot trials using UAV based remote sensing. Remote Sens. Environ. 8: 1–24. https://doi.org/10.3390/rs8121031
Inskeep W. P., and P. R. Bloom, 1987 Soil chemical factors associated with soybean chlorosis in Calciaquolls of Western Minnesota. Agron J. 79: 779–786.
Jannink J. L., A. J. Lorenz, and H. Iwata, 2010 Genomic selection in plant breeding: From theory to practice. Briefings Funct. Genomics Proteomics 9: 166–177. https://doi.org/10.1093/bfgp/elq001
Jeong J., and E. L. Connolly, 2009 Iron uptake mechanisms in plants: functions of the FRO family of ferric reductases. Plant Sci. 176: 709–714. https://doi.org/10.1016/j.plantsci.2009.02.011
Jessen H. ., R. W. Dragonuk, Hintz, and W. R. Fehr, 1988 Alternative breeding strategies for the improvement of iron efficiency in soybean. J. Plant Nutr. 11: 717–726.
Kaiser D. E., J. A. Lamb, and P. R. Bloom, 2011 Managing Iron Deficiency Chlorosis in Soybean. Univ. Minnesota Ext.
Kaiser D. E., J. A. Lamb, P. R. Bloom, and J. A. Hernandez, 2014 Comparison of field management strategies for preventing iron deficiency chlorosis in soybean. Agron. J. 106: 1963–1974. https://doi.org/10.2134/agronj13.0296
Karcher D. E., and M. D. Richardson, 2005 Batch analysis of digital images to evaluate turfgrass characteristics. Crop Sci. 45: 1536–1539. https://doi.org/10.2135/cropsci2004.0562

King K. E., G. A. Peiffer, M. Reddy, N. Lauter, S. F. Lin, *et al.*, 2013 Mapping of Iron and Zinc Quantitative Trait Loci in Soybean for Association To Iron Deficiency Chlorosis Resistance. J. Plant Nutr. 36: 2132–2153. https://doi.org/10.1080/01904167.2013.766804

Koenning S. R., 2000 Density-Dependent Yield of Heterodera glycines-Resistant and -Susceptible Cultivars. J. Nematol. 32: 502–7.

Li J., and L. Ji, 2005 Adjusting multiple testing in multilocus analyses using the eigenvalues of a correlation matrix. Heredity (Edinb). 95: 221–227. https://doi.org/10.1038/sj.hdy.6800717

Liesch A. M., D. A. Ruiz Diaz, K. L. Martin, B. L. Olson, D. B. Mengel, *et al.*, 2011 Management strategies for increasing soybean yield on soils susceptible to iron deficiency. Agron. J. 103: 1870–1877. https://doi.org/10.2134/agronj2011.0191

Lin S., S. Cianzio, and R. Shoemaker, 1997a Mapping genetic loci for iron deficiency chlorosis in soybean. Mol. Breed. 3: 219–229. https://doi.org/10.1023/A:1009637320805

Lin S. F., D. Grant, S. Cianzio, and R. Shoemaker, 2000 Molecular characterization of iron deficiency chlorosis in soybean. J. Plant Nutr. 23: 1929–1939. https://doi.org/10.1080/01904160009382154

Lorenz A. J., 2013 Resource allocation for maximizing prediction accuracy and genetic gain of genomic selection in plant breeding: A simulation experiment. G3 Genes, Genomes, Genet. 3: 481–491. https://doi.org/10.1534/g3.112.004911

Lucena J. J., and L. Hernandez-Apaolaza, 2017 Iron nutrition in plants: an overview. Plant Soil 418: 1–4. https://doi.org/10.1007/s11104-017-3316-8

Mamidi S., S. Chikara, R. J. Goos, D. L. Hyten, D. Annam, *et al.*, 2011 Genome-Wide Association Analysis Identifies Candidate Genes Associated with Iron Deficiency Chlorosis in Soybean. Plant Genome J. 4: 154. https://doi.org/10.3835/plantgenome2011.04.0011

Mamidi S., R. K. Lee, J. R. Goos, and P. E. McClean, 2014a Genome-wide association studies identifies seven major regions responsible for iron deficiency chlorosis in soybean (Glycine max). PLoS One 9: 1–13. https://doi.org/10.1371/journal.pone.0107469

Mamidi S., R. K. Lee, J. R. Goos, and P. E. McClean, 2014b Genome-wide association studies identifies seven major regions responsible for iron deficiency chlorosis in soybean (Glycine max). PLoS One 9: e107469. https://doi.org/10.1371/journal.pone.0107469

Mansur L., 1992 Resistance to Iron-Deficiency Chlorosis in PI 437654 Soybean. Crop Sci. 32: 1137. https://doi.org/10.2135/cropsci1992.0011183x003200050014x

Martín-Fernández C., Á. Solti, V. Czech, K. Kovács, F. Fodor, *et al.*, 2017 Response of soybean plants to the application of synthetic and biodegradable Fe chelates and Fe complexes. Plant Physiol. Biochem. 118: 579–588. https://doi.org/10.1016/j.plaphy.2017.07.028

McCarville M. T., C. C.Marett, M. P.Mullaney, G. D. Gebhart, and G. L. Tylka, 2017

Increase in soybean cyst nematode virulence and reproduction on resistant soybean varieties in Iowa from 2001 to 2015 and the effects on soybean yields. Plant Heal. Prog. 18: 146–155. https://doi.org/10.1094/PHP-RS-16-0062

Melakeberhan H., J. D. Ey, V. C. B. Aligar, T. E. C. A. J. R, I. B. Unit, *et al.*, 2013 Effect of soil pH on the pathogenesis of Heterodera glycines and Meloidogyne incognita on Glycine max genotypes. 6: 585–592.

Merry R., K. Butenhoff, B. W. Campbell, J.-M. Michno, D. Wang, *et al.*, 2019 Identification and Fine-Mapping of a Soybean Quantitative Trait Locus on Chromosome 5 Conferring Tolerance to Iron Deficiency Chlorosis. Plant Genome 12: 3. https://doi.org/10.3835/plantgenome2019.01.0007

Meuwissen T. H. E., B. J. Hayes, and M. E. Goddard, 2001 Prediction of total genetic value using genome-wide dense marker maps. Genetics 157: 1819–1829.

Moran Lauter A. N., G. A. Peiffer, T. Yin, S. A. Whitham, D. Cook, *et al.*, 2014 Identification of candidate genes involved in early iron deficiency chlorosis signaling in soybean (Glycine max) roots and leaves. BMC Genomics 15: 1–25. https://doi.org/10.1186/1471-2164-15-702

Moreira F. F., H. R. Oliveira, J. J. Volenec, K. M. Rainey, and L. F. Brito, 2020 Integrating High-Throughput Phenotyping and Statistical Genomic Methods to Genetically Improve Longitudinal Traits in Crops. 11: 1–18. https://doi.org/10.3389/fpls.2020.00681

Morris D. R., R. H. Loeppert, and T. J. Moore, 1990 Indigenous soil factors influencing iron chlorosis of soybean in calcareous soils. Soil Sci. Soc. Am. J. 54: 1329–1336.

Mourtzinis S., and S. P. Conley, 2017 Delineating soybean maturity groups across the United States. Agron. J. 109: 1397–1403. https://doi.org/10.2134/agronj2016.10.0581

Naeve S. L., 2006 Iron deficiency chlorosis in soybean: Soybean seeding rate and companion crop effects. Agron. J. 98: 1575–1581. https://doi.org/10.2134/agronj2006.0096

Naeve S. L., and G. W. Rehm, 2006 Genotype x environment interactions within iron deficiency chlorosis-tolerant soybean genotypes. 98: 808–814. https://doi.org/10.2134/agronj2005.0281

Naik H. S., J. Zhang, A. Lofquist, T. Assefa, S. Sarkar, *et al.*, 2017 A real - time phenotyping framework using machine learning for plant stress severity rating in soybean. Plant Methods 13–23. https://doi.org/10.1186/s13007-017-0173-7

Narayanan B., B. Floyd, K. Tu, L. Ries, and N. Hausmann, 2019 Improving soybean breeding using UAS measurements of physiological maturity. Proc. SPIE 27. https://doi.org/10.1117/12.2519072

Neely L., A. Rana, M. V Bagavathiannan, J. Henrickson, E. B. Putman, *et al.*, 2016 Unmanned aerial vehicles for high- throughput phenotyping and agronomic research. PLoS One 7: 1–26. https://doi.org/10.5061/dryad.65m87

Neilson E. H., A. M. Edwards, C. K. Blomstedt, B. Berger, B. L. Møller, *et al.*, 2015 Utilization of a high-throughput shoot imaging system to examine the dynamic phenotypic responses of a C4 cereal crop plant to nitrogen and water deficiency over

time. J. Exp. Bot. 66: 1817–1832. https://doi.org/10.1093/jxb/eru526
Niblack T. L., N. K. Baker, and D. C. Norton, 1992 Yield losses due to Heterodera glycines in Iowa. Plant Dis. 76: 943–948.
Niblack T. L., P. R. Arelli, G. R. Noel, C. H. Opperman, J. H. Orf, *et al.*, 2002 A revised classification scheme for genetically diverse populations of Heterodera glycines. J. Nematol. 34: 279–288.
Niblack T. L., A. L. Colgrove, K. Colgrove, and J. P. Bond, 2008 Shift in Virulence of Soybean Cyst Nematode is Associated with Use of Resistance from PI 88788. Plant Heal. Prog. 9: 29. https://doi.org/10.1094/php-2008-0118-01-rs
Nutter F. W., G. L. Tylka, J. Guan, A. J. D. Moreira, C. . C. Marett, *et al.*, 2002 Use of Remote Sensing to Detect Soybean Cyst Nematode-Induced Plant Stress. 34: 222–231.
O'Rourke J. A., D. V. Charlson, D. O. Gonzalez, L. O. Vodkin, M. A. Graham, *et al.*, 2007a Microarray analysis of iron deficiency chlorosis in near-isogenic soybean lines. BMC Genomics 8: 1–13. https://doi.org/10.1186/1471-2164-8-476
O'Rourke J. A., M. A. Graham, L. Vodkin, D. O. Gonzalez, S. R. Cianzio, *et al.*, 2007b Recovering from iron deficiency chlorosis in near-isogenic soybeans: A microarray study. Plant Physiol. Biochem. 45: 287–292. https://doi.org/10.1016/j.plaphy.2007.03.008
O'Rourke J. A., R. T. Nelson, D. Grant, J. Schmutz, J. Grimwood, *et al.*, 2009 Integrating microarray analysis and the soybean genome to understand the soybeans iron deficiency response. BMC Genomics 10: 1–17. https://doi.org/10.1186/1471-2164-10-376
Pauli D., P. Andrade-Sanchez, A. E. Carmo-Silva, E. Gazave, A. N. French, *et al.*, 2016a Field-based high-throughput plant phenotyping reveals the temporal patterns of quantitative trait loci associated with stress-responsive traits in cotton. G3 Genes, Genomes, Genet. 6: 865–879. https://doi.org/10.1534/g3.115.023515
Pauli D., S. C. Chapman, R. Bart, C. N. Topp, C. J. Lawrence-Dill, *et al.*, 2016b The quest for understanding phenotypic variation via integrated approaches in the field environment. Plant Physiol. 172: 622–634. https://doi.org/10.1104/pp.16.00592
Pederson P., G. L. Tylka, A. P. Mallarino, A. E. Macguidwin, N. C. Koval, *et al.*, 2010 Correlation between Soil pH, Heterodera glycines Population Densities, and Soybean Yield. Crop Sci. 50: 1458–1464.
Peiffer G. A., K. E. King, A. J. Severin, G. D. May, S. R. Cianzio, *et al.*, 2012 Identification of candidate genes underlying an iron efficiency quantitative trait locus in soybean. 158: 1745–1754. https://doi.org/10.1104/pp.111.189860
Reynolds D., F. Baret, C. Welcker, A. Bostrom, J. Ball, *et al.*, 2019 What is cost-efficient phenotyping? Optimizing costs for different scenarios. Plant Sci. 282: 14–22. https://doi.org/10.1016/j.plantsci.2018.06.015
Reynolds M., S. Chapman, L. Crespo-Herrera, G. Molero, S. Mondal, *et al.*, 2020 Breeder friendly phenotyping. Plant Sci. 110396. https://doi.org/10.1016/j.plantsci.2019.110396

Riggs R. D., and D. P. Schmitt, 1988 Complete Characterization of the Race Scheme for Heterodera glycines. J. Nematol. 20: 392–5.

Rodrigues F. A., G. Blasch, P. Defourny, J. I. Ortiz-Monasterio, U. Schulthess, *et al.*, 2018 Multi-temporal and spectral analysis of high-resolution hyperspectral airborne imagery for precision agriculture: Assessment of wheat grain yield and grain protein content. Remote Sens. 10. https://doi.org/10.3390/rs10060930

Rodríguez-Álvarez M. X., D. J. Lee, T. Kneib, M. Durbán, and P. Eilers, 2015 Fast smoothing parameter separation in multidimensional generalized P-splines: the SAP algorithm. Stat. Comput. 25: 941–957. https://doi.org/10.1007/s11222-014-9464-2

Rogovska N., 2006 Use of precision agriculture technologies in studying the relationships among soil pH , calcium carbonate equivalent , soybean cyst nematode population density , and soybean yield

Rogovska N. P., A. M. Blackmer, and A. P. Mallarino, 2007 Relationships between soybean yield , soil pH , and soil carbonate concentration. 71: 1251–1256. https://doi.org/10.2136/sssaj2006.0235

Rogovska N. P., A. M. Blackmer, and G. L. Tylka, 2009 Soybean Yield and Soybean Cyst Nematode Densities Related to Soil pH, Soil Carbonate Concentrations, and Alkalinity Stress Index. 1019–1026. https://doi.org/10.2134/agronj2008.0086x

Roitsch T., L. Cabrera-Bosquet, A. Fournier, K. Ghamkhar, J. Jiménez-Berni, *et al.*, 2019 Review: New sensors and data-driven approaches—A path to next generation phenomics. Plant Sci. 282: 2–10. https://doi.org/10.1016/j.plantsci.2019.01.011

Ross J. P., and C. A. Brim, 1957 Resistance of soybeans to the soybean cyst nematode as determined by a double-row method. Plant Dis. 41: 923–924.

Sagan V., M. Maimaitijiang, P. Sidike, K. Eblimit, K. T. Peterson, *et al.*, 2019 UAV-based high resolution thermal imaging for vegetation monitoring, and plant phenotyping using ICI 8640 P, FLIR Vue Pro R 640, and thermomap cameras. Remote Sens. 11. https://doi.org/10.3390/rs11030330

Severin A. J., G. A. Peiffer, W. W. Xu, D. L. Hyten, B. Bucciarelli, *et al.*, 2010 An integrative approach to genomic introgression mapping. Plant Physiol. 154: 3–12. https://doi.org/10.1104/pp.110.158949

Silva J., and R. Uchida, 2000 Essential nutrients for plant growth: nutrient functions and deficiency symptoms, pp. 31–55 in *Plant Nutrient Management in Hawaii's Soils, Approaches for Tropical and Subtropical Agriculture*,.

Singh A., B. Ganapathysubramanian, A. K. Singh, and S. Sarkar, 2016 Machine learning for high-throughput stress phenotyping in plants. Trends Plant Sci. 21: 110–124. https://doi.org/10.1016/j.tplants.2015.10.015

Song Q., D. L. Hyten, G. Jia, C. V. Quigley, E. W. Fickus, *et al.*, 2013 Development and Evaluation of SoySNP50K, a High-Density Genotyping Array for Soybean. PLoS One 8: 1–12. https://doi.org/10.1371/journal.pone.0054985

Song Q., J. Jenkins, G. Jia, D. L. Hyten, V. Pantalone, *et al.*, 2016 Construction of high resolution genetic linkage maps to improve the soybean genome sequence assembly Glyma1.01. BMC Genomics 17: 33. https://doi.org/10.1186/s12864-015-2344-0

Soybase.org, SoyBase and the Soybean Breeder's Toolbox
Sun J., J. E. Rutkoski, J. A. Poland, J. Crossa, J.-L. Jannink, *et al.*, 2017 Multitrait, Random Regression, or Simple Repeatability Model in High-Throughput Phenotyping Data Improve Genomic Prediction for Wheat Grain Yield. Plant Genome 10: plantgenome2016.11.0111. https://doi.org/10.3835/plantgenome2016.11.0111
Tardieu F., L. Cabrera-Bosquet, T. Pridmore, and M. Bennett, 2017 Plant Phenomics, From Sensors to Knowledge. Curr. Biol. 27: R770–R783. https://doi.org/10.1016/j.cub.2017.05.055
Tylka G. L., and C. C. Marett, 2014 Distribution of the Soybean Cyst Nematode , Heterodera glycines , in the United States and Canada : 1954 to 2014. Plant Heal. Br. 15: 85–87. https://doi.org/10.1094/PHP-BR-14-0006.The
Vasconcelos M. W., and M. A. Grusak, 2014 Morpho-physiological parameters affecting iron deficiency chlorosis in soybean (Glycine max L .). Plant Soil 374: 161–172. https://doi.org/10.1007/s11104-013-1842-6
Velazco J. G., M. X. Rodríguez-Álvarez, M. P. Boer, D. R. Jordan, P. H. C. Eilers, *et al.*, 2017 Modelling spatial trends in sorghum breeding field trials using a two-dimensional P-spline mixed model. Theor. Appl. Genet. 130: 1375–1392. https://doi.org/10.1007/s00122-017-2894-4
Wahabzada M., A. Mahlein, C. Bauckhage, and U. Steiner, 2015 Metro maps of plant disease dynamics — automated mining of differences using hyperspectral images. PLoS One 1–20. https://doi.org/10.1371/journal.pone.0116902
Wang J., T. L. Niblack, P. Microbiology, J. A. Tremain, W. J. Wiebold, *et al.*, 2003 Soybean Cyst Nematode Reduces Soybean Yield Without Causing Obvious Aboveground Symptoms
Wang J., P. E. McClean, R. Lee, R. J. Goos, and T. Helms, 2008 Association mapping of iron deficiency chlorosis loci in soybean (Glycine max L. Merr.) advanced breeding lines. Theor. Appl. Genet. 116: 777–787. https://doi.org/10.1007/s00122-008-0710-x
Weiss M. G., 1943 Inheritance and Physiology of Efficiency in Iron Utilization in Soybeans. Genetics 28: 253–68.
White J. W., P. Andrade-Sanchez, M. A. Gore, K. F. Bronson, T. A. Coffelt, *et al.*, 2012 Field-based phenomics for plant genetics research. F. Crop. Res. 133: 101–112. https://doi.org/10.1016/j.fcr.2012.04.003
White J. W., and M. M. Conley, 2013 A flexible, low-cost cart for proximal sensing. Crop Sci. 53: 1646–1649. https://doi.org/10.2135/cropsci2013.01.0054
Wiersma J. V, 2005 Partial Solutions to Iron Deficiency in Soybean. 934: 924–934. https://doi.org/10.2134/agronj2004.0309
Wu R., C. X. Ma, M. Lin, Z. Wang, and G. Casella, 2004 Functional mapping of quantitative trait loci underlying growth trajectories using a transform-both-sides logistic model. Biometrics 60: 729–738. https://doi.org/10.1111/j.0006-341X.2004.00223.x
Wu G. Z., and H. W. Xue, 2010 Arabidopsis beta-Ketoacyl-[Acyl Carrier Protein]

Synthase I Is Crucial for Fatty Acid Synthesis and Plays a Role in Chloroplast Division and Embryo Development. Plant Cell 22: 3726–3744. https://doi.org/10.1105/tpc.110.075564

Xavier A., B. Hall, A. A. Hearst, K. A. Cherkauer, and K. M. Rainey, 2017 Genetic architecture of phenomic-enabled canopy coverage in glycine max. Genetics 206: 1081–1089. https://doi.org/10.1534/genetics.116.198713/-/DC1.1

Yu N., L. Li, N. Schmitz, L. F. Tian, J. A. Greenberg, *et al.*, 2016a Development of methods to improve soybean yield estimation and predict plant maturity with an unmanned aerial vehicle based platform. Remote Sens. Environ. 187: 91–101. https://doi.org/10.1016/j.rse.2016.10.005

Yu N., L. Li, N. Schmitz, L. F. Tian, J. A. Greenberg, *et al.*, 2016b Development of methods to improve soybean yield estimation and predict plant maturity with an unmanned aerial vehicle based platform. Remote Sens. Environ. 187: 91–101. https://doi.org/10.1016/j.rse.2016.10.005

Zarco-Tejada P. J., S. L. Ustin, and M. L. Whiting, 2005 Temporal and spatial relationships between within-field yield variability in cotton and high-spatial hyperspectral remote sensing imagery. Agron. J. 97: 641–653. https://doi.org/10.2134/agronj2003.0257

Zhang J., H. S. Naik, T. Assefa, S. Sarkar, and R. V. C. Reddy, 2017a Computer vision and machine learning for robust phenotyping in genome-wide studies. Sci. Rep. 7: 1–11. https://doi.org/10.1038/srep44048

Zhang J., H. S. Naik, T. Assefa, S. Sarkar, and R. V. C. Reddy, 2017b Computer vision and machine learning for robust phenotyping in genome-wide studies. Sci. Rep. 7: 1–11. https://doi.org/10.1038/srep44048

Zheng J., Y. Li, and S. Chen, 2006 Characterization of the virulence phenotypes of Heterodera glycines in Minnesota. J. Nematol. 38: 383–390.

Zhou J., D. Yungbluth, C. N. Vong, A. Scaboo, and J. Zhou, 2019 Estimation of the maturity date of soybean breeding lines using UAV-based multispectral imagery. Remote Sens. 11. https://doi.org/10.3390/rs11182075

Appendix A – UAS data collection protocol for Phantom 3

Overview:

The goal of this handout is to provide the information necessary for someone to collect data using a Phantom 3 Advanced or Phantom 3 Professional drone.

General pipeline:

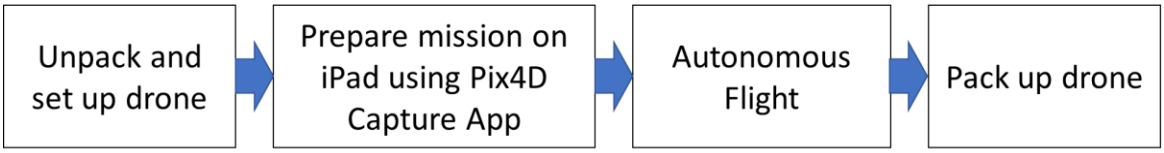

Materials Needed:

1. UAV case with all components inside (See figure 1)
2. iPad or iPhone with DJI Go App and Pix4D Capture App Downloaded
3. Lightning cable for ipad
4. SD card (can be stored in drone camera)

Before going to field:

1. Make sure both drone batteries are fully charged
    a. To check charge of battery, tap button on battery once
2. Make sure remote controller is fully charged
    a. To check charge of battery, tap button on controller once
3. Make sure iPad is charged
4. Make sure weather is permitting
    a. Wind should be less than 25mph

b. Don’t fly in the rain or severe weather conditions

c. Best to check “UAV forecast” app for weather conditions

Unpacking and setting up drone:

1. Place landing/take-off pad on level ground (When available)
2. Open drone case and place drone on landing pad
3. Remove gimbal mount and lens cover
4. Add rotors to drone
    a. Black screw top matches black node on propeller (see figure 2)
5. Power on remote controller
6. Power on Drone
    a. Press once, then immediately following press down and hold
    b. Gimbal will calibrate and drone will beep
    c. Open iPad, Password = 777777
7. Connect phone/ipad to controller via lightning cable
8. Open **DJI GO APP**
9. Check for any error or warning messages
10. Make sure home point is set
11. Completely close out of DJI Go App
    a. Double click home button and swipe up to close app

Flying a previously planned mission:

12. Open Pix4D capture App

13. Click Project List
14. Click on project corresponding to the correct field
15. Click duplicate
16. Click duplicate
17. Double check that the mission covers the field you expect
18. Click save (Bottom right next to the start button) - then ok
19. Click start
20. Click next
21. Click start (This is when the drone will take off)

During Flight:

22. While in flight
    a. Have awareness of drone location
    b. Be on lookout for other air traffic
    c. Keep eye on app to see that images are being captured properly
    d. monitor drone battery level
23. The drone will return home at the completion of the mission
    a. If experienced, catching the drone legs with two hands is preferred
    b. Use caution to not put hands near propellers
24. Close app
25. Power off controller
26. Power off UAV

27. Pack everything back into case

After Flight:

28. Return to lab, transfer data to Shared Folder

FIGURES (Appendix A):

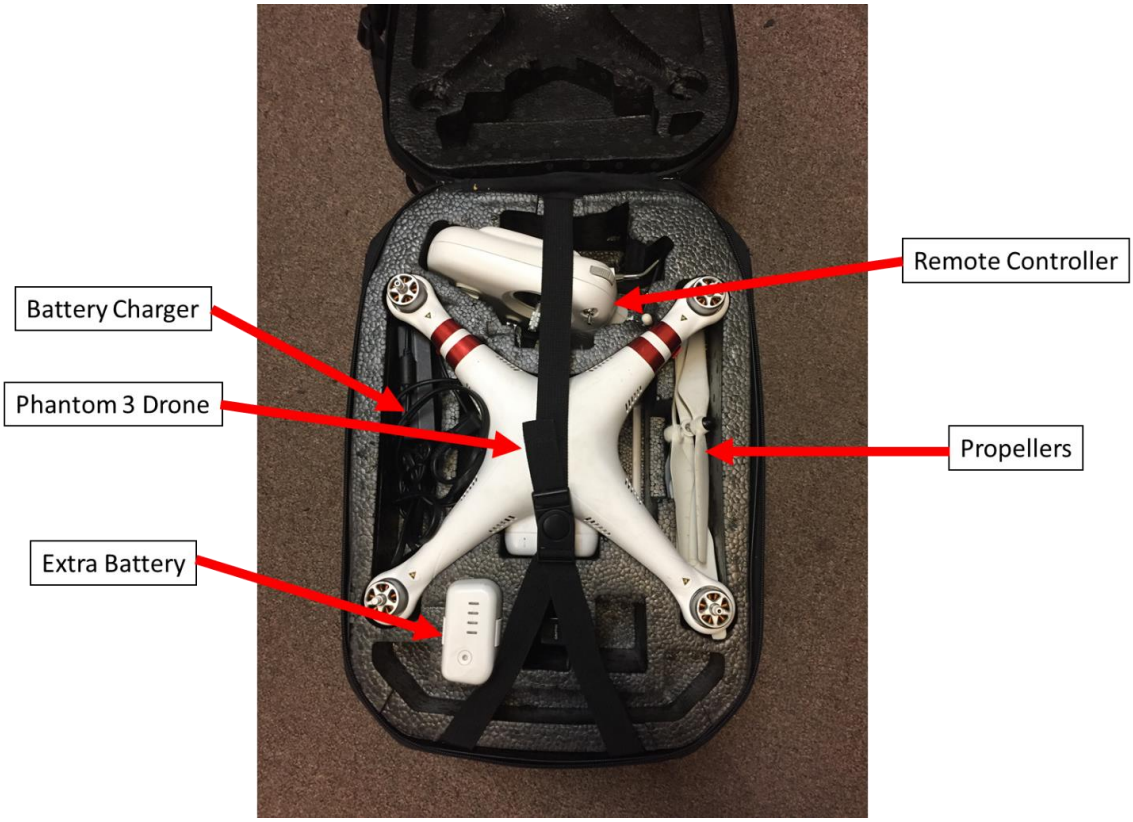

Figure 1. Drone case components. The drone case consists of a battery charger, the drone, an extra battery, remote controller, and propellers.

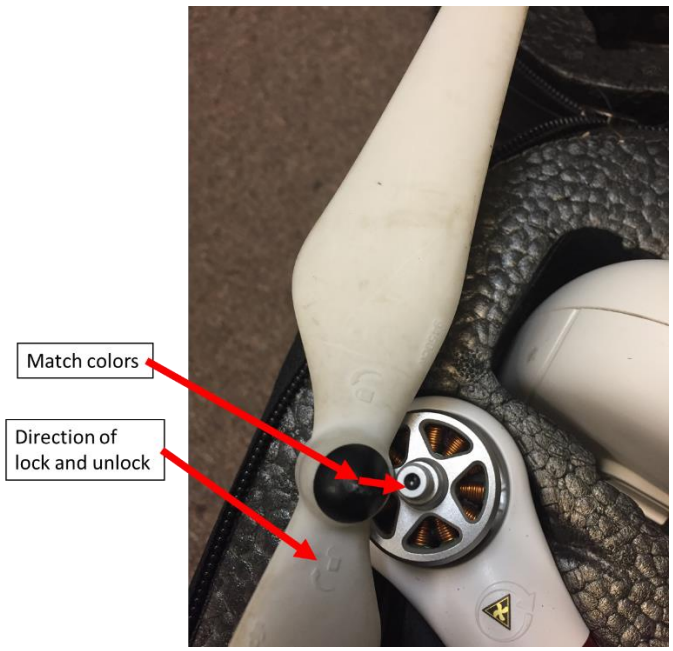

Figure 2. Propeller attachment. In order to attach propellers, one must match the color on the propeller with the color on the drone rotor.

Figure 3. Pix4D capture app – preparing mission

Appendix B – UAS data collection protocol for Inspire 1

Overview:

The goal of this handout is to provide the information necessary for someone to collect data using the Inspire 1 drone

General pipeline:

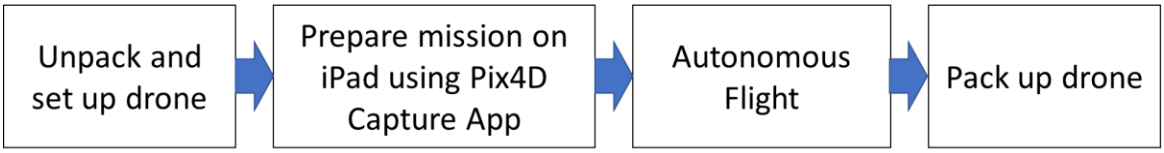

Materials Needed:

- UAV case with all components inside
- iPad or iPhone with DJI Go App and Pix4D Capture App Downloaded
- Lightning cable for ipad
- SD card (can be stored in drone camera)

Before going to field:

- Make sure both drone batteries are fully charged
    - To check charge of battery, tap button on battery once
- Make sure remote controller is fully charged
    - To check charge of battery, tap button on controller once
- Make sure iPad is charged
- Make sure weather is permitting

- Wind should be less than 25mph
- Don’t fly in the rain or severe weather conditions

Unpacking, setting up, and flying drone:

- Open case and set on landing pad
- Turn on drone (push power once, then press and hold)
- Turn on Controller (push power once, then press and hold)
- Raise drone (Toggle switch many times on controller)
- Attach camera (Either Sentera or X3 RGB)
- Attach 4 rotors to drone (red to red and white to white)
- Place drone in an open space
- Turn on ipad – password is all 7’s
- Clear all open apps (double tap home button and swipe away an open apps)
- Open DJI Go App (blue icon)
  - Check for any errors
  - Check to see that the green arrow home button is set
  - You would use this app if you wanted to manually fly and take pictures
- Open Pix4D capture app (Green icon with white box in it)
- Go to Project List
- Open Project
- DUPLICATE project -> Yes
- Hit save icon in lower right

- Hit start
- Hit next
- Drone takeoff checklist
- Hit start
- Drone will takeoff and complete mission
- Double check that camera icons are dropping along the flight plan
- Double check that camera is taking pictures
- Hit the camera icon in upper right to see a live feed of camera
- You'll know pictures are taking correctly if there are flashes of the live camera feed
- Drone will land automatically
    - Can also land manually if preferred

After Flight:

- Return to lab, transfer data to shared folder